2011

CHEMICAL EVOLUTION AND RESIDENCE TIME OF GROUNDWATER IN THE WILCOX AQUIFER OF THE NORTHERN GULF COASTAL PLAIN

Estifanos Haile
University of Kentucky, estifanos.haile@gmail.com

STUDENT AGREEMENT:

I represent that my thesis or dissertation and abstract are my original work. Proper attribution has been given to all outside sources. I understand that I am solely responsible for obtaining any needed copyright permissions. I have obtained and attached hereto needed written permission statements(s) from the owner(s) of each third-party copyrighted matter to be included in my work, allowing electronic distribution (if such use is not permitted by the fair use doctrine).

I hereby grant to The University of Kentucky and its agents the non-exclusive license to archive and make accessible my work in whole or in part in all forms of media, now or hereafter known. I agree that the document mentioned above may be made available immediately for worldwide access unless a preapproved embargo applies.

I retain all other ownership rights to the copyright of my work. I also retain the right to use in future works (such as articles or books) all or part of my work. I understand that I am free to register the copyright to my work.

REVIEW, APPROVAL AND ACCEPTANCE

The document mentioned above has been reviewed and accepted by the student's advisor, on behalf of the advisory committee, and by the Director of Graduate Studies (DGS), on behalf of the program; we verify that this is the final, approved version of the student's dissertation including all changes required by the advisory committee. The undersigned agree to abide by the statements above.

Estifanos Haile, Student

Dr. Alan E. Fryar, Major Professor

Dr. Alan E. Fryar, Director of Graduate Studies

CHEMICAL EVOLUTION AND RESIDENCE TIME OF GROUNDWATER IN THE WILCOX AQUIFER OF THE NORTHERN GULF COASTAL PLAIN

DISSERTATION

A dissertation submitted in partial fulfillment of the
requirements for the degree of Doctor of Philosophy in the
College of Arts and Sciences
at the University of Kentucky

By
Estifanos Haile
Lexington, Kentucky

Director: Dr. Alan E. Fryar, Associate Professor of Geology
Lexington, Kentucky

2011

ABSTACT OF DISSERTATION

CHEMICAL EVOLUTION AND RESIDENCE TIME OF GROUNDWATER IN THE WILCOX AQUIFER OF THE NORTHERN GULF COASTAL PLAIN

This study aims to integrate groundwater geochemistry and mathematical modeling to determine the dominant geochemical processes and groundwater residence time within the Wilcox aquifer in the northern Gulf Coastal Plain. Groundwater samples were collected and analyzed for major ion chemistry, stable isotopes (^{18}O, ^{2}H, and ^{13}C), and radioisotope ^{36}Cl content. Geochemical modeling enabled the identification of major sources and sinks of solutes in the aquifer. A two-dimensional, finite-difference, numerical model was used to determine the deep groundwater flow rate and transport of ^{36}Cl in the aquifer. Major ion chemistry shows a chromatographic pattern along the flow path in which a gradual increase of Na^{+} and decrease of Ca^{2+} and Mg^{2+} is evident. The most plausible inverse models in the downgradient section of the aquifer indicate that oxidation of organic matter (OM), which may be associated with discontinuous lenses of lignite, and consequent release of CO_2 sustain the reduction of Fe(III) (oxyhydr)oxides and sulfate and the dissolution of carbonate minerals (calcite and, in some instances, siderite). These processes, in turn, result in pyrite precipitation and exchange of Ca^{2+} for Na^{+} on clay-mineral surfaces. Models constrained with ^{13}C are consistent with mole transfers between pairs of wells in close proximity, but not for the entire flow path. The observed range of $\delta^{13}C$ of dissolved inorganic carbon (-7.3‰ to -12.4‰) is interpreted as a result of both oxidation of OM and dissolution of carbonates. Calculated values of $^{36}Cl/Cl$ show an abrupt discontinuity between the upgradient and downgradient sections that was also observed in $\delta^{18}O$ and $\delta^{2}H$ data. The gradual enrichment of ^{18}O and ^{2}H along the flow path could be the result of diffusion. The distinct differences in $\delta^{18}O$ and $\delta^{2}H$ between the upgradient and downgradient Wilcox aquifer suggest that the latter preserves a paleoclimatic signal.

KEYWORDS: Groundwater Chemistry, Residence Time, Hydrostratigraphy, Wilcox Aquifer, Gulf Coastal Plain, Stable Isotopes, Radioisotopes

Estifanos Haile
Student's signature

November 22nd, 2011
Date

CHEMICAL EVOLUTION AND RESIDENCE TIME OF GROUNDWATER IN THE WILCOX AQUIFER OF THE NORTHERN GULF COASTAL PLAIN

By

Estifanos Haile

Dr. Alan E. Fryar
Director of Dissertation

Dr. Alan E. Fryar
Director of Graduate Studies

November 22nd, 2011
Date

ACKNOWLEDGMENTS

First, I wish to thank my advisor Dr. Alan E. Fryar for his initial design of the project, guidance, and above all, his patience. Dr. Fryar trusted that eventually I would make it, even when at times I fell into desperation. I would like to thank the dedication of my former (Prof. William Thomas and Dr. Stephen Fisher) and present (Drs. James Dinger, Stephen Workman, Christopher Barton, and Frank Ettensohn) committee members.

I would like to thank the Department of Earth and Environmental Sciences and the Graduate School at the University of Kentucky for giving me this opportunity. This study was made possible through the support of the Kentucky Water Resources Research Institute and the Gulf Coast Association of Geological Societies. Furthermore, I would like to extend my sincere appreciation to administrators of municipal wells and the Arkansas Geological Survey for facilitating sampling.

The list of people to thank is very long; nevertheless, I will try to include as many of them as I can. I would not have been able to settle in and get all the cultural shocks out of the way in one fell swoop without the help of Dr. James W. Ward. Thank you, James and Katy Ward, for all the help, encouragement, discussions, and being good friends. My stay at the University of Kentucky would not have been enjoyable without the presence of former and current students and friends, including Tricia Coakley, John May, Dr. Kenneth Macpherson, Brent Wilhelm, Dr. Brian Cook, Dr. John Allen, Dr. Devi Udgata, Ganesh Tripathi, Peter Idstein, John Warden, and others I may have missed.

Finally, I would like to thank my parents Haile Ghebremichael and Mehret Tekle for all their patience and support. The last two years would not have been possible without the presence of my wife Emily Eastridge. She has always given me moral support and a good sense of humor while also dealing with her own Master's thesis.

TABLE OF CONTENTS

LIST OF TABLES

LIST OF FIGURES

Chapter 1 Introduction

The hydrogeology and hydrogeochemistry of regional clastic aquifers in North America have been extensively studied during the past five decades, motivated by scientific interests and social/economic relevance. These aquifers are major water resources for domestic, agricultural, and industrial purposes (Maupin and Barber, 2005). Effective usage and management of groundwater depend on understanding sources of recharge and flow conditions, complemented by geochemical studies, in target aquifers. An integrated assessment of the connection between geochemical processes and groundwater flow in an aquifer provides a greater understanding of spatial variations in groundwater quality and its availability.

Solute and isotope compositions of groundwater, in conjunction with geochemical and transport models, can be used as proxies to infer sources and fluxes of groundwater. Chemical, biological, and physical processes, such as dissolution - precipitation, ion exchange, oxidation - reduction (redox), microbial respiration, diffusion, and advection, affect the chemical composition of groundwater (Appelo and Postma, 1999). One of the earliest studies that addressed processes controlling solute compositions in regional clastic aquifers was by Foster (1950), who inferred that groundwater composition changes from Ca-HCO_3 to Na-HCO_3 as a result of cation exchange. Hydrochemical facies distributions in aquifer systems are influenced by aquifer parameters (e.g., porosity, permeability, thickness, and lithology). In the early 1980's, various authors (e.g., Plummer and Back, 1980; Chapelle and Knobel, 1983) used a mass-balance approach to interpret the spatial variations and geochemical processes from observed groundwater quality data. This method was later incorporated into computer codes, such as NETPATH (Plummer et al., 1994), to calculate net geochemical changes by tracing an upgradient water composition (initial component) to a downgradient water composition (final component) along a flow path, using a user-specified set of reactions. A slightly more advanced code that includes reactive transport, PHREEQC, was developed by Parkhurst and Appelo (1999). Commonly, plausible models have been calibrated against mineralogical compositions with a certain degree of freedom of possible phases in order to account for source-sink terms of aqueous species (e.g., Appelo, 1994).

Basin-scale groundwater flow models are useful to delineate recharge zones and estimate probable ranges of groundwater residence time. Groundwater residence time is a function of aquifer material properties and recharge rate. Groundwater flow is driven by topography, stratigraphic orientation, aquifer depth, thickness and type of overburden (for sediment compaction-driven flow), extent and type of formation water (density differences), and thermal variations with depth (Bethke, 1985). Flux through the aquifers is estimated from mass-balance calculations. Uncertainties in model parameters (e.g., horizontal and vertical hydraulic conductivity, specific storage, specific yield, porosity, diffusion coefficient) can greatly influence estimated flux amounts. Models applied to regional clastic aquifers that took into consideration the above parameters have inferred residence times on the order of 10^4 years for flow paths on the scale of 100 km (Castro and Goblet, 2003a; 2005).

The purpose of this study is to develop a quantitative understanding of the processes that control groundwater geochemistry of a major regional clastic aquifer, the lower Wilcox aquifer in the northern Gulf Coastal Plain of the USA, and to determine flow rates and residence time of groundwater in the aquifer under natural conditions. Studies of regional confined aquifers in the Atlantic and Gulf Coastal Plains have shown a transition from fresh to brackish water at distances of ~100 km downgradient from the recharge zone (e.g., Clark et al., 1997; Penny et al., 2003; Lee et al., 2007). In comparison, the lower Wilcox aquifer has a distinctively low total dissolved solids (TDS) content compared to overlying and underlying aquifers. This is exhibited by Cl^- concentrations < 10 mg/L at a flow distance $\gtrsim$ 300 km from the recharge zone (Arthur and Taylor, 1986; Hosman et al., 1968). The questions addressed in this work are: (1) how effectively is the section of the aquifer addressed in this study confined? (2) To what extent is the aquifer open to modern meteoric recharge or cross-formational flows? (3) What geochemical processes control observed water quality? (4) What is the residence time of water in the Wilcox aquifer? In order to answer these questions, I hypothesize that the confined section of the aquifer is not actively recharged at present, and groundwater chemistry is mainly controlled by oxidation of organic matter that triggers the dissolution of carbonate minerals in the aquifer. The approach used to address these questions combines: (1) analysis of groundwater chemistry to identify spatial patterns in major

ions; (2) geochemical modeling along a regional groundwater flow path to identify major reactions that control the facies distribution; and (3) numerical modeling of solute transport in conjunction with stable-isotope data to constrain estimates of groundwater residence time in the Wilcox aquifer.

Chapter 2 Background

2.1 Overview

The lower Wilcox is one of the major Tertiary to Quaternary aquifers in the Gulf Coastal Plain, which are collectively referred to as the Gulf Coast aquifer system (GCAS). Hydrostratigraphically, the GCAS is divided into the Mississippi Embayment aquifer system (MEAS) of Tertiary age in the north and the Coastal Lowland aquifer system of Quaternary age in the south (Hosman, 1996; Hosman and Weiss, 1991; Williamson and Grubb, 2001) (Figures 2.1 and 2.2). Both aquifer systems are covered by Mississippi River alluvium of Holocene age. The stratigraphic relationships and classification into hydrostratigraphic units are summarized in Table 2.1. The MEAS comprises five major aquifers and four confining layers of Tertiary age covered by the Quaternary-age alluvial aquifer (Hosman et al., 1968). The MEAS is the main supply of groundwater in the south-central USA, which encompasses southern Illinois, southwestern Kentucky, western Tennessee, northwestern Mississippi, eastern Arkansas, and southeastern Missouri (Hosman et al., 1968). It has supported extensive agricultural activity in the region, particularly cultivation of soybean, rice, and cotton, for more than 100 years (Maupin and Barber, 2005).

The study area is located in southeastern Missouri and northeastern Arkansas. Major physiographic features include Crowley's Ridge and the Saint Francis River to the west and the Mississippi River to the east. As reviewed by Williamson and Grubb (2001), the topography is characterized by a gently sloping land surface that varies from ~120 m above sea level (asl) in the northern limits of the study area to ~60 m above sea level south of the Tennessee-Mississippi state line (Figure 2.3). The climate is warm and humid. Annual precipitation varies from 89 cm in southeastern Missouri to 132 cm in Arkansas. Potential evapotranspiration, as estimated from pan evaporation, ranges from 89 to 114 cm/yr in the north and increases towards the south up to 127 cm/yr (Williamson and Grubb, 2001).

2.2 Regional structure and stratigraphy

A major structure in the Gulf Coast basin is the Mississippi Embayment. It is a southwest-plunging trough formed during the Late Cretaceous to Tertiary periods

(Stearns, 1957). The embayment was formed by the opening of the Gulf of Mexico and reactivation of the underlying Late Precambrian to Early Cambrian Reelfoot Rift, followed by down-warping and down-faulting of successive Paleozoic and younger sediments (Kane et al., 1981; Thomas, 1991; Liu and Zoback, 1997). The axis of the Mississippi Embayment coincides with the Mississippi River and is about ~600 km long. The embayment has a width of ~200 km near its northern boundary in Kentucky and Missouri, and ~500 km at its southern boundary in Louisiana and Mississippi.

The Gulf Coastal Plain consists of a thick clastic sequence of prograding fluvio-deltaic and shallow-marine strata deposited during the Cenozoic era. The sediment consists of interbedded sand, silt, and clay. Generally, stratigraphic units thicken toward the axis of the embayment, and along the axis they thicken southward toward the Gulf of Mexico, where the sequence is covered by Pleistocene-Holocene alluvium of the Mississippi River and its tributaries. Outcrops of the Paleocene-Eocene units are limited to margins of the basin (Figure 2.1). The boundary between the Paleocene-Holocene Mississippi Embayment clastic deposits and Oligocene to Holocene Coastal Lowland deposits marks the beginning of the most recent transgressive cycle (Fillon et al., 2005).

The inland extent of the basin is defined by the Cretaceous onlap (Galloway et al., 1991). The depositional history of the Mississippi Embayment is characterized by a major regression of the sea toward the present shoreline of the Gulf of Mexico during the Late Cretaceous and Tertiary eras. Fillon et al. (2005) summarized the transgression and regression cycles for the Paleocene to Eocene sequences from biostratigraphic data and delineated maximum flooding surfaces. Minor transgression events are marked by laterally continuous clay beds that presently act as confining layers to permeable sandy layers (Hosman and Weiss, 1991).

A stratigraphic correlation table of the Tertiary to Quaternary sediments for the entire Gulf Coast sequence was developed by Hosman and Weiss (1991) (Table 2.1). The Midway Group represents the uppermost surface of marine transgression during the Late Cretaceous and the beginning of regression during the Early Paleocene. It consists of dense marine clay and grades into calcareous facies towards the Gulf of Mexico. On top of the Midway, deposition of the lower Wilcox began in a prograding fluvio-deltaic

environment. The lower Wilcox consists of thick sand beds that grade laterally into silt and clay facies deposited in a deltaic environment. Transgression temporarily resumed, leaving a thin clay layer separating the lower Wilcox from the middle Wilcox. Slow regression accompanied by a larger sedimentation rate in a deltaic system deposited a thick layer, identified as the middle Wilcox sequence, composed largely of fine sand, silt, and clay. The cycle continued until Early Miocene time, accompanied by the onset of deposition of Coastal Lowland sediments. Miocene and Pliocene sediments accumulated in the Coastal Lowlands but not in the Mississippi Embayment. During the Pleistocene and Holocene, fluvial and proglacial aggradation deposits by the Mississippi River covered the Tertiary units (Fillon et al., 2005).

2.3 Hydrostratigraphic units

The stratigraphy of the region is characterized by a sequence of sandy layers acting as aquifers and silty to clayey layers that act as confining units. The MEAS is separated from Cretaceous carbonate rocks by a basal clay (Arthur and Taylor, 1986). The Cenozoic geologic units from oldest to youngest are the Midway Group, Wilcox Group, Claiborne Group, Jackson Formation, Vicksburg Formation, loess and alluvial deposits of Pleistocene to Holocene age. They constitute 11 formations with age ranging from Paleocene to Holocene. A summary of the geologic and hydrostratigraphic units constructed by Grubb (1998) is given in Table 2.1.

The Paleocene-Eocene sequence comprises two major geologic groups, the Wilcox Group and the Claiborne Group. The underlying clay unit, the Midway Group, represents the bottom confining unit (Williamson and Grubb, 2001). The Claiborne Group consists of alternating clay and sand layers. The top confining unit, the Jackson and Vicksburg formations, which consist of thick marine clay beds, separate the Paleocene-Eocene sequence from the Quaternary alluvium (Pettijohn, 1996).

The Wilcox Group transitions from massive and laterally continuous sand beds at the bottom (lower Wilcox) to thin and laterally discontinuous sand, silt and clay beds toward the top (middle Wilcox) (Hosman, 1996). The reference to the upper Wilcox has been phased out in recent reports (e.g. Hart et al., 2008) because its hydraulic properties are similar to those of the lower Claiborne aquifer. The geologic units that were defined as

the upper Wilcox (like the Meridian Sand Member) have been reclassified with the lower Claiborne aquifer. The outcrop of the Wilcox Group, which includes the lower Wilcox aquifer, is localized to a narrow strip along the western boundary of the study area, mainly on the hills of Crowley's Ridge (Figures 2.1 and 2.3). It dips toward the south and toward the axis of the basin that roughly coincides with the present-day Mississippi River.

The major semi-confined and confined aquifers are the lower Wilcox, middle Wilcox and lower to middle Claiborne aquifers. The aquifers are identified from the confining units based on sand-to-clay proportion. Table 2.2 shows the sand-to-clay ratio of the aquifers and confining units and short lithologic descriptions of units compiled by Hart et al. (2008) from earlier works by Williamson and Grubb (2001) and Hosman (1996). Depth to the lower Wilcox aquifer ranges from outcrop to 600 m below ground surface (Figure 2.4a), and thickness varies from 25 m near the outcrop to 200 m along the axis of the embayment (Figure 2.4b). The lateral extent of the lower Wilcox toward the south is defined by a facies change from sandy to clayey composition.

The aquifer material is predominantly quartz sand (> 90%), with minor feldspar content and traces of carbonates (calcite and siderite), pyrite, and clay minerals. Oman (1986) has described sand from the Wilcox Group in the New Madrid Seismic Zone as pyritic and containing occasional glauconitic clay layers. The Wilcox Group is sometimes referred to as the lignitic layer because of an abundance of lignite beds, most of which occur south of the Monroe Uplift in southeastern Arkansas (Warwick et al., 2008).

2.4 Hydrogeology

The demand for fresh water supply has led to a number of hydrogeologic and groundwater quality studies. Several of these studies have been conducted as part of the Mississippi Embayment Regional Aquifer Study project by the U.S. Geological Survey (USGS). Most of these were aimed on descriptions of groundwater chemistry and groundwater-flow models for the entire aquifer system, which were not aquifer-specific.

The geologic and hydrostratigraphic framework of the aquifer system is well documented. However, uncertainties about flow mechanisms and geochemical processes persist due to the complexity of the geology of the aquifer system. Additional

complications result from the fact that extensive groundwater pumping has altered the hydraulic gradient, especially around urban areas. Most of the groundwater-flow models developed by USGS have been designed to reconstruct “pre-pumpage” hydraulic conditions, arbitrarily assumed to have occurred circa 1982, while little has been done to characterize the spatial variability and processes that control it.

Systematic regional hydrogeologic studies of the Mississippi Embayment were mostly conducted by USGS in three phases starting from 1964 until the present. The focus of the first phase of the study was a general description of aquifers (especially the top alluvial layer) and water-quality characterization (e.g., Speer et al., 1964; Cushing et al., 1970). In the second phase, the Mississippi Embayment was included as part of a larger regional study, in which the Gulf Coastal Plain aquifers were subdivided into three regional aquifer systems: the Mississippi Embayment, Texas Coastal Uplands, and Coastal Lowland aquifer systems (Hosman and Weiss, 1991; Weiss, 1992). These studies classified the geologic units into hydrostratigraphic units, with sandy layers as aquifers and clayey layers as confining units (Table 2.1). Hosman (1996) refined these classifications and addressed the problems related with geologic correlation and sediment heterogeneity in defining the hydrostratigraphic units. The most recent studies (Hart et al., 2008; Hart and Clark, 2008; Clark and Hart, 2009) involved developing digital surface maps for tops of hydrostratigraphic units based on 2,600 geophysical well logs (normal resistivity, spontaneous potential, and natural gamma logs) for the entire MEAS, and refining the regional groundwater flow model. Arthur and Taylor (1998) delineated groundwater flow directions based on hydraulic-head maps and analyzed transmissivity for Paleocene and Eocene aquifers. A conceptual model was developed by Grubb (1998) and later extended by Williamson and Grubb (2001) to represent pre-development groundwater-flow conditions. The regional groundwater-flow directions obtained from models using pre-1982 data show that the natural flow direction was toward the south to the west of the Mississippi River and toward the west east of the river (Williamson and Grubb, 2001).

Table 2.2 shows that the lower Claiborne and lower Wilcox strata contain large percentages of sand as compared to other Paleocene and Eocene units (Williamson and Grubb, 2001). It should be noted that the sand-to-clay proportions for each unit are

calculated for the entire Gulf Coast, regardless of facies change. Therefore, sand contents in the up-dip portion of the basin for the lower Claiborne and lower Wilcox aquifers should be higher than the given values. The middle Wilcox has a lower sand content and thus lower hydraulic conductivity, but its transmissivity is enhanced by a larger thickness (Grubb, 1998).

The largest portion of the lower Wilcox aquifer is confined; the unconfined and semi-confined part is very narrow and limited to the outcrop area on the western part of the study area (Crowley's Ridge), and north of the New Madrid seismic zone. Historical water level data from a well in the confined section of the lower Wilcox aquifer shows a continuous decrease of water level from 1958 at least until 2000 due to pumpage (Figure 2.5). It is reasonable to assume that the confined section of the aquifer is only replenished slowly, as in a piston-flow model, as groundwater flows downgradient. Natural discharge from the aquifer is hypothesized to occur by upward cross-formational flow at the updip margin of the brackish/saline water zone, as described by Arthur and Taylor (1986).

Recently, Yeatts (2004), Schrader (2007), and Pugh (2010) developed potentiometric surface maps for the Wilcox aquifer in northeastern Arkansas based on hydraulic-head measurements from 2003, 2006, and 2009, respectively (Figure 2.6). The major groundwater flow direction in the Wilcox aquifer is toward the southeast. However, the potentiometric surface maps show that there has been a steady decline of the hydraulic head in the confined section of the Wilcox aquifer near the pumping center around West Memphis, Arkansas, consistent with Figure 2.5.

2.5 Groundwater chemistry

The chemical composition and origin of groundwater in regional clastic aquifers of the USA has been studied for more than 80 years (Chapelle, 2003). One of the earliest discussions was on the origin of groundwater in which Na^+ and HCO_3^- are the dominant ions (Cederstrom, 1946; Foster, 1950; Chapelle, 2003; Schwartz and Zhang, 2003). Sodium-bicarbonate waters are found in aquifers across much of North America, including sandstones beneath the Colorado Plateau (Zhu, 2000) and the Great Plains (Thorstenson et al., 1979; Dutton and Simpkins, 1986; Hendry and Schwartz, 1990; Parkhurst et al., 1996). Sodium-bicarbonate waters have been identified in unlithified

Cretaceous and Tertiary sediments in the Coastal Plain, such as the Aquia Formation in Maryland (Chapelle and Knobel, 1985), the Potomac and Pamunkey Groups in Virginia (Cederstrom, 1946), the Black Creek Formation in South Carolina (Chapelle, 2003), and the Wilcox Group in Tennessee, Mississippi, Arkansas, and Texas (Fogg and Kreitler, 1982; Pettijohn, 1996). In both lithified and unlithified aquifers, these waters occur down-dip from recharge areas under confined conditions. The Na^+ in Na-HCO_3 waters results mainly from exchange with Ca^{2+} and Mg^{2+} on clay minerals as relatively fresh Ca-HCO_3 groundwater flows away from the recharge zone.

The most comprehensive compilation of hydrochemical data for each hydrostratigraphic unit within the Mississippi Embayment was conducted by Pettijohn (1996). Groundwater chemistry from the Wilcox aquifer is generally characterized by low total dissolved solids (TDS). West of the Mississippi River, Ca^{2+}, Mg^{2+}, and SO_4^{2-} concentrations decrease down-gradient. From north to south, Na^+ and HCO_3^- become increasingly dominant ions. The Wilcox aquifer also contains zones of elevated Fe^{2+}, H_2S, and CH_4. The pinchout of the lower Wilcox coincides with a change in water quality from fresh, low TDS ($Cl^- < 10$ mg/L) to $Cl^- > 250$ mg/L. Its position is similar to the freshwater - brackish water interface at a salinity of 1000 mg/L mapped by Arthur and Taylor (1986) in Mississippi (Figure 2.7). Downgradient, approaching the boundary with the Coastal Lowland aquifer system, the water composition becomes a Na-Cl type because of the presence of salt domes and mixing with formation water (Williamson and Grubb, 2001). As water levels decline in overlying aquifers, such as the surficial Mississippi River Valley alluvial aquifer (Czarnecki, 2006), there could be increased outflow/discharge of water from deeper aquifers (Williamson and Grubb, 2001). This would lead in decline of hydraulic head in the deeper aquifers, and potentially, upwelling of saline water from greater depths.

2.6 Background on stable isotopes and ^{36}Cl in groundwater

Stable isotopes of water (^{18}O and ^{2}H) have been used to identify regionally different groundwater flow paths and trace sources of recharge (Mook, 2001). A specific isotopic signature of groundwater is the result of isotopic fractionation due to physical processes such as evaporation, condensation, melting, and diffusion, or chemically by isotopic

exchange between compounds or phases (Geyh, 2001). Gat (1996) concluded that, at ambient temperatures, the stable-isotopic composition of groundwater is conserved, whereas at elevated temperature, the isotopic composition can be perturbed due to isotopic exchange with solid phases. LaBolle et al. (2008) hypothesized that in confined aquifers, with negligible interactions with the atmosphere and low groundwater temperature, oxygen and hydrogen isotopic fractionation can occur by diffusion.

Observed ^{36}Cl levels in groundwater reflect atmospheric and in-situ production, radioactive decay, and mixing with other sources of chloride (Davis et al., 1998). Groundwater dating using ^{36}Cl data (reported as ^{36}Cl/Cl) is dependent on the assumption of the initial value and its source (Davis et al., 1998). The half-life of ^{36}Cl is $3.01\times10^5 \pm 4\times10^3$ years (Bentley et al., 1986). Davis et al. (1998) outlined problems in determining the initial ^{36}Cl in recharge. The authors suggested that long-term records from ice-cores can be used as a proxy for the initial value. However, other authors have used the long-term average of modern atmospheric ^{36}Cl (e.g. Purdy et al., 1996; Lee et al., 2007). The residence time (t) for groundwater is calculated as:

$$t = \frac{-1}{\lambda} \ln\left(\frac{^{36}\mathrm{Cl}}{^{36}\mathrm{Cl}_0}\right) \lambda = \frac{\ln(2)}{T_{1/2}} \qquad (2.1)$$

where $T_{1/2}$ is half-life.

There are four mechanisms of ^{36}Cl production. (1) It is produced by reactions in the atmosphere caused by cosmic radiation and enters groundwater as atmospheric fallout with recharging water. The reaction is triggered by proton-induced spallation of ^{40}Ar in the atmosphere (Andrews et al., 1986). Chlorine-36 is also produced by (2) neutron activation of ^{35}Cl in the atmosphere (Fontes et al., 1984). This was an effect of nuclear bomb testing in the last century along with elevated ^{3}H. Peaks of ^{36}Cl and ^{3}H in shallow groundwater profiles are used as markers of recent groundwater recharge ($\lesssim$ 50 years) (Bentley et al., 1986). Brahana et al. (1985) reported ^{3}H composition of < 1 pCi/L for wells from deep aquifers of the MEAS, suggesting that they contain no anthropogenic ^{36}Cl from nuclear explosions. Figure 2.8 summarizes the above-mentioned mechanisms. (3) Spallation of ^{39}K and ^{40}Ca on rock outcrops and subcrops by atmospheric neutron flux contributes about 2% of the total ^{36}Cl produced (Bentley et al., 1986). (4) Andrews et al.

(1986) estimated that about 10% of the ^{36}Cl produced is from decay of U and Th in sediments, which releases neutrons that collide with ^{35}Cl atoms that are present in groundwater. When the aquifer of interest has high dissolved Cl^- concentration (e.g., because of the presence of connate waters or evaporite layers in the aquifer), proportionally a significant amount of ^{36}Cl is produced by the activation of ^{35}Cl (Andrews et al., 1986).

2.7 Paleoenvironment indicators

Natural environmental tracers provide further information on groundwater fluxes that can complement hydraulic information. These tracers are used to estimate rates and sources of recharge, groundwater residence times, and cross-formational mixing (see Cook and Herczeg [2000], and references therein). Tracers that are commonly measured in groundwater include stable isotopes of H_2O (^{18}O, ^{2}H), radioisotopes (^{3}H, ^{14}C, ^{36}Cl), and noble gases (He, Ne, Ar, Kr, Xe). Residence time is estimated using tracers that vary in concentration with time. Perhaps the most commonly used environmental tracer to characterize flow in regional aquifers for pre-modern (pre-1950s) groundwater is ^{14}C (e.g., Phillips et al., 1989; Clark et al., 1998), which has a halftime of 5730 years and is thus useful for dating to a limit of ~40-50 ka (Cook and Herczeg, 2000). However, reliability of measured values depends on the source and sink terms used. Radiocarbon dating is influenced by C cycling, such as oxidation of dissolved organic matter and dissolution and precipitation of carbonates. Table 2.3 summarizes groundwater ages determined with various isotopes (mainly ^{14}C) in regional aquifer systems in the continental United States.

Studies of radioisotope, stable isotope (^{2}H, ^{18}O), and noble gas concentrations and their spatial variability have been used to determine Pleistocene-Holocene paleoclimatic signatures in regional aquifers (Phillips and Castro, 2003). Stable isotopes in groundwater have been used to infer sources and temperatures of recharge because fractionation is temperature-dependent, but noble gases provide more precise information on recharge temperatures because the aqueous solubility of those gases is known as a function of temperature (Aeschbach-Hertig et al., 2002; Ma et al., 2004). Concentrations of dissolved atmospheric noble gases can thus be utilized to derive groundwater temperatures at the

time of infiltration. Studies integrating analysis of radioisotopes with stable isotopes and/or noble gases in North America have included aquifers beneath the Colorado Plateau (Zhu et al., 1998), the San Juan basin (Phillips et al., 1986; Stute et al., 1995), the Great Plains (Plummer et al., 1990; Dutton, 1995; Clark et al., 1998), the Michigan basin (Ma et al., 2004), the Gulf Coastal Plain (Stute et al., 1992; Castro and Goblet, 2003b) and the Atlantic Coastal Plain (Clark et al., 1997; Aeschbach-Hertig et al., 2002). Collectively, these studies have documented paleotemperatures of the last glacial maximum (~21 ± 1.5 ka) at about 5 to 9 °C cooler than present day (Jackson et al., 2000).

Contemporaneous ^{18}O and ^{2}H values that are more depleted than modern values in some areas (e.g., the Madison aquifer in the northern Great Plains [Plummer et al., 1990]) and more enriched in other places (e.g., the Cambro-Ordovician aquifer in Iowa [Siegel, 1991]) have been observed. The lack of consistent spatio-temporal shifts in ^{18}O and ^{2}H values probably reflects the combined effects of temperature (which tends to vary with latitude) and atmospheric circulation (e.g., isotopically depleted Pacific-sourced moisture vs. isotopically enriched Gulf of Mexico-sourced moisture) (Ma et al., 2004). Such studies within the Gulf Coastal Plain and adjoining regions have been scarce. Penny et al. (2003) used ^{18}O, ^{2}H, and ^{36}Cl to assess mixing of groundwater with connate water and residence times in Cretaceous aquifers of the Alabama Coastal Plain. Musgrove and Banner (1993) used H, O, and Sr isotopes to determine sources of groundwater and mixing of saline and fresh waters in Paleozoic carbonate aquifers of the Ozark Plateau in Missouri. Brahana et al. (1985) reported values of ^{18}O, ^{2}H, and ^{14}C mainly for the McNairy and Nacatoch sands of Cretaceous age that lie directly below the lower confining unit (Midway Group).

Table 2.1: Setting of geologic units into hydrostratigraphic units for the study area. Thickness and sand percentage estimates given by Williamson and Grubb (2001).

System	Series	Group	Formation	Thickness (m)		Hydrostratigraphy
				Max.	Ave.	
Quaternary	Holocene		Alluvium	370	170	Alluvium
	Pleistocene		Loess			
Tertiary	Oligocene	Vicksburg	Vicksburg	2000	175	Vicksburg-Jackson confining unit
	Eocene	Jackson	Jackson			
		Claiborne	Cockfield	760	150	Upper Claiborne aquifer
			Cook Mountain	1050	110	Middle Claiborne confining unit
			Sparta Sand	770	145	Middle Claiborne aquifer
			Memphis Sand ("500-foot" sand)			
			Cane River Formation Zilpha Clay	380	70	Lower Claiborne confining unit
			Carrizo Sand Meridian Sand	395	80	Lower Claiborne
	Upper Paleocene	Wilcox	Flour Island	1590	380	Middle Wilcox aquifer
			Fort Pillow Sand ("1400-foot" sand)	395	90	Lower Wilcox aquifer
			Old Breastworks			Old Breastworks confining unit
		Midway	Porters Creek Clay	1150	260	Midway confining unit

Table 2.2: Summary description of individual layers, and their respective sand to clay proportions used for the model.

Layer name	Sand:clay ratio (%)	Description
Alluvium	55 : 45	Coarse gravel, sand, silt and clay; fining-upward sequence
Upper Claiborne	50 : 50	Interbedded fine sand, silt, clay and some lignite;sand beds are thicker at base of aquifer
Middle Claiborne confining unit	0 : 100	Marine clay
Middle Claiborne	50 : 50	Continental derived sand with clay
Lower Claiborne	75 : 25	Thick fine to coarse sand, interbedded with thin layers of clay and silt
Middle Wilcox	40 : 60	Thin interbedded layers of sand, silt, and clay
Lower Wilcox	65 : 35	Thick, laterally continuous and massive sand layer
Midway confining unit	0 : 100	Marine clay

Table 2.3: Regional aquifer systems with published data on ^{14}C-age, $\delta^{18}O$ and $\delta^{2}H$. Data for ^{14}C-age, $\delta^{18}O$ and $\delta^{2}H$ are presented in Figures 5.4a, b, and c, respectively.

Map Code	Aquifer	Location	Reference	Geologic age	Type	Dist. km	Depth m	Num. of samples[a]
1a[b]	Upper Floridan	FL	Plummer and Sprinkle (2001)	Eoc. – Olig.	Carb.	206	131–457	6
1b	Floridan	GA	Plummer (1993)	L Paleoc. – E Mioc.	Carb.	270		10
2a[c]	Black Creek/U Cape Fear	NC	Kennedy and Genereux (2007)	Cretac.	Clastic	93	81–263	6
2b	Aquia	MD	Aeschbach-Hertig et al. (2002)	Paleoc.	Clastic	81.3	95–189	19
3	Marshall	MI	Ma et al. (2004), Ma (2009)	Missi.	Clastic	180	73–122	12
4a	Cambrian-Ordovician	WI	Klump et al. (2008)	Camb. – Ordo.	Clastic	50		7
4b	Cambrian-Ordovician	IA	Siegel (1991)	Camb. – Ordo.	Clastic			1
5	Madison	WY/MT/SD	Plummer et al. (1990)	Missi.	Carb.	250	791–2790	18
6a	San Juan Basin	NM	Phillips et al. (1986)	Paleoc.	Clastic			15
6b[d]	N aquifer	AZ	Zhu et al. (1998)	Tri. – Jur.	Clastic			
7a	Dakota	NE	Stotler et al. (2010)	Cretac.	Clastic	200	169–439	6
7b[e]	Dakota	CO/KS	Clark et al. (1998)	Cretac.	Clastic	500	910–1338	6
7[f]	Dakota	OK/KS	Dutton (1995)	Cretac.	Clastic		34–346	25
8	Central Oklahoma	OK	Parkhurst et al. (1996)	Perm.	Clastic	40	42–900	22
9	Carrizo-Wilcox	TX	Boghici (2008)	U Paleoc. – Eoc.	Clastic	85		6
10[g]	Ozark	MO/AR/OK	Musgrove and Banner (1993)	Penn. – Perm.	Carb.			21
11	McNairy	MO	Brahana et al. (1985)	Cretac.	Clastic		65–656	18

[a] counts of samples used to average $\delta^{18}O$ and $\delta^{2}H$ values. Includes only samples in which the ^{14}C-age falls between 10 and 30 ka; [b] data for flow path III; [c] no $\delta^{2}H$ values; [d] no stable isotope data; [e] data for Group 2; [f] data for Central and Northern High Plains; [g] no ^{14}C data

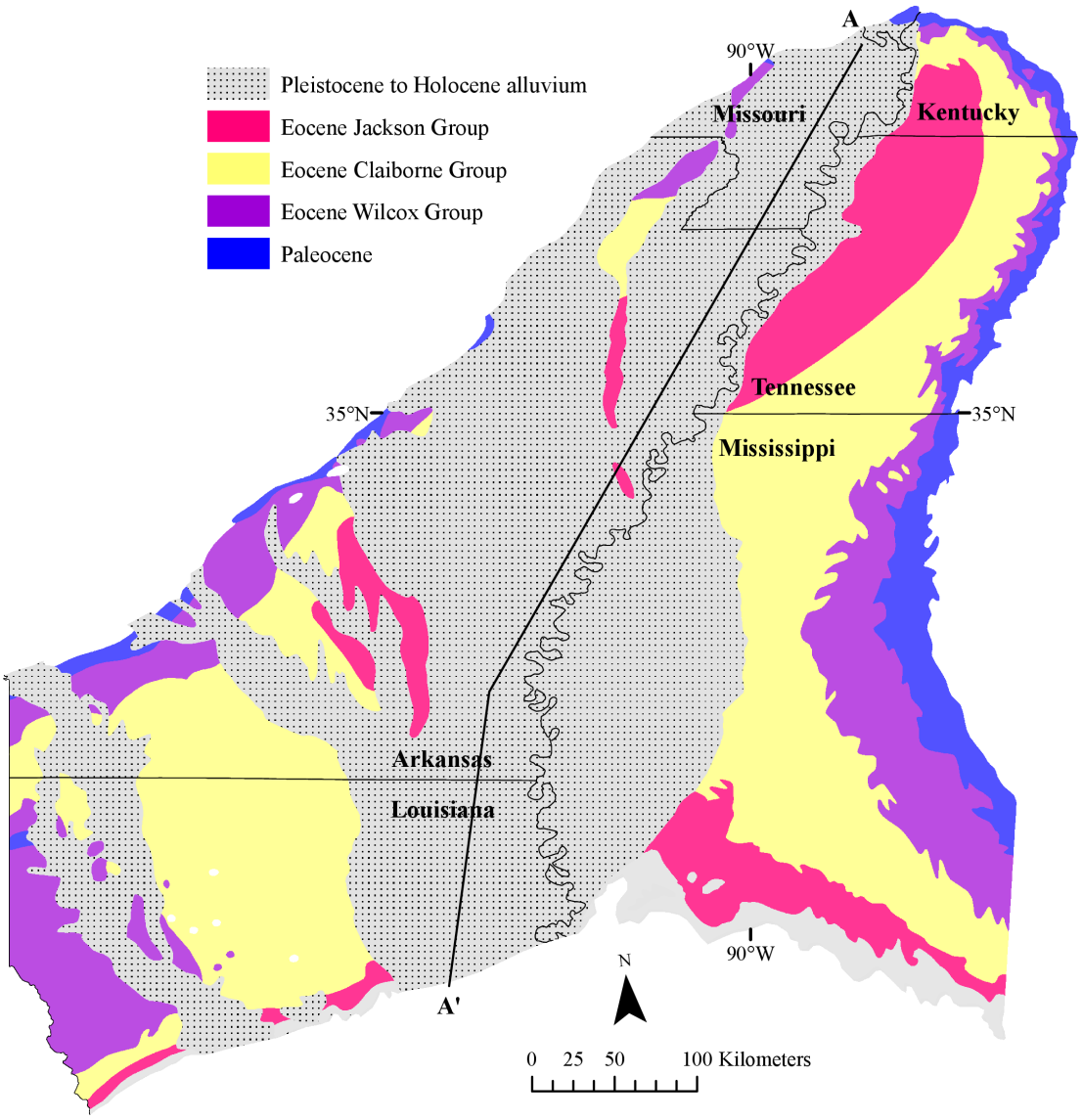

Figure 2.1: Surface exposure of Paleocene to Holocene sediments in the Gulf Coast region (modified from Williamson and Grubb, 2001).

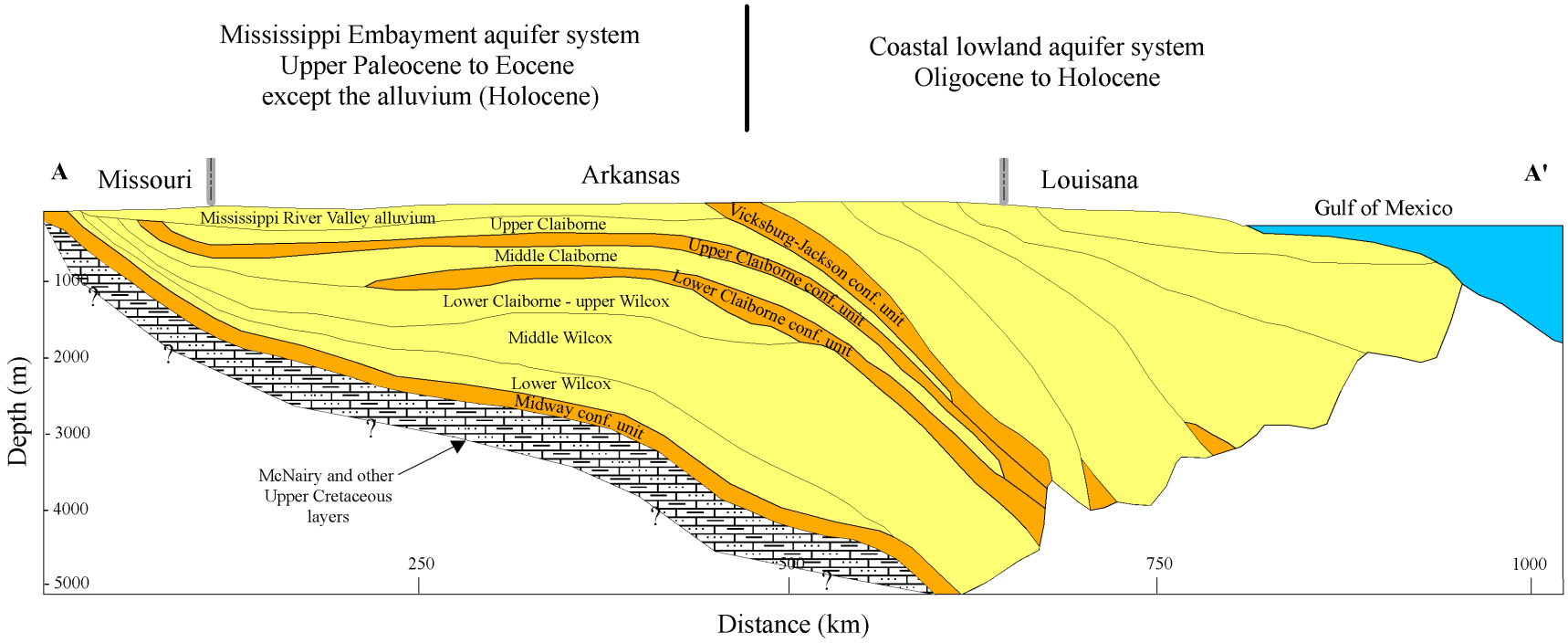

Figure 2.2: A north-south schematic cross-section of the Gulf Coast aquifer system (modified from Williamson and Grubb, 2001).

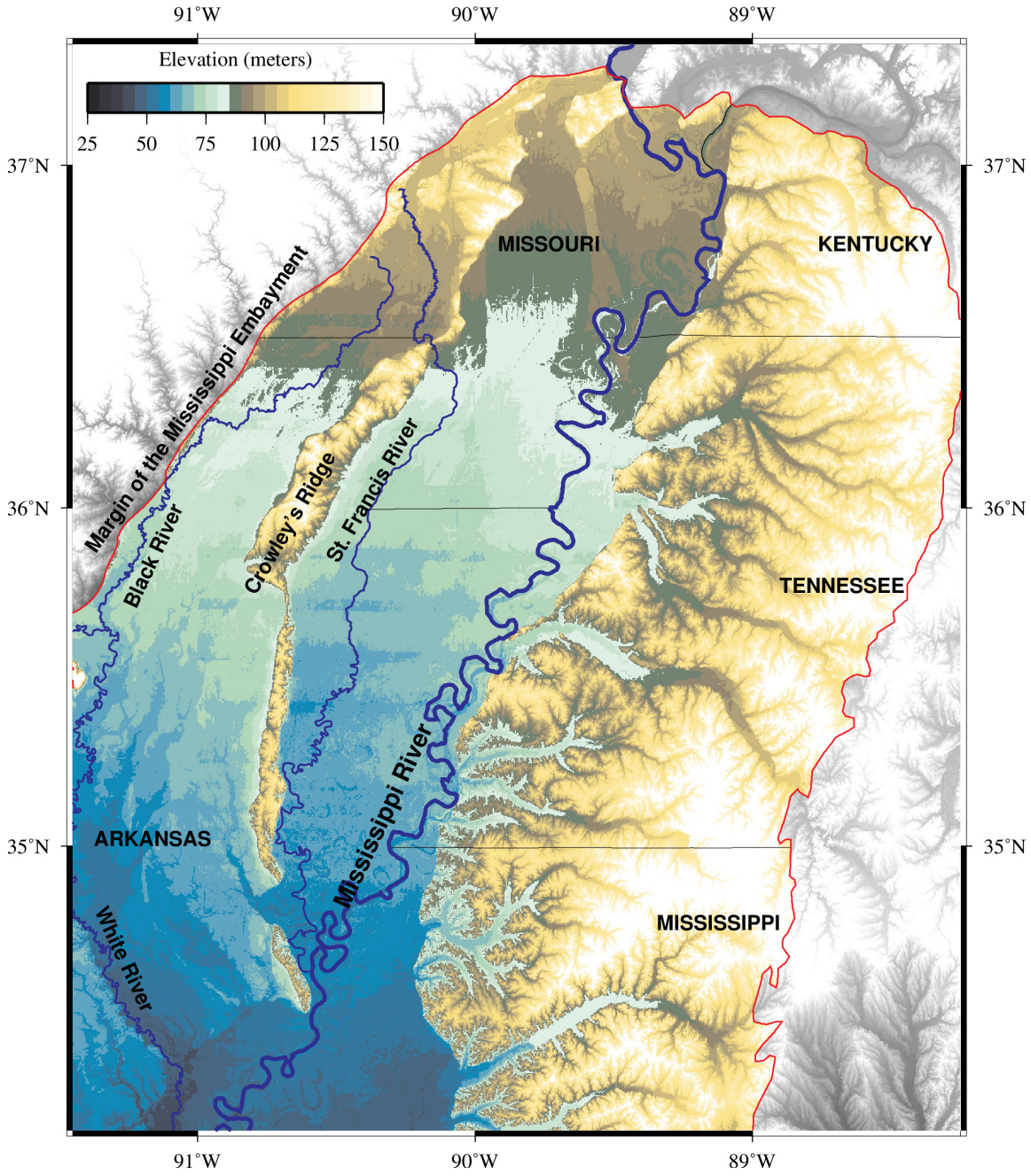

Figure 2.3: Location map and topographic features of the study area (digital elevation model from http://seamless.usgs.gov).

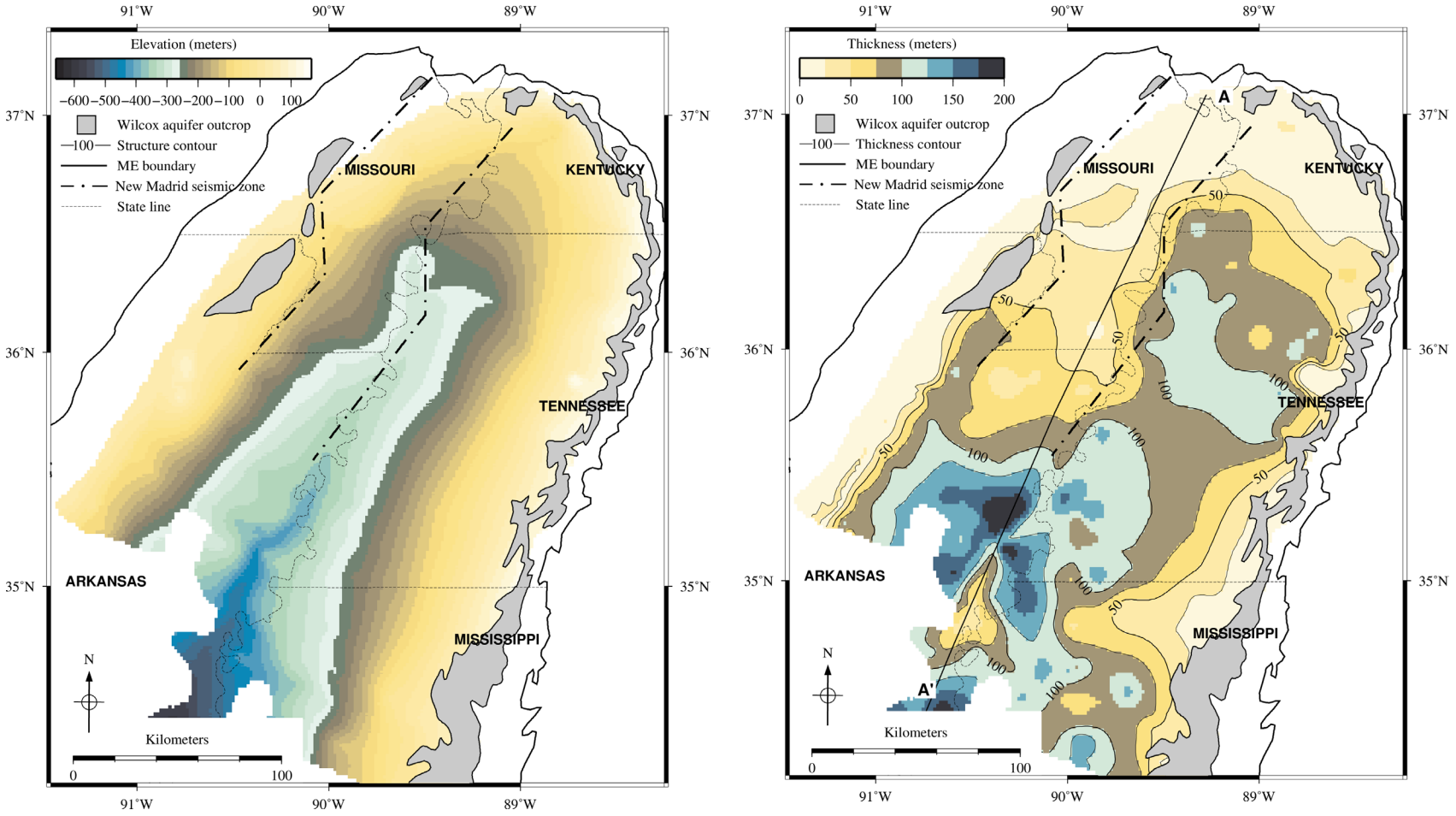

Figure 2.4: Structural (a) and thickness (b) contour maps of the Wilcox aquifer (modified from Hart et al., 2008). Line A-A' represents cross-section shown in Figure 3.2.

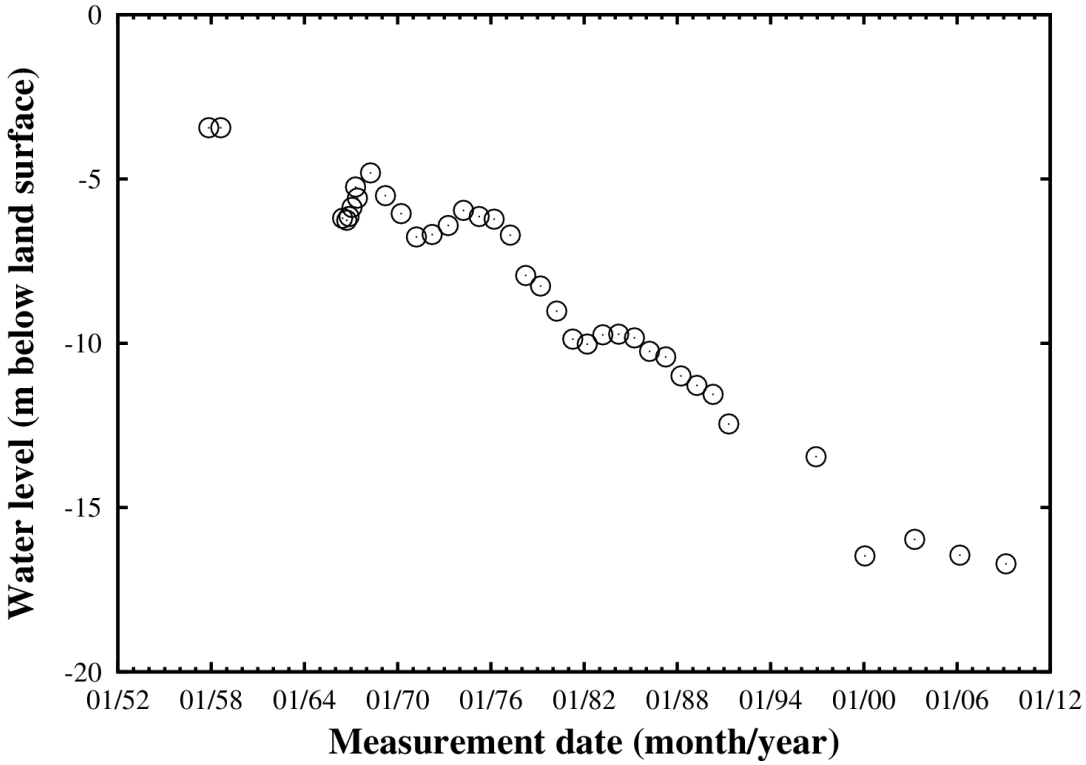

Figure 2.5: Historical water-level measurements from well that taps from the lower Wilcox aquifer located at Earle, AR (well # 17 in this study). Data from National Water Information System (http://waterdata.usgs.gov/nwis).

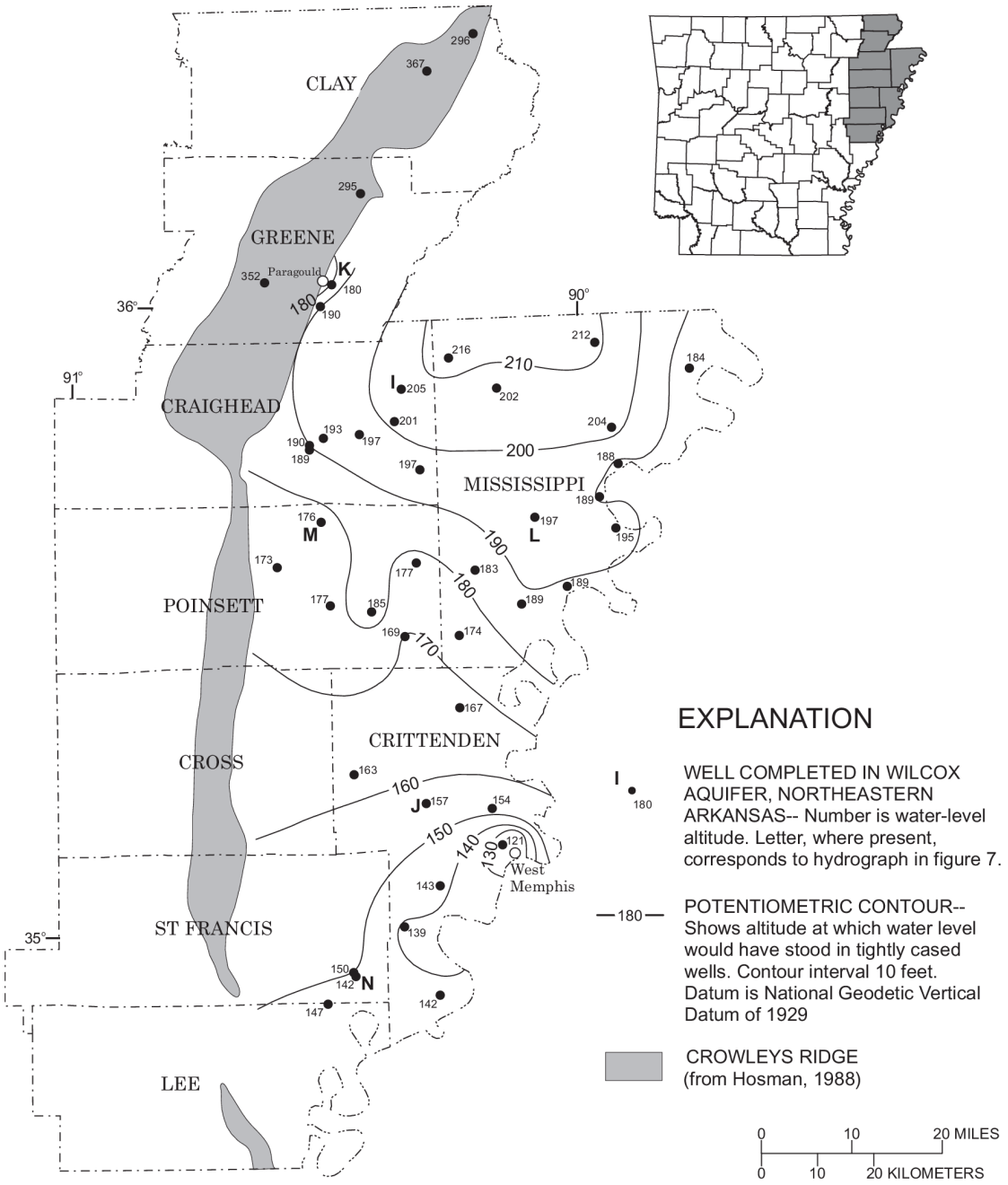
CLAY
GREENE
CRAIGHEAD
POINSETT
CROSS
ST FRANCIS
LEE
CRITTENDEN
MISSISSIPPI
Paragould
West Memphis
36°
35°
91°
90°
296
367
295
352
180
190
216
210
212
184
205
202
201
204
193
197
190
189
200
188
176
M
197
L
195
173
177
183
189
185
169
174
170
167
163
160
J
157
154
150
140
130
121
143
139
150
142
N
147
142
EXPLANATION
I
180
WELL COMPLETED IN WILCOX AQUIFER, NORTHEASTERN ARKANSAS-- Number is water-level altitude. Letter, where present, corresponds to hydrograph in figure 7.
180
POTENTIOMETRIC CONTOUR-- Shows altitude at which water level would have stood in tightly cased wells. Contour interval 10 feet. Datum is National Geodetic Vertical Datum of 1929
CROWLEYS RIDGE (from Hosman, 1988)
0 10 20 MILES
0 10 20 KILOMETERS

Figure 2.6 (a)

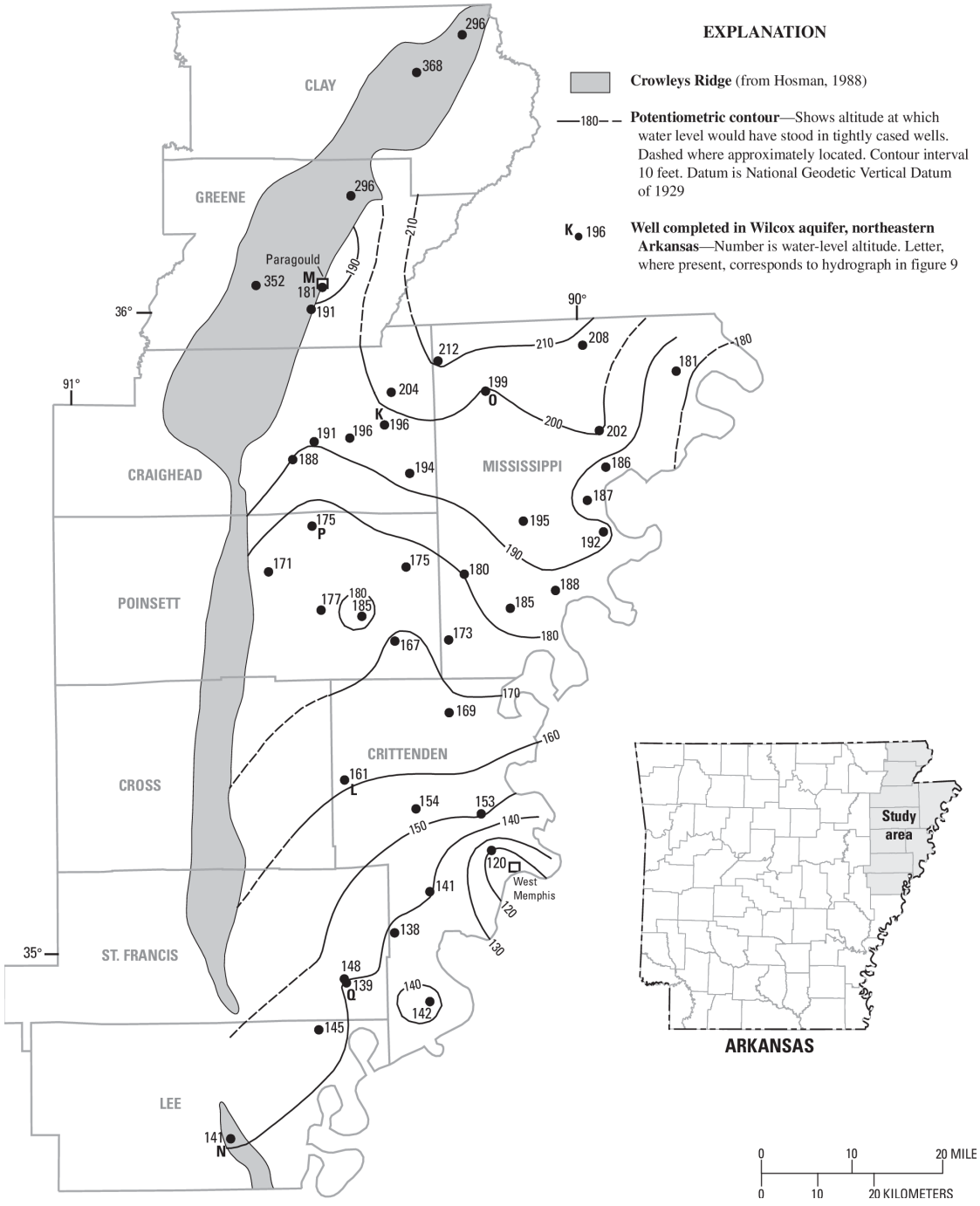
EXPLANATION
Crowleys Ridge (from Hosman, 1988)
180
Potentiometric contour—Shows altitude at which water level would have stood in tightly cased wells. Dashed where approximately located. Contour interval 10 feet. Datum is National Geodetic Vertical Datum of 1929
K 196
Well completed in Wilcox aquifer, northeastern Arkansas—Number is water-level altitude. Letter, where present, corresponds to hydrograph in figure 9
CLAY
GREENE
CRAIGHEAD
POINSETT
CROSS
ST. FRANCIS
LEE
MISSISSIPPI
CRITTENDEN
Paragould
West Memphis
36°
35°
91°
90°
Study area
ARKANSAS
0 10 20 MILE
0 10 20 KILOMETERS

Figure 2.6 (b)

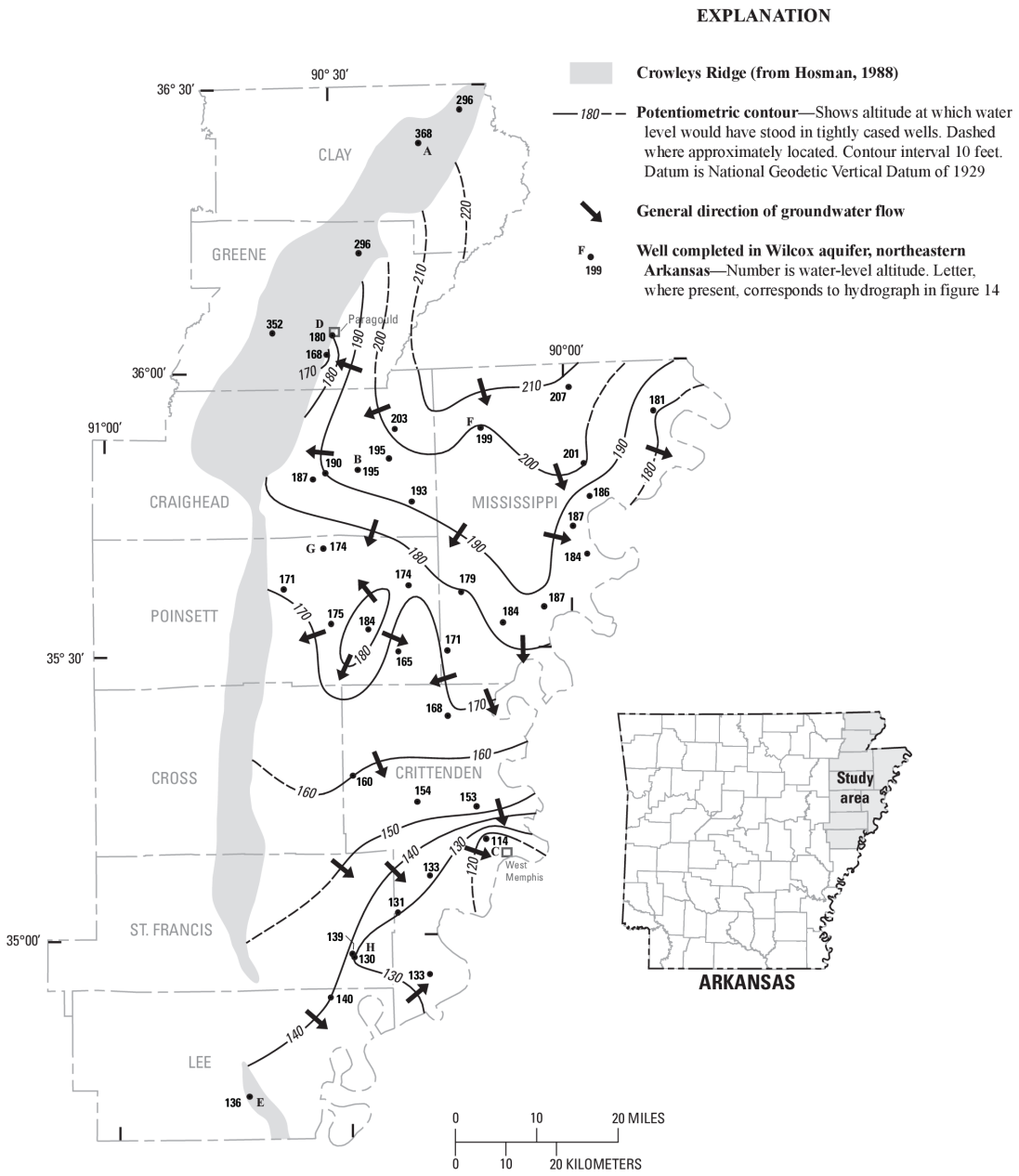

Figure 2.6 (c)

Figure 2.6: Change of potentiometric surface of the Wilcox aquifer in northeastern Arkansas for the years of (a) 2003 (Yeatts, 2004), (b) 2006 (Schrader, 2007), and (c) 2009 (Pugh, 2010). Note that contour intervals are given in feet.

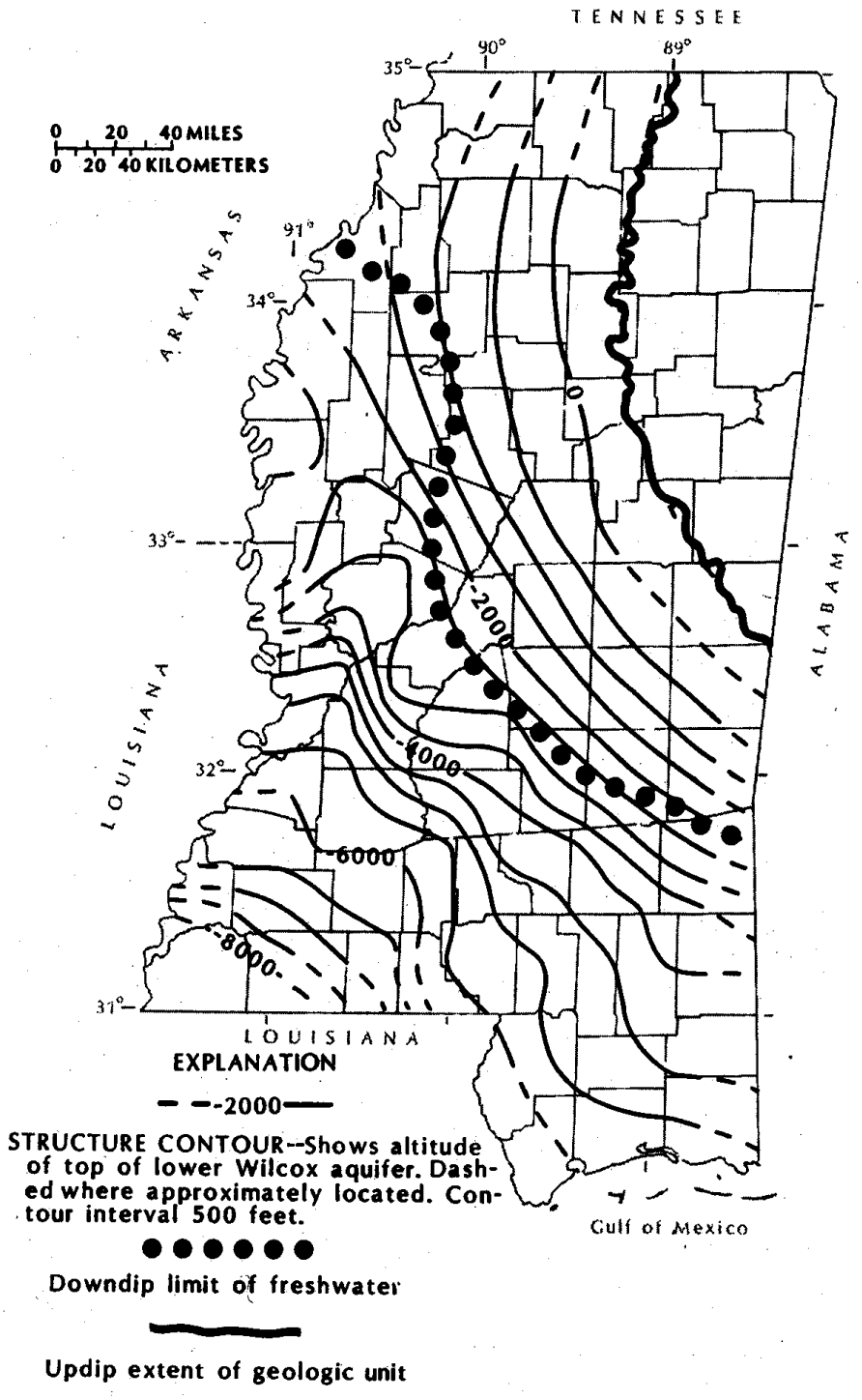

Figure 2.7: Map showing high TDS boundary and top to lower Wilcox aquifer south of the study area in the state of Mississippi. Compare the fresh water boundary (dotted line) with the boundary of the lower Wilcox in Figure 3.1 (reproduced from Arthur and Taylor, 1986).

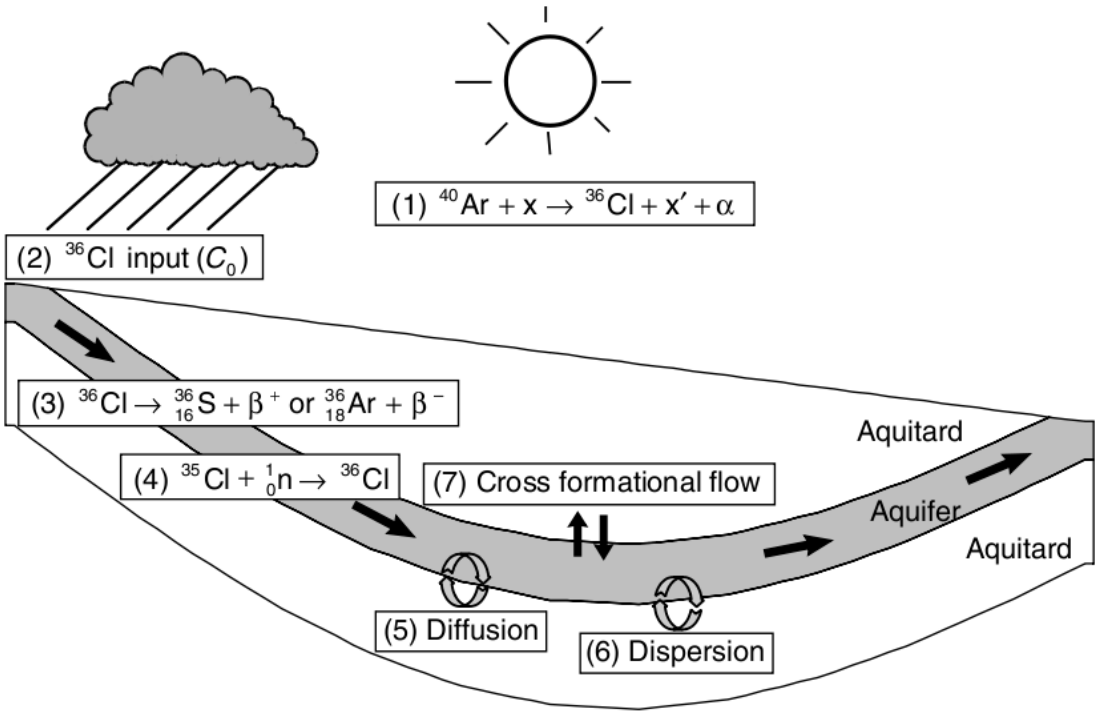

Figure 2.8: Sources of ^{36}Cl from the atmosphere and its interactions in the subsurface as transported by groundwater (Park et al., 2002).

Chapter 3 Methods

3.1 Field and laboratory methods

Samples were collected during May to July in 2006 and 2007 (Table A.1). A total of 21 groundwater samples were collected from the Wilcox aquifer (the lower Wilcox except near the updip and downdip limits). Six samples from the overlying Claiborne aquifer and one sample from the McNairy were collected for comparison purposes (Figure 3.1). For visualization purpose, the approximate positions of the wells were projected to a cross-section reconstructed from data by Hart et al. (2008) (Figure 3.2). Background information on respective well-completion depths was obtained from the National Water Information System (NWIS) database. Wells were selected based on their locations along the inferred regional flow path in the lower Wilcox aquifer. Yeatts (2004) and Schrader (2007) collected hydraulic head data only from northeastern Arkansas. Because this study includes the Wilcox aquifer in southeastern Missouri, additional data from the NWIS for Missouri (collected near the same time) in conjunction with data collected by Schrader (2007) were used to create an interpolated potentiometric surface map using surface spline methods (Figure 3.3). Fifty-six wells were used for the interpolation. Because some wells within short distances exhibited large differences in hydraulic heads, representative wells within a 2.5-km radial distance were selected to avoid data clustering and variability due to heavy pumping. With slight variations, the generated potentiometric surface map is similar to those of Yeatts (2004) and Schrader (2007) for northeastern Arkansas.

Eh, pH, alkalinity, temperature, and electrical conductivity (EC) were measured on-site following the methods described by Wood (1981). Prior to sample collection, pH, Eh, temperature, and EC were monitored until measurements stabilized. An in-line flow cell fitted with a pH electrode, platinum redox electrode and temperature probe was used to minimize outgassing of samples and contact with the atmosphere. The pH electrode was calibrated using standard pH 4, 7 and 10 buffer solutions and the redox electrode was referenced to ZoBell's solution (ZoBell, 1946). Groundwater samples were filtered with high-capacity, in-line, disposable 0.45-µm capsule filters. Following Mukherjee and Fryar (2008), redox-sensitive parameters were measured by CHEMets (Chemetrics, Calverton,

VA, USA) medium-to-low range field kits: NO_3^- – N (Cd reduction/azo dye formation method [APHA, 1995a]), NO_2^- – N (azo dye formation method [APHA, 1995b]), NH_4^+ – N (nesslerization method [APHA, 1992]), Fe^{2+} (1,10-phenanthroline method [Tetlow and Wilson, 1964]), and HS^- (methylene blue method [EPA, 1979; APHA, 1995c]). Sulfide was also qualitatively determined by odor and taste. Dissolved oxygen (O_2) samples were collected in 300-mL biological oxygen demand (BOD) bottles and were measured within 8 hours using titration according to the Winkler method (Hach, Loveland, CO, USA). Samples for cations (except NH_4^+) were collected in 125-mL white high-density polyethylene (HDPE) bottles and were acidified in the field with 1.5 mL 6N HNO_3 to pH < 3. Samples for analysis of N species (NH_4^+, NO_3^- and NO_2^-) and other anions were collected in separate 125-mL white HDPE bottles. Nitrogen species were preserved by adding 1.5 mL $CHCl_3$ in the field (Böttcher et al., 1990). Dissolved organic carbon (DOC) samples were collected in 40-mL amber glass vials with solid caps to which 1.5 mL of 50% H_2SO_4 were added to out-gas dissolved inorganic carbon (DIC). Methane (CH_4) samples were collected in separate 40-mL amber glass vials with septa with no headspace. Samples for alkalinity were collected in BOD bottles without headspace and analyzed within 24 hours by a digital titrator (Hach kit) and magnetic stirrer by titrating a 100-mL sample with 1.6 N H_2SO_4 to pH < 4.5 (Wood, 1981). The titration data were used to calculate inflection points of HCO_3^- and CO_3^{2-} concentrations using the U.S. Geological Survey (USGS) alkalinity calculator (http://or.water.usgs.gov/alk/). Samples for analysis of ^{13}C of DIC were collected in solid-capped 40-mL amber glass vials poisoned in the field with five drops of $HgCl_2$.

Solute concentrations were analyzed in the laboratories of the University of Kentucky (UK). Analysis of cations and anions were done at the Environmental Research and Teaching Laboratory at UK (ERTL). Major cations and some trace metals were measured by multi-element scans using an inductively coupled plasma-optical emission spectrometer (VarianVista Pro ICP-OES). Accuracy of analysis was assessed with blanks, laboratory-controlled standards, and spiked samples. Precision was determined by duplicate and triplicate analysis. The precision of analysis was generally better than 5%. Anions (preserved and unpreserved) were measured using an ion chromatograph (IC) (Dionex ICS-2000) with AS18 column (at ERTL). N-species were measured using an

auto-analyzer (Bran-Luebbe AAIII) in the UK Department of Forestry. The error was generally <6% for the IC and <3% for the auto-analyzer. The CH_4 samples were analyzed using a gas chromatograph with flame ionization detector in the UK Department of Plant and Soil Sciences (Shimadzu GC-14A with Chromatopac C-R5A). DOC was measured using a Phoenix 8000 UV-Persulfate TOC analyzer at the Kentucky Geological Survey.

Stable-isotope ratios of $^{18}O/^{16}O$ and $^{2}H/^{1}H$ were measured for groundwater samples. Rainwater samples collected between January 1997 and January 1998 from two sites approximately 6 kilometers apart in McCracken County, Kentucky (the U.S. Department of Energy Paducah Gaseous Diffusion Plant [PGDP] and Tennessee Valley Authority [TVA] Shawnee Fossil Plant) were also analyzed. Approximate location of the sites is shown in Figure 3.1. Rainwater samples were collected in polypropylene separatory funnels containing silicone oil to inhibit fractionation due to evaporation (Warren W. Wood, U.S. Geological Survey, personal communication to A.E. Fryar, 1992; Scholl, 2006), and were stored in glass bottles in a refrigerator prior to analysis. Results were compared with previously reported ^{18}O data for the same samples analyzed in 1998 at the University of Georgia. The $^{18}O/^{16}O$ and $^{2}H/^{1}H$ ratios were measured at the Isotope Geochemistry Laboratory at the University of Arizona in July 2007 using a continuous-flow isotope-ratio mass spectrometer (IRMS) (ThermoQuest Finnigan DeltaPlusXL). Results are reported as δ values relative to the VSMOW (Vienna Standard Mean Ocean Water) standard, where

$$\delta^{18}O(‰) = \left[\frac{{}^{18}O_{sa}/{}_{16}O_{sa}}{{}^{18}O_{std.}/{}_{16}O_{std.}} - 1 \right] \times 1000$$

and sa and std. refer to the sample and standard, respectively. The analytical precisions (1σ) for $\delta^{18}O$ and $\delta^{2}H$ were ± 0.08‰ and ± 0.9‰, respectively.

Stable isotope (^{13}C and ^{34}S) analyses were performed at the Isotope Geochemistry Laboratory at the University of Arizona using a continuous-flow isotope-ratio mass spectrometer (IRMS) (ThermoQuest Finnigan DeltaPlusXL). Sulfur-34 was isolated using the anion exchange method of Carmody et al. (1998). Direct precipitation of $BaSO_4$

was not possible for several of the samples because the SO_4^{2-} content in samples is mostly < 10 mg/L. The analytical precisions (1σ) for $\delta^{13}C$ and $\delta^{34}S$ were ±0.25‰ VCDT and ±0.15‰ VPDB, respectively, where VCDT refers to the Vienna Cañon Diablo Troilite standard and VPDB refers to the Vienna Pee Dee Belemnite standard.

A total of 10 groundwater samples were collected for ^{36}Cl analysis in 20-liter polyethylene carboys, but only four of the samples were extracted successfully. Chloride was concentrated in the laboratory using ion exchange media. Samples were prepared using a chromatographic column, 10 mm internal diameter and 75 cm length, packed with AG 1-X8 analytical-grade anion-exchange resin (Bio-Rad, Hercules, CA). Prior to usage, the resin was conditioned with 1.5 M HNO_3 in order to remove any residual chloride. Because the Cl^- concentration of samples was very small (< 5 mg/L), on average 20 liters of each sample were eluted by gravity through the column to concentrate a sufficient mass of Cl^-. A 1% HNO_3 solution was used to extract the concentrated Cl^- from the resin, and $AgNO_3$ was added in excess to the extract to precipitate AgCl. ^{36}Cl was analyzed using an accelerator mass spectrometer (AMS) in the Purdue Rare Isotope Measurement Laboratory (PRIME Lab) at Purdue University.

3.2 Geochemical modeling

To determine the speciation, saturation indices, and mole transfers for the inverse models, PHREEQC version 2.12 (Parkhurst and Appelo, 1999) was used. Saturation indices, SI=log(IAP/K), where IAP is the ion activity product and K is the equilibrium solubility constant of a phase at ambient temperature, were calculated for groundwater with thermodynamic values of phases from the PHREEQC database. An SI value greater than zero (supersaturation) indicates precipitation of phases is thermodynamically favorable, while SI < 0 (undersaturation) suggests dissolution (Drever, 1997). The equilibrium redox potential was determined using field-measured Eh values, which are close to values calculated by using Fe^{3+}/Fe^{2+} or SO_4^{2-}/H_2S redox couples. There were discrepancies because Fe^{3+} and H_2S were not detected in all of the samples, but they were solved by adding a very small amount of these components (about 10 ng/L) to the solution.

Assuming the chemical compositions of groundwater between two points along a

flow path represent initial and final end members, inverse chemical models can calculate the theoretical resultant mole-transfer amounts between those points by various chemical reactions (Parkhurst et al., 1996). The calculations also account for mixing proportions of initial water with water from underlying or overlying units. Reaction-path models were calculated using PHREEQC (and tested again with NETPATH [Plummer et al., 1994] with ^{13}C constraint) for pairs of wells located approximately along the regional groundwater flow path. The model setup procedure involves defining (1) the aqueous species affected by reactions and/or mixing, (2) initial and final compositions along the flow path, and (3) the mass transfers that are expected to occur out of a set of reactions formulated. The mass-balance models were tested for reactions with and without mixing.

The selected primary aqueous species are major ions (Ca^{2+}, Mg^{2+}, Na^{+}, K^{+}, HCO_3^{-}, and Cl^{-}). Mole-transfer amounts of exchangeable cations as CaX_2, MgX_2, NaX, and KX (where X is an anion), carbonates (calcite, dolomite, and siderite), organic carbon as CH_2O, amorphous $Fe(OH)_3$, and pyrite were evaluated. Some possible constraints (e.g., Mn and Sr) were not included in the mass-balance calculations because of lack of information about the solid phases in which they reside. Clay-mineral phases were not included because Al is near or below detection limit in all samples (i.e., Al is assumed to be conserved in the solid phase [Tardy, 1971]). Halite and gypsum (or anhydrite) were used as proxies for cross-formational mixing. Table 3.1 summarizes model boundary conditions. Inaccuracies in the choices of end-member waters and in analytical data are handled by PHREEQC by including user-defined uncertainty values for the initial and final solutions. Uncertainty values equivalent to the mass-balance errors of individual wells were satisfactory to calculate minimal numbers of models. Possible reaction paths between points are indicated by the arrows in Figure 3.3.

Mineral phases used in geochemical modeling were selected in part based on analysis of drill cuttings from the Wilcox Group. Grain-mounted polished thin-sections were prepared for transmitted- and reflected-light microscopy. Cuttings from three wells were taken from the Arkansas Geological Survey core library. The locations of the wells are indicated in Figure 3.1. The wells were selected based on their lateral and depth proximity to sampled wells. Wells 2392 and 2393 are very close to sample 12 (Keiser) and sample 9 (Dogwood). Sampling depths for well numbers 2392 and 2393 were 1010

to 1340 ft (~ 307.8 to 408.4 m) and 1180 to 1300 ft (~ 359.7 to 396.2 m), respectively, at 30-ft (~ 9.1-m) intervals. For well 137, sampling depth was 1360 to 1670 ft (~ 414.5 to 509.0 m) at 10-ft (~ 3.0-m) intervals. Drill cuttings from well 137 were mainly composed of clay and were aggregated to 30-ft (~ 9.1-m) intervals.

3.3 Groundwater flow modeling

The two-dimensional basin hydrology modeling program, BASIN2 (Bethke et al., 2002), was used to simulate regional groundwater flow and residence time by tracking the transport and decay of ^{36}Cl through the Wilcox aquifer. BASIN2 uses a finite-difference grid consisting of nodal blocks arranged into columns and rows of a cross-section along the regional groundwater flow path. The cross-section was constructed to represent the hydrostratigraphy of the MEAS sediments in the study area. The regional groundwater flow path was inferred based on potentiometric surface maps created by Yeatts (2004) and Schrader (2007) (Figure 2.6). It roughly coincides with the north-south cross-section shown in Figure 3.2. A no-flow boundary to the east is defined by the axis of the basin, which roughly coincides with the modern-day Mississippi River. The outcrop area to the north and west (Crowley's Ridge) is the recharge area.

A steady-state flow condition with open left (north) and right (south), closed bottom, and open upper boundaries was assumed for the model. Thickness and composition (sand-to-clay proportion) of seven different hydrostratigraphic units (i.e., Midway confining unit, lower Wilcox aquifer, middle Wilcox confining unit, lower to middle Claiborne aquifer, middle Claiborne confining unit, upper Claiborne aquifer, and the Mississippi River alluvial aquifer) were synthesized from stratigraphic data compiled by Hart et al. (2008) (Figure 3.2). Variable thicknesses of individual layers were permitted, maintaining a 20-m vertical grid interval, except for the lowermost confining unit, for which the thickness was assumed to be uniformly 50 meters. Actual thicknesses and depths to the tops of all hydrostratigraphic units were reproduced at 40 points along the inferred flow path at an interval of 9 km. Data for depths of units were taken from Hart et al. (2008) based upon interpolation of 2800 geophysical well logs. The total distance of the cross section is 370 km. Horizontal and vertical model grid spacings are 2 km and 20 m, respectively, in a curvilinear coordinate system that follows the basin stratigraphy

(Figure 3.4).

The most significant parameters that affect the flow and transport model are porosity and permeability. The details of the equations for calculating porosity development as a function of effective stress (hydrostatic and burial) are given by Bethke et al. (2002). The permeability of each hydrostratigraphic unit, which is dependent on the size, shape, and packing of grains, was assigned based on sand proportion given by Williamson and Grubb (2001) (Table 2.2). The lower and middle Claiborne aquifers have been lumped together because they exist as undifferentiated units. The permeability calculation is based on the linear relation between porosity and the logarithm of permeability observed for clastic material given as:

$$\text{Log}(k) = A\,\phi + B \tag{3.1}$$

where k is the intrinsic permeability (cm^2), ϕ is the porosity, and A and B are empirical constants (Bethke et al., 2002). A represents the change of permeability with respect to porosity, which is a function of depth, and B is the minimum log-transformed permeability that can be assigned to the aquifer or aquitard. For example, because the permeability of sand decreases sharply with decreased porosity, whereas the porosity of clay does not change significantly with depth, A is assigned a higher value for sandy layers than for clayey layers. The resulting permeability values of the porous media (in this case sand and clay) within a hydrostratigraphic unit are then averaged for each nodal block using arithmetic, geometric, and/or harmonic methods at various depths. The drawback to this approach is that, depending on the sand-to-clay ratio of the aquifer, multiple non-representative permeability values can be calculated.

Alternatively, permeability values can be derived from hydraulic conductivity (K) values for individual hydrostratigraphic units. Clark and Hart (2009), Pugh (2008), and Prudic (1991) reported K values for the individual layers in the MEAS based on field measurements and hydraulic-head-calibrated models (Table 3.2). Hydraulic conductivity depends on properties of the fluid as well as of the porous medium. BASIN2 uses the intrinsic permeability coefficient (k) as input, which is a property of the porous medium alone (independent of the fluid properties),

$$K = C\,d^2 \tag{3.2}$$

where C is the grain shape factor and d is the mean pore diameter (Fetter, 2001). The relationship between K and k is given as:

$$K=k\left(\frac{\gamma}{\mu}\right)=k\left(\frac{\rho g}{\mu}\right) \tag{3.3}$$

where γ is the specific unit weight of the fluid (N/m^2), ρ is the fluid density (g/cm^3), g the acceleration due to gravity (9.81 m/s) and μ the dynamic viscosity ($g\ cm^{-1}\ s^{-1}$) of the fluid (Fetter, 2001). For water, viscosity and density are functions of pressure and temperature. At 20 °C and 1 atm pressure, the density and dynamic viscosity of water are 998.2 kg/m^3 and 1.002×10^{-6} $kg\ m^{-1}\ s^{-1}$, respectively. Under these conditions the intrinsic permeability can be calculated from the hydraulic conductivity as:

$$k = 1.023 \times 10^{-7}\ K \tag{3.4}$$

(Fetter, 2001). Table 3.2 shows that reported permeability values based on hydraulic conductivity vary by up to a factor of four among different studies. Values were used in sensitivity analysis to estimate upper and lower limits for permeability values derived from sand-to-clay proportions.

BASIN2 simulations were calibrated against hydraulic-head data collected by Schrader (2007) and measured groundwater temperature data from the lower Wilcox aquifer. Calibration against hydraulic-head data is based on numerical solutions of gravity-driven flow, summarized as follows from Bethke et al. (2002). Assuming the model has attained a steady state, Darcy's law and mass conservation define the flow field in terms of the following partial differential equation:

$$\frac{\partial}{\partial x}\left[\frac{k_x}{\mu}\frac{\partial \Phi}{\partial x}\right]+\frac{\partial}{\partial z}\left[\frac{k_z}{\mu}\frac{\partial \Phi}{\partial z}\right]=0 \tag{3.5}$$

where k_x and k_z are permeability (m^2) in lateral and vertical directions, μ is fluid viscosity, and Φ is the hydraulic potential. The hydraulic potential is defined by Hubbert (1940) as the mechanical energy of a unit volume of groundwater:

$$\Phi = P - \rho\, gz \tag{3.6}$$

where P is the pressure, z is the elevation head, and ρ and g are as defined previously. BASIN2 assumes elevation above sea level as negative, hence the negative sign in

equation 3.6. By combining equations 3.5 and 3.6, the continuity equation is obtained as follows:

$$\frac{\partial}{\partial x}\left[\frac{k_x}{\mu}\frac{\partial P}{\partial x}\right]+\frac{\partial}{\partial z}\left[\frac{k_z}{\mu}\left(\frac{\partial \Phi}{\partial z}-\rho g\right)\right]=0 \tag{3.7}$$

The above equations are solved using finite-difference methods. BASIN2 calculates heat transfer based on the thermal conductivity (which is a function of porosity) and groundwater advection. Heat flow can be set for the top and bottom layers until temperatures match measured values (Bethke et al., 2002). The program allows specification of constant surface temperature in degrees Celsius for the top layer and heat flow rate from below the bottom layer in heat flow units (HFU). Surface temperature and heat flow rate from underneath were set to 15°C and 0.7 HFU, respectively. Near surface groundwater temperature is 1 to 2°C higher than mean annual air temperature (Heath, 1983). Therefore the surface temperature was set to 15°C based upon reported mean annual air temperature of 14°C to 16°C by Williamson and Grubb (2001) in the study area.

Two critically sensitive variables, permeability and diffusion coefficient, affect ^{36}Cl transport along the flow path. The coefficient of hydrodynamic dispersion (D) for ^{36}Cl transport can be calculated as:

$$D_L = \alpha_L v_x + D^* \tag{3.8}$$

$$D_t = \alpha_t v_z + D^* \tag{3.9}$$

Here α is the dispersivity, L and T refer to coefficients along and transverse to the mean direction of groundwater flow, respectively, and v_x and v_z are the average linear groundwater velocity in lateral and vertical directions. The diffusion coefficient (D^*) becomes important in low-k confining units where v is very small (Bethke et al., 2002).

Table 3.1: Mineral phases, exchange species, and constraints used for the inverse modeling in the Wilcox aquifer.

Phases	calcite(+,-), dolomite(+), siderite(+,-), $FeOH_{3(a)}$(+), pyrite(-), CH_2O(+), halite(+)*, anhydrite(+)*
Exchange species	CaX_2, MgX_2, NaX, KX
Constraints	Na^+, K^+, Ca^{2+}, Mg^{2+}, Fe_T, SO_4^{2-}, Cl^-, HCO_3^-
^{13}C	Organic matter (-25‰)
	Calcite (0‰)

+, dissolution; -, precipitation; *, contribution by diffusion

Table 3.2: Table showing hydraulic conductivity (K) values reported by Prudic (1991), Pugh (2008), and Clark and Hart (2009). Permeability (k) calculated using equation 3.3. Abbreviations U, M, and L in aquifer names mean upper, middle, and lower, respectively.

Aquifer	Prudic (1991)			Pugh (2008)			Clark and Hart (2009)		
	K	k		K	k		K	k	
	$\times10^{-3}$ cm/s	$\times10^{-8}$ cm^2	log darcy	$\times10^{-3}$ cm/s	$\times10^{-8}$ cm^2	log darcy	$\times10^{-3}$ cm/s	$\times10^{-8}$ cm^2	log darcy
Alluvium	111	130	2.1	63	74	1.9	212	247	2.4
U Claiborne	28	32	1.5	3	3	0.5	9	11	1.0
M Claiborne	26	31	1.5	3	4	0.6	12	14	1.2
M Wilcox	6	7	0.8	1	1	0	1	1	0
L Wilcox	45	53	1.7	3	4	0.6	9	10	1.0

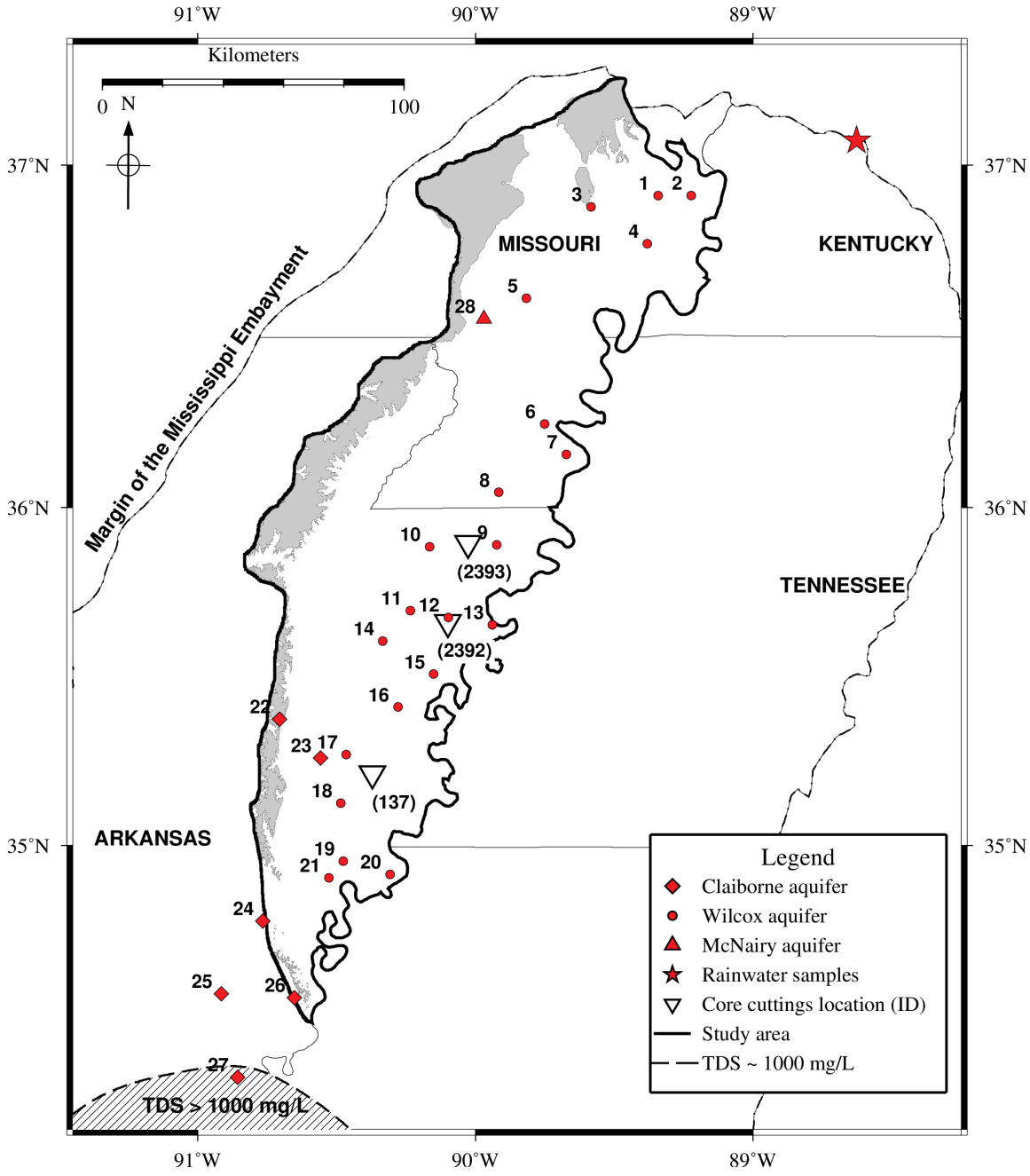

Figure 3.1: Map showing boundary of the study area, sample locations, and extent of fresh water in the lower Wilcox aquifer west of the Mississippi River. Hatched region indicates where groundwater TDS amount is ≳ 1000 mg/L.

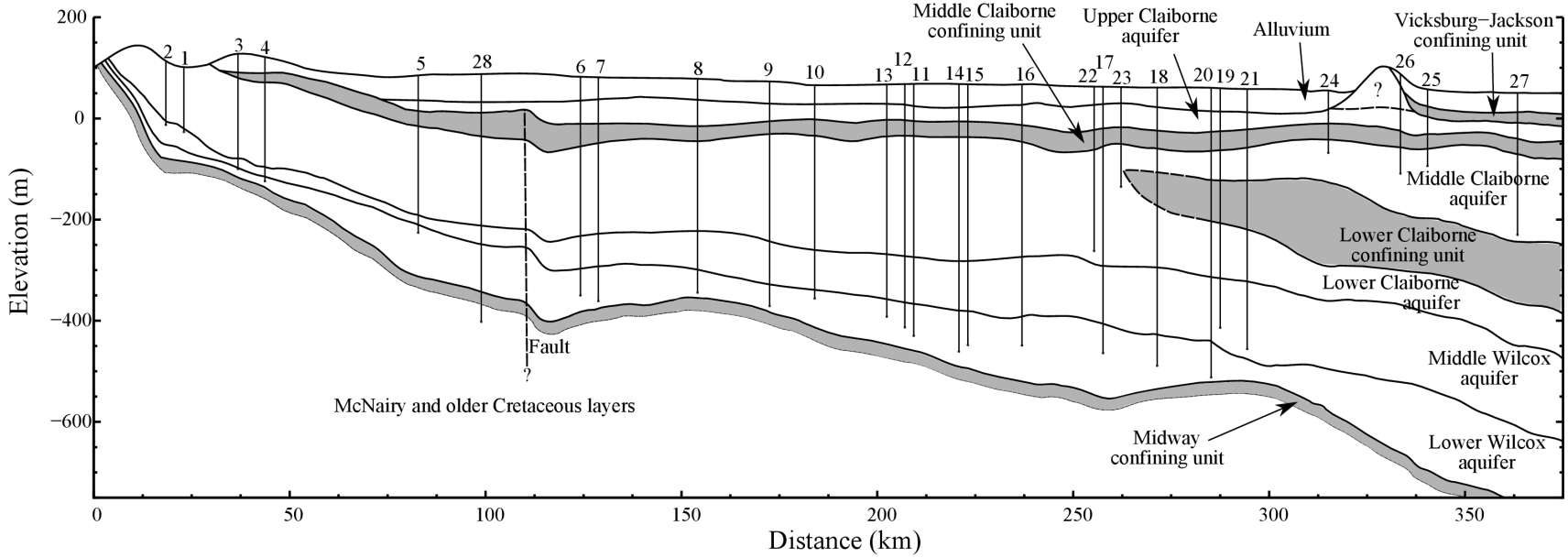

Figure 3.2: A north-south cross-section through the Mississippi Embayment aquifer system derived from individual aquifer structural contour maps (Hart et al., 2008). Sampled wells (Figure 3.1) are projected to the cross section for illustration purposes.

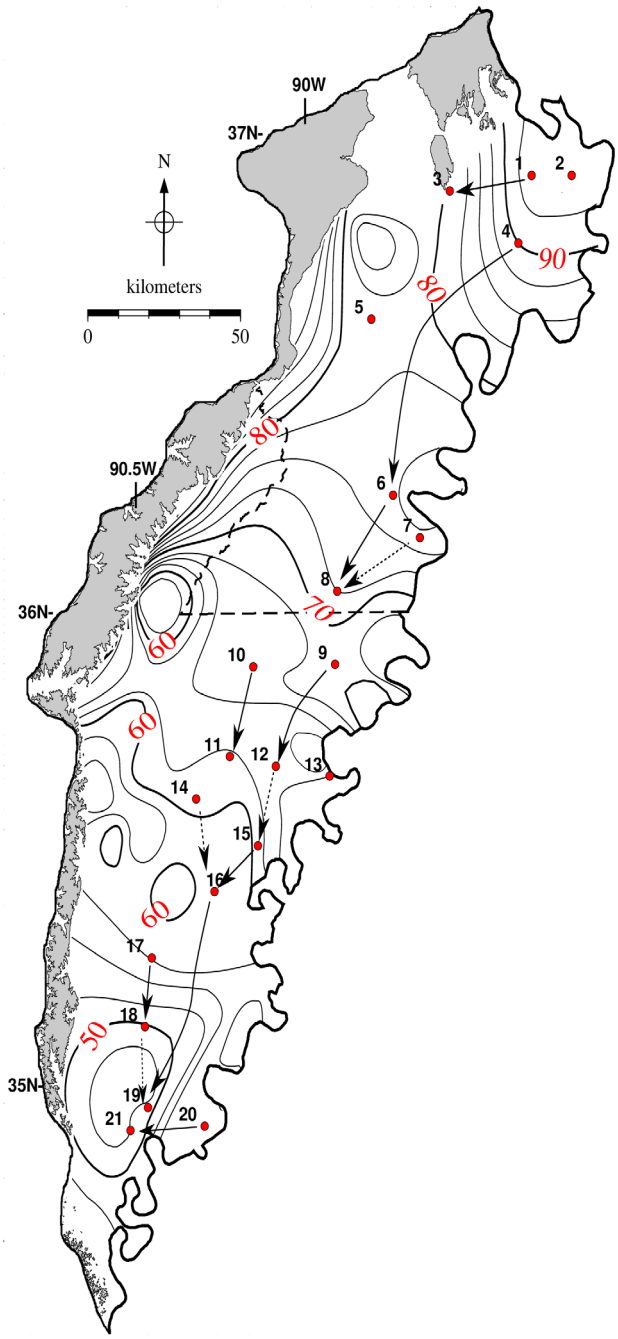

Figure 3.3: Potentiometric surface of the Wilcox aquifer generated by using spline interpolation. Contour interval is 2.5 meters and major contours at 10 meters interval are labeled with red. Solid circles represent sampled wells from the lower Wilcox aquifer, and arrows indicate initial and final end member water samples determined with inverse geochemical models.

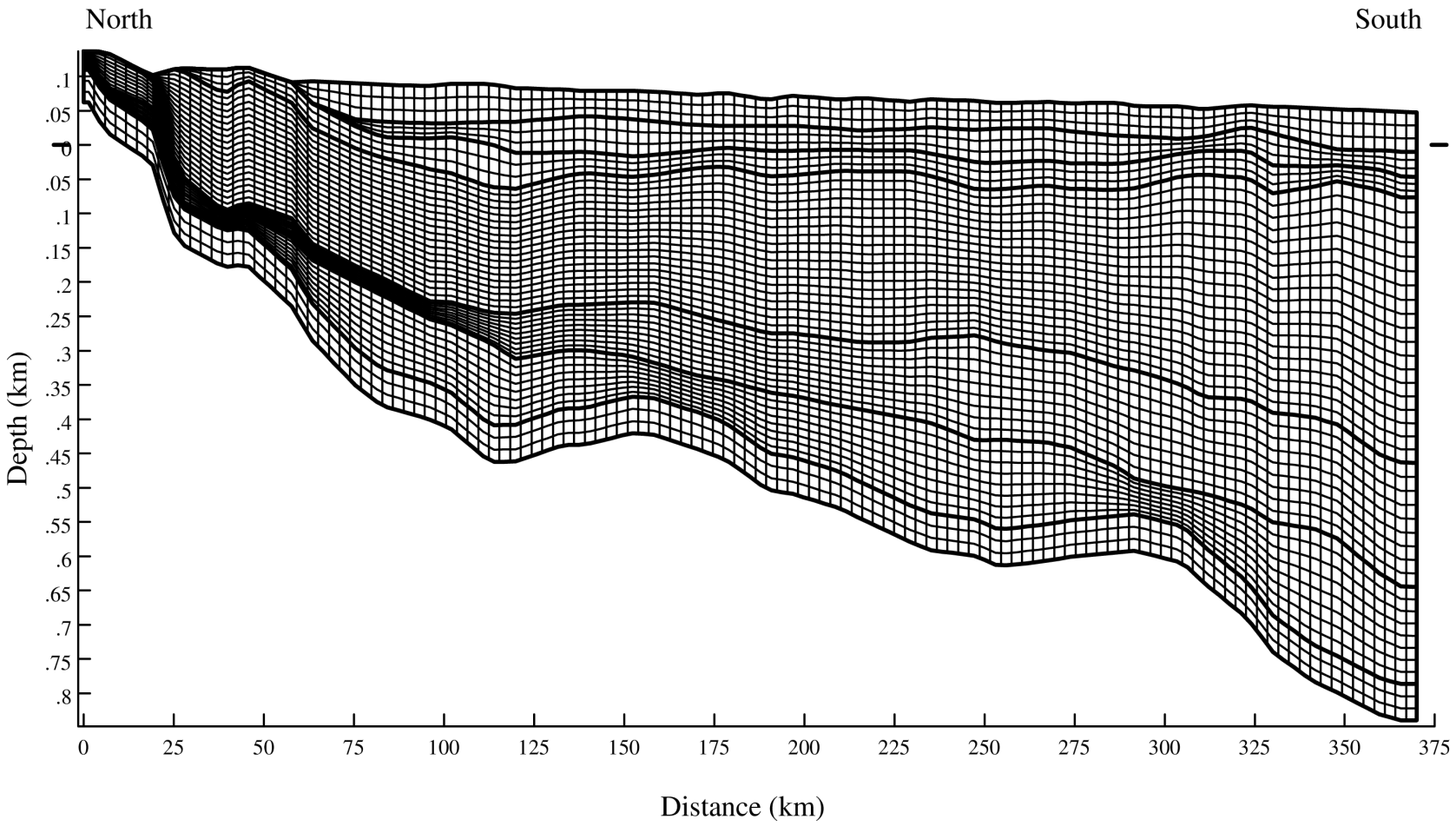

Figure 3.4: The finite difference mesh used for the 2-D transport model. Vertical and horizontal grid sizes are 20 m and 2 km, respectively.

Chapter 4 Results

4.1 Solute chemistry

Results from field observations and laboratory analyses for all groundwater samples are listed in Tables A.2 and A.3. Groundwater from the Wilcox aquifer has distinctively low solute concentrations as compared to water from the overlying Claiborne (samples 22 – 27) and underlying McNairy (sample 28) aquifers. Calcium is the dominant cation in the upgradient sections of the aquifer (ranges: 26.3 – 70.5 mg/L) and decreases along the flow path to 0.3 mg/L. Conversely, Na^+ increases progressively from 4.8 – 10.3 mg/L in the upgradient section to 67.2 mg/L in the downgradient section. Bicarbonate concentrations vary slightly throughout the entire section (102 – 137 mg/L), except for sample 2 from the upgradient section (Wyatt, MO) with 353.8 mg/L. Elevated amounts of Na^+ (186.1 – 313.8 mg/L) and Cl^- (83.3 – 311.2 mg/L) occur in the underlying (McNairy) and overlying (Claiborne) aquifers. The charge balance error for the Wilcox samples is ±10% except for samples 13 and 21, which showed excess cation contents (11 – 13% balance error).

The lower Wilcox shows distinctive hydrochemical facies variations along the regional flow path. Using the Piper plot (Figure 4.1), the groundwater chemistry can be characterized into Ca-(Mg)-HCO_3 type (samples 1 to 5 in the upgradient section) and Na-HCO_3 type (samples 6 to 21 from the downgradient section). Overlying and underlying aquifers do not show chemically distinctive water types. Instead, they have intermediate compositions between the above-mentioned hydrochemical facies. Nevertheless, proportional anion amounts show dominance from HCO_3^- to Cl^-, which can represent mixing between brackish and fresh-water end-members.

A convenient way to examine spatial variation of solutes and other parameters along a flow path is to use bivariate plots of solutes as a function of distance. The starting point for the flow path was selected as the northernmost well, which corresponds to the recharge area (Figure 3.2). Figure 4.2 shows concentrations of dissolved Ca^{2+}, Mg^{2+}, Na^+, and K^+ plotted as a function of distance along the flow path. Near the outcrop area (at distances between 0 and ~75 km along the flow path), Ca^{2+} and Mg^{2+} are the dominant cations. Downgradient, Na^+ concentrations increase markedly while Ca^{2+} and Mg^{2+} concentrations decrease. The concentration of K^+ does not show

any marked change, except samples 18, 20, and 21 have lower K^+ concentrations by a factor of five as compared to other samples.

The Eh of the groundwater samples ranges between -149 and 103 mV. The majority of the samples have Eh below -10 mV, but four samples are above zero (0 to 102 mV). Most samples have dissolved O_2 less than 1 mg/L. Based on the observed Eh range, dissolved O_2 was probably introduced by aeration during sampling (Parkhurst et al., 1996). Mukherjee and Fryar (2008) observed similarly low but detectable levels of O_2 in samples collected from public water-supply wells tapping a semi-confined, anoxic regional aquifer in the western Bengal basin of India. Sulfate gradually decreases and CH_4 gradually increases along the flow path (Figure 4.3). Ferrous iron peaks at a distance between 100 and 150 km from the recharge zone (Figure 4.3b); nitrate and nitrite are below detection limit in all samples. Field measurements of Fe(II) are higher than laboratory measured total Fe in all samples, except two samples (numbers 6 and 8) from the Wilcox aquifer and one sample (number 23) from the Claiborne aquifer. This could be due to precipitation of iron oxide in sample bottles (samples were acidified to pH < 3) or it could be a problem of accuracy of the CHEMets method. NH_4^+ was detected in all the samples, but based on the data, no relationship with position along the flow path is evident. The pH of the upgradient wells is circumneutral (6.5 – 7.5) and increases to 8.5 in downgradient wells.

Temperature measurements for wells in the upgradient section range from 17 to 19 °C (close to annual average air temperature [Heath, 1983]). Temperatures in downgradient wells (24 to 28 °C) show an increase of ~ 2.5 °C per 100 meters of depth (Figure 4.4).

The groundwater has low salinity at great depth (up to 600 m below sea level) and long flow path distance (up to 350 km) from the recharge zone. The Cl^- concentration is less than 10 mg/L along the major flow path (Figure 4.5). Except for a few outliers, Cl^- averages about 2 mg/L with no significant variations along the flow path. This implies that the aquifer is not actively influenced by cross-formational mixing with brackish water.

4.2 Geochemical modeling

Saturation indices (SI values) were calculated for phases likely to be present in the aquifer matrix, including carbonates (calcite, dolomite, and siderite), pyrite, Fe (oxyhydr)oxides

(goethite and $Fe(OH)_{3(a)}$), and SiO_2 phases (Table A.4). Sulfates (anhydrite and gypsum) were also included in the geochemical calculations in order to account for a source of SO_4^{2-}, possibly by diffusion from confining units containing connate water (e.g., Pucci and Owens, 1989; Chapelle and McMahon, 1991) or cross-formational leakage. Water samples are undersaturated with respect to calcite, dolomite, and $Fe(OH)_{3(a)}$ and supersaturated with respect to goethite. Siderite is observed to be supersaturated in lower Wilcox upgradient wells (samples 1 – 5), but is undersaturated in six of nine downgradient wells.

Based on changes in major ion compositions along the flow path, pairs of initial and final samples were chosen for mass-balance modeling. Selected pairs with plausible reaction-path calculations are presented in Table A.5. Major assumptions are that the system has attained steady-state flow conditions and that observed differences in water chemistry between two points are due to reaction with solid phases. Preliminary models indicated that mixing with brackish water was volumetrically insignificant. Based on their major-ion compositions and location along the flow path, wells in the upgradient section (samples 1 to 5) were considered to represent modified recharge water. Dissolution of calcite and other carbonates was assumed closed to the atmosphere. Based on charge balance error, maximum uncertainty was set to 0.15 in PHREEQC. All in all, 20 pairs of wells were tested and 62 plausible inverse models were obtained. The mole-transfer model outputs reported in Table A.5 are interpreted as semi-quantitative. Most plausible reaction models obtained from inverse modeling involved oxidation of SOM, dissolution of calcite, precipitation of pyrite, and cation exchange.

Petrographic analysis indicated the mineralogical composition and authigenic nature of solid phases within the aquifer matrix. In all thin sections the dominant mineral observed was primary quartz with traces of micas. Significant amounts of authigenic pyrite (Figure 4.6a, b) and Fe-(oxyhydr)oxide rims around siderite were evident (Figure 4.6c).

4.3 Stable isotopes

Results for $\delta^{13}C$ values range between -12.38‰ and -6.89‰ (Table A.3). No relationship is evident between $\delta^{13}C$ and location of wells or TOC content in the groundwater. For samples measured for $\delta^{34}S$ (7, 13, 18, 22, and 23), $\delta^{34}S$ tends to increase as SO_4^{2-}.decreases (Table A.3)

The rainwater samples (Table A.6) represent an aggregate of precipitation events over periods of two to six weeks. For samples collected on the same day at the DOE and TVA sites, values of $\delta^{18}O$ and $\delta^{2}H$ vary by as much as 0.74‰ and 4.60‰, respectively. Samples for the same time interval collected at the two stations were averaged. Two samples were discarded because of discoloration and other visual evidence of atmospheric contamination; another sample broke in storage. Overall average values for January 1997 – January 1998 were calculated using the following equation:

$$X = \frac{\Sigma X_i P_i}{\Sigma P_i}$$

where X is volume weighted average (VWA) for $\delta^{18}O$ or $\delta^{2}H$, X_i represents $\delta^{18}O$ or $\delta^{2}H$ measured for each sample or pair of samples, and P_i is cumulative rainfall amount between sampling days. The results for $\delta^{18}O$ from 2007 are enriched by 0.5‰ on average relative to the initial analyses from 1998. Differences between the two sets of analyses could have resulted from interlaboratory differences or sample storage. However, because samples were stored in sealed glass bottles in a refrigerator, fractionation during storage would have been limited. Overall, 12 representative samples were acquired. Results of 2007 analyses range from -10.4‰ to -2.9‰ (VWA = -5.8‰) for $\delta^{18}O$ and -67.6‰ to -10.0‰ (VWA = -33.4‰) for $\delta^{18}H$. A linear regression of these samples yields a local meteoric water line (LMWL) with an equation $\delta^{2}H = 7.5\delta^{18}O + 10.6$ (Figure 4.7a), which has a slightly lower slope than the global meteoric water line ($\delta^{2}H = 8\delta^{18}O + 10$) (Craig, 1961).

Oxygen-18 and deuterium results for the groundwater samples are reported in Table A.3. The groundwater samples plot along the LMWL (Figure 4.7b). The isotopic compositions of the groundwaters are within the range of present-day precipitation. The $\delta^{18}O$ and $\delta^{2}H$ of groundwater from the unconfined Wilcox aquifer range from -6.1 to -5.5‰ and -37.0 to -32.1‰, respectively. For the confined section of the Wilcox aquifer, $\delta^{18}O$ and $\delta^{2}H$ range from -6.8 to -5.7‰ and -41.3 to -32.7‰, respectively. By comparison, $\delta^{18}O$ and $\delta^{2}H$ of groundwater from the Claiborne aquifer range from -6.0 to -5.1‰ and -34.6 to -28.1‰, respectively. Including data from Brahana et al. (1985), $\delta^{18}O$ and $\delta^{2}H$ of groundwater from the McNairy aquifer range from -6.3 to -5.4‰ and -37.5 to -32.0‰, respectively (Figure 4.7b).

Figure 4.8 shows variation of $\delta^{18}O$ and $\delta^{2}H$ along the regional flow path. There are distinct trends for wells in the recharge area and wells from the confined part of the flow system. In both the confined Wilcox and Claiborne aquifers, values of $\delta^{18}O$ and $\delta^{2}H$ become progressively heavier along the flow path. In the confined section of the Wilcox aquifer, ^{18}O is enriched by ~ 1‰/150 km and ^{2}H by ~ 6‰/150 km.

4.4 Flow model and chlorine-36

Results of $^{36}Cl/Cl$ ratios from collected samples show an overall decrease along the flow path, with values ranging from 212×10^{-15} to 40×10^{-15}. Table 4.1 presents the results along with two data points from the Claiborne aquifer reported by Davis et al. (1998). Higher $^{36}Cl/Cl$ ratios represent relatively young groundwater that has high atmospheric ^{36}Cl and small ^{35}Cl (Davis et al., 2003).

The transport model was calibrated against the measured $^{36}Cl/Cl$ ratio. Use of four samples, which represent only the downgradient section, might not reveal statistically significant variations. Age was calculated from the measurements using equation 2.1, but the calculated age values were used only to check if outputs of residence time and ^{36}Cl distribution across the basin conform. Measured Cl^- concentrations were used to estimate the probable value of atmospheric ^{36}Cl flux and contribution by diffusion from underlying aquifers.

The model assumes that the surface of the MEAS is open to fresh water recharge with a constant $^{36}Cl/Cl$ ratio of ~ 250×10^{-15}, within the range reported by Davis et al. (2003) (Figure 4.9). BASIN2 can consider additional sources of ^{36}Cl other than the input from atmospheric recharge, primarily neutron activation of ^{35}Cl. However, production of ^{36}Cl by this process, as compared to natural decay of the isotope, is very small. Only under certain conditions where aquifer sediments contain abundant U, Th, or evaporite minerals that can contribute excess ^{35}Cl is the process important. There are no reported analyses of solid-phase U and Th from the Wilcox Group (lower Wilcox aquifer). Default values for U and Th in sand (U = 1.4 ppm, Th = 3.9 ppm) and clay (U = 3.2 ppm, Th = 11.7 ppm) provided by the authors of the software were used at the beginning. Inclusion of neutron activation of ^{35}Cl with the above values slightly increased the calculated ^{36}Cl, but did not change the $^{36}Cl/Cl$ pattern across the basin.

Chlorine-36 can also diffuse into groundwater along the basin's bottom boundary. This input source was neglected because Cl^- concentrations averaged 2 mg/L and only increased by a factor of two to five downgradient (Figure 4.5). Inverse geochemical models also show that there is no significant cross-formational mixing of the groundwater from the Wilcox aquifer with that from underlying (or overlying) units.

The sensitivity analysis first explored how variations in D^* may affect the ^{36}Cl concentration. Based on the range of values in Table 3.2, permeability for sandy layers was allowed to vary from 10^0 to 10^2 darcys whereas permeability for clayey layers was set to 10^{-3} darcys (1 darcy = 10^{-8} cm^2). The diffusion constant was progressively increased in four sets of simulations (for each permeability value of sand) from 10^{-8} to 10^{-5} cm^2/s for both sand and clay. Transverse and longitudinal dispersivity were set to the program's default values of 100 cm and 1000 cm, respectively, for both sand and clay. Estimates of $^{36}Cl/Cl$ ratio were sensitive to variations of diffusion constant and permeability (Figure 4.10a) whereas residence time was more sensitive to permeability (Figure 4.10b). Figure 4.11 shows $^{36}Cl/Cl$ ratios across the basin with $D^* = 10^{-6}$ cm^2/s.

Figures 4.12 and 4.13 show representative model fits against field-measured hydraulic head and temperature, respectively. Calculated heads represent predevelopment levels and therefore they tend to be higher than measured head values (Figure 4.12). These parameters showed only minor changes with permeability variations. For temperature, the model was fitted by setting surface temperature to 15°C, which corresponds to the approximate recharge temperature.

Table 4.1: Results of $^{36}Cl/Cl$ measurements.

Well ID	Locality	Aquifer	$^{36}Cl/Cl$ $\times 10^{-15}$	Cl (mg/L)	Distance (km)	Age ka
13	Osceola	Wilcox	211.9±6%	1.06	78	–
18	Shell Lake	Wilcox	89.6±4%	2.19	271	360
20	Horseshoe Lake	Wilcox	59.9±5%	2.75	285	535
21	Brickeys	Wilcox	41.0±7%	7.07	294	700
	Birdeye[a]	–	205	3.24	255	–
	Parkin[a]	Claiborne	70	2.87	262	553

[a] Davis et al. (1998)

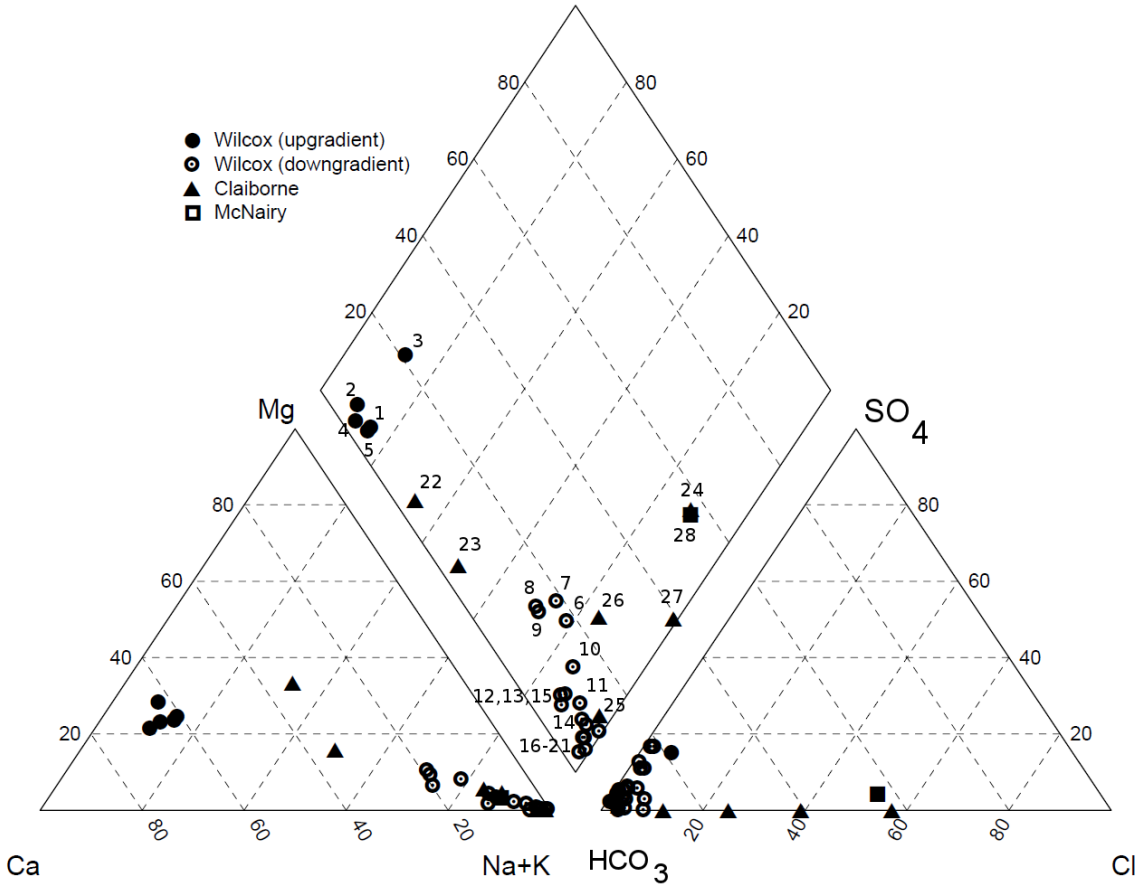

Figure 4.1: A Piper plot (Piper, 1944) showing the hydrochemical facies of samples from the Claiborne, Wilcox, and McNairy aquifers.

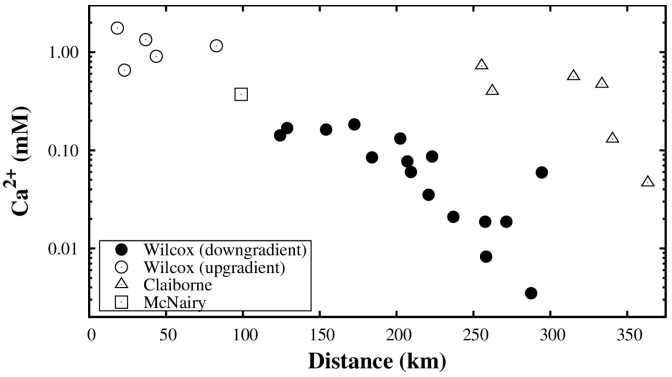

(a)

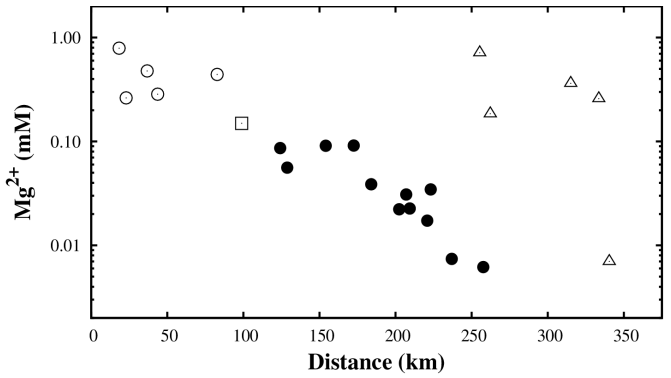

(b)

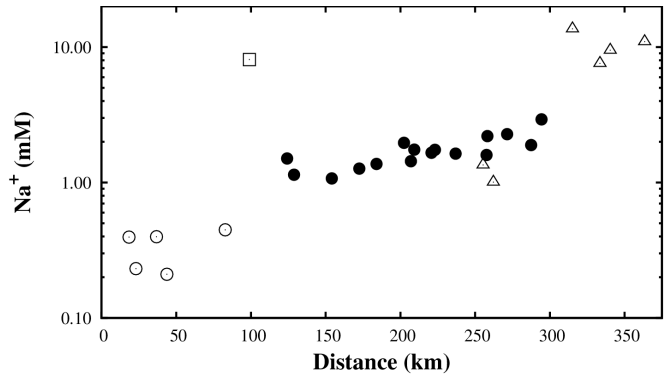

(c)

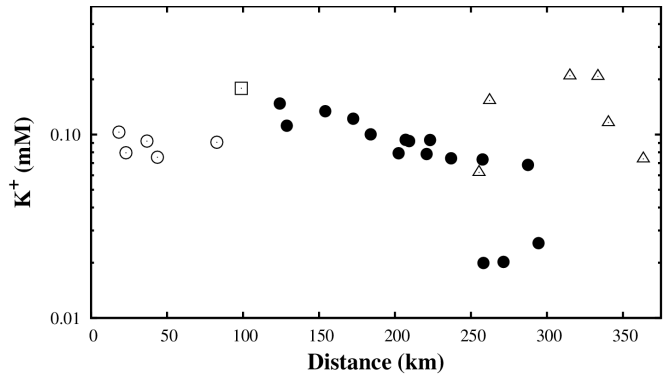

(d)

Figure 4.2: Graphs showing the concentrations of dissolved (a) Ca^{2+}, (b) Mg^{2+}, (c) Na^{+}, and (d) K^{+} plotted versus distance along the flow path.

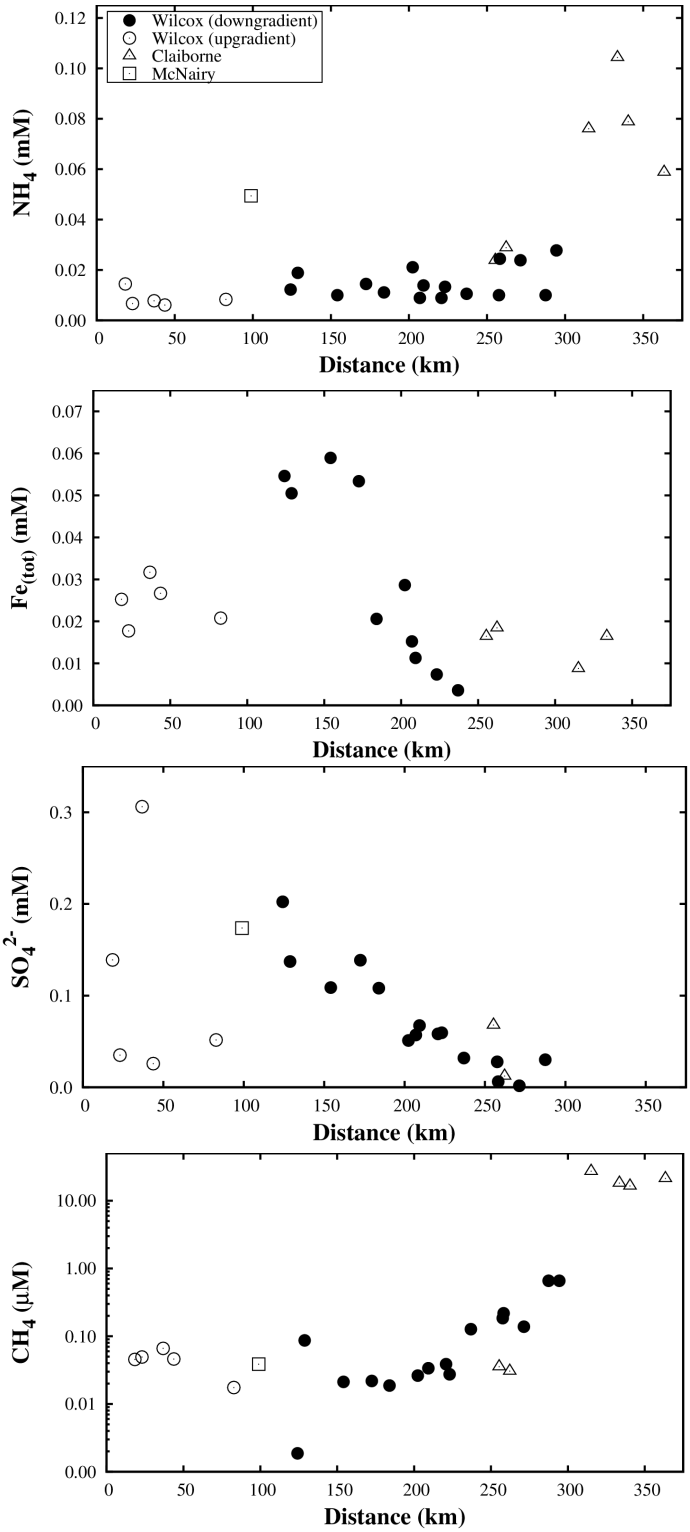

Figure 4.3: Graphs showing the concentrations of redox-sensitive dissolved solutes. (a) NH^{4+}, (b) $Fe_{(tot)}$, (c) SO_4^{2-}, and (d) CH_4 plotted versus distance along the flow path.

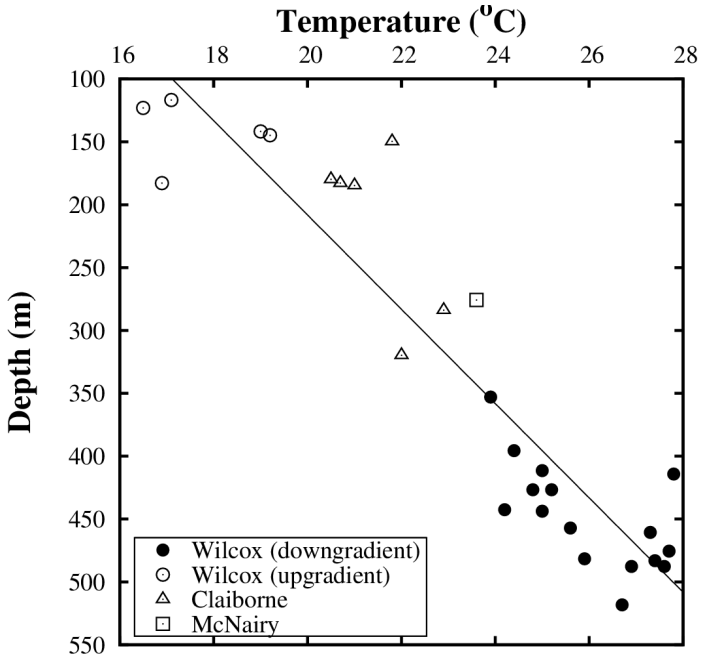

Figure 4.4: Variation of groundwater temperature with depth. The slope of the regression line is ~2.5 °C/100 m.

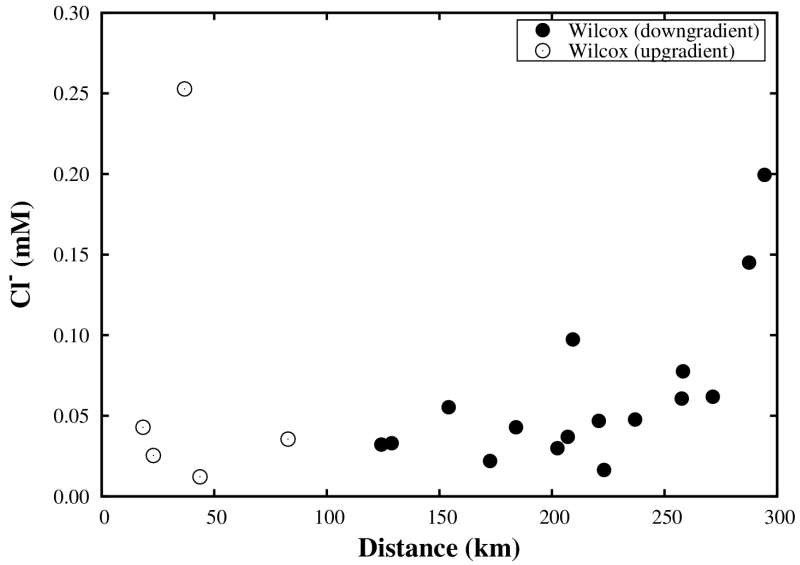

Figure 4.5: Chloride concentration in groundwater from wells located along flow path.

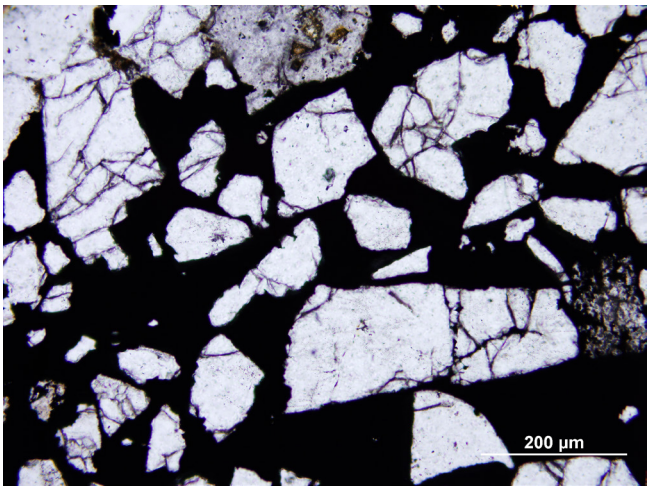

(a)

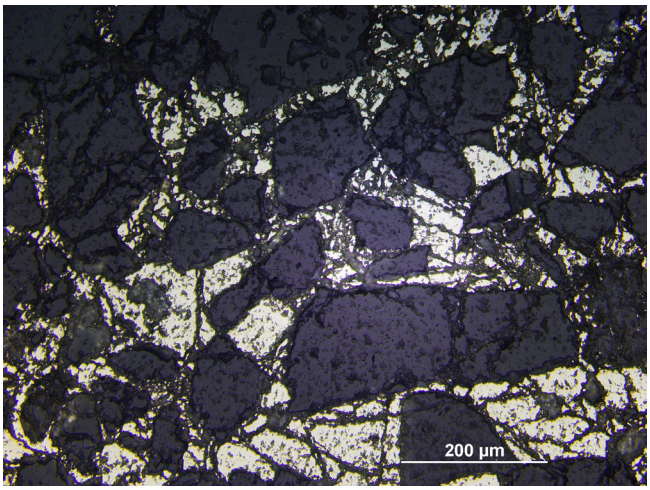

(b)

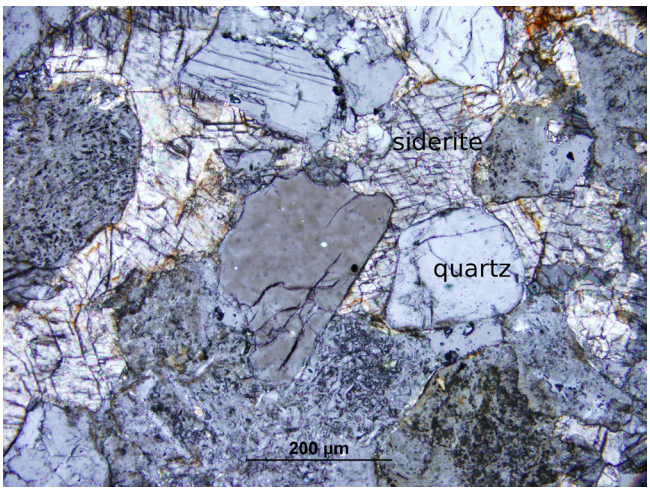

(c)

Figure 4.6: Authigenic pyrite surrounding quartz in photomicrographs appears dark in plane polarized light (a) and yellowish under reflected light (b). (c) Siderite weathering to Fe(oxyhydr)oxides around the edge.

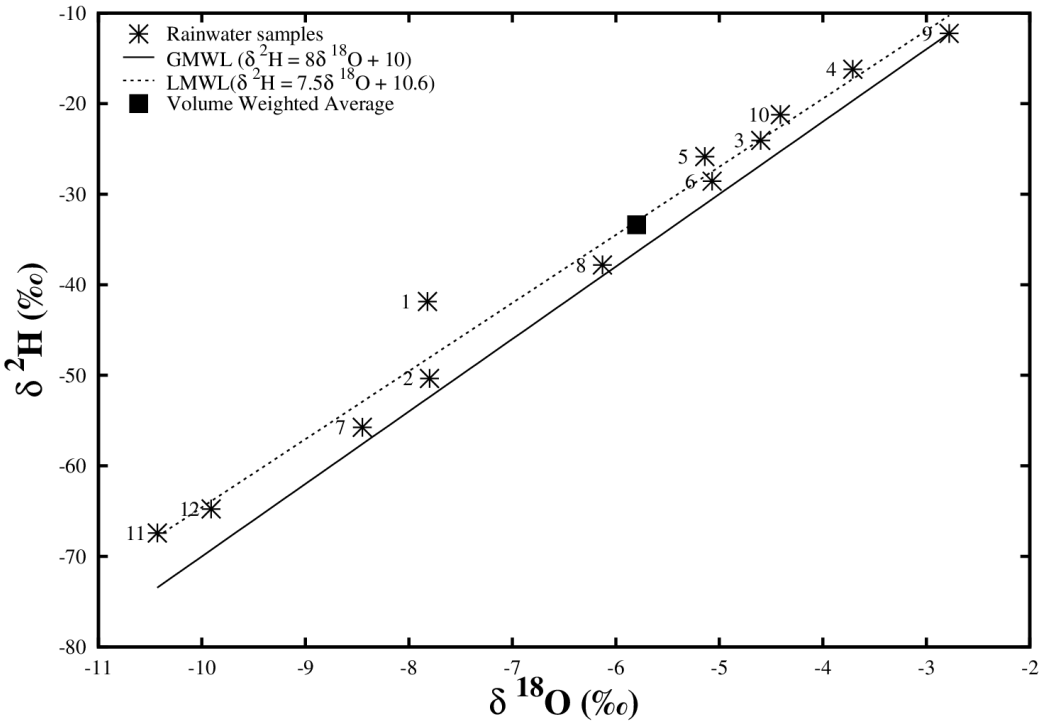

(a)

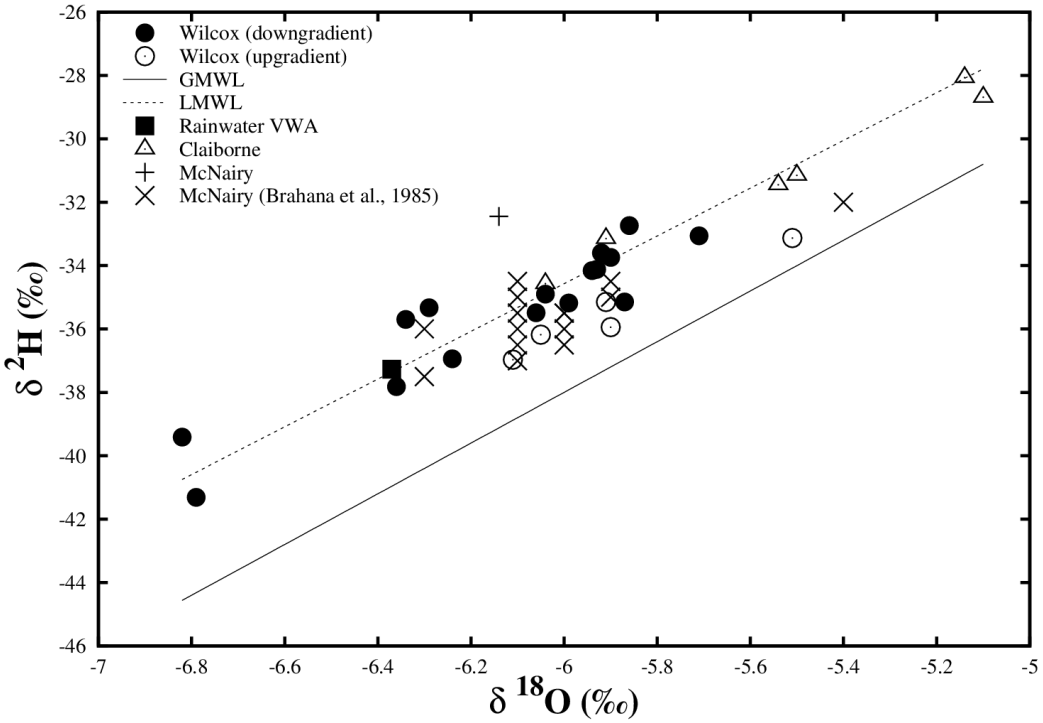

(b)

Figure 4.7: Plot showing the relationship between ^{18}O and ^{2}H (a) in rainwater from Paducah, Kentucky (numbers on graph correspond to Table A.6) and (b) in groundwater from the study area. All samples plot along a local meteoric water line (LMWL). The global meteoric water line (GMWL) is given as a reference.

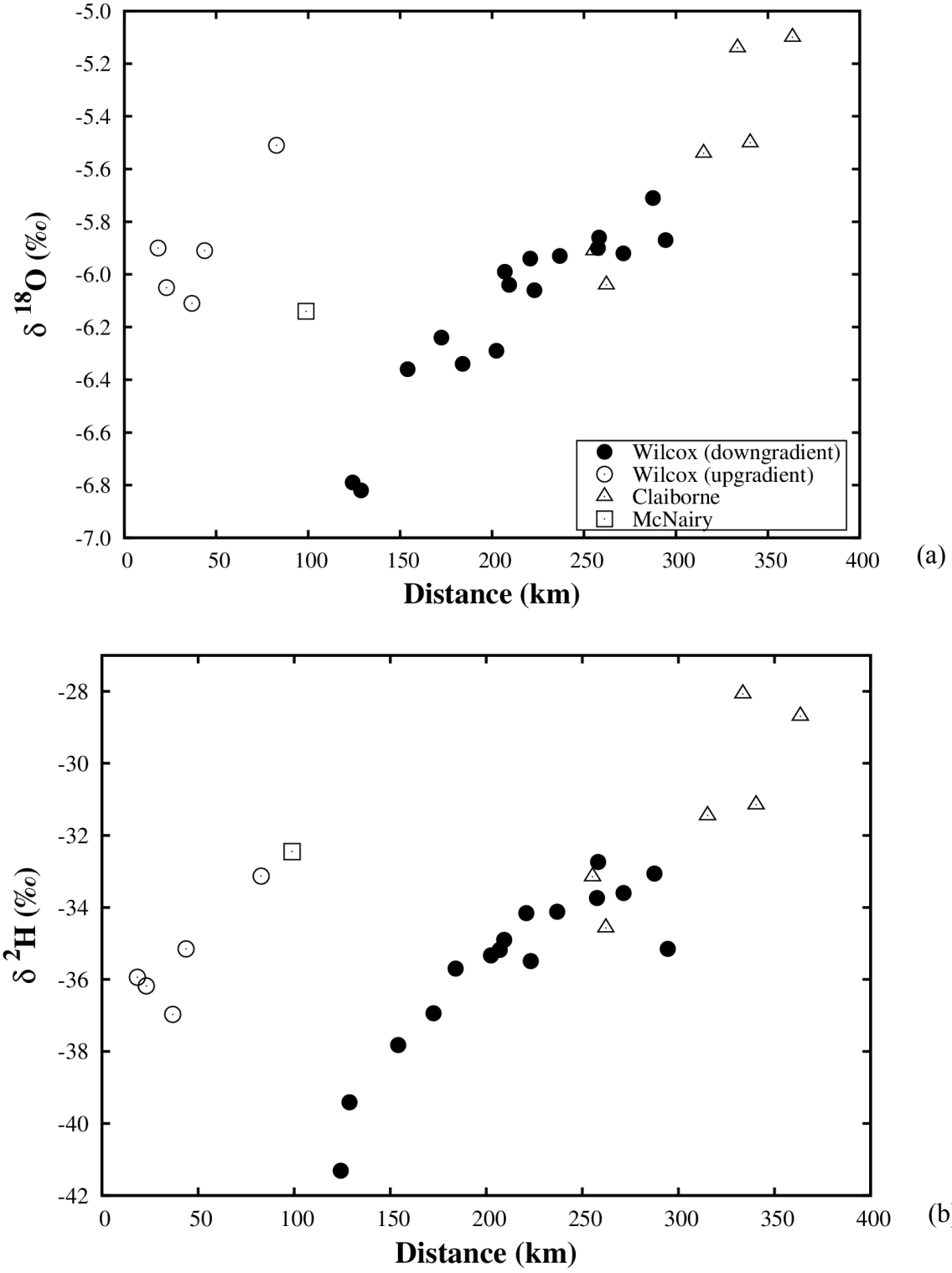

Figure 4.8: Variation of (a) $\delta^{18}O$ and (b) $\delta^{2}H$ along flow path. The abrupt shift might represent compartmentalization of aquifers between the upgradient and downgradient section.

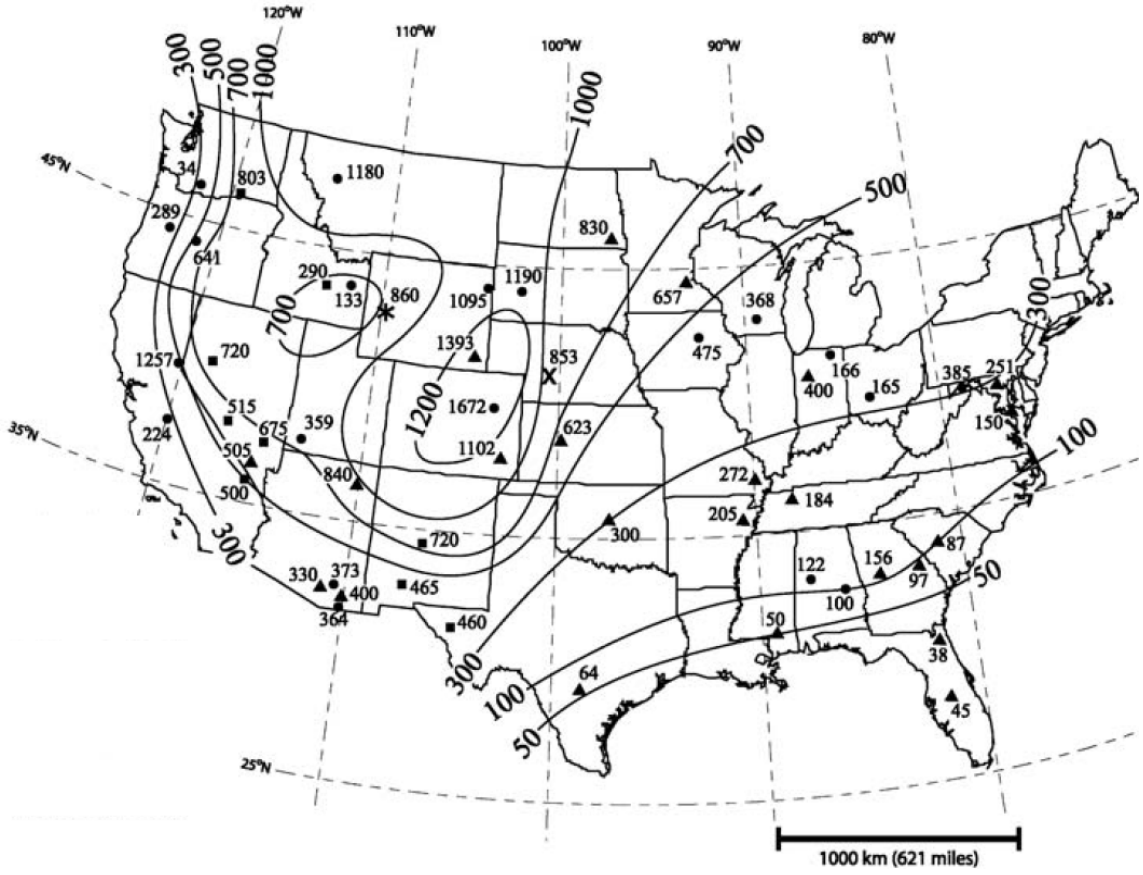

Figure 4.9: Projected pre-anthropogenic 36Cl/Cl ($\times 10^{-15}$) isopleths for continental United States based on compiled empirical data of shallow wells in clastic, carbonate, and glacial aquifer; glacial ice, and soil leachate (from Davis et al., 2003).

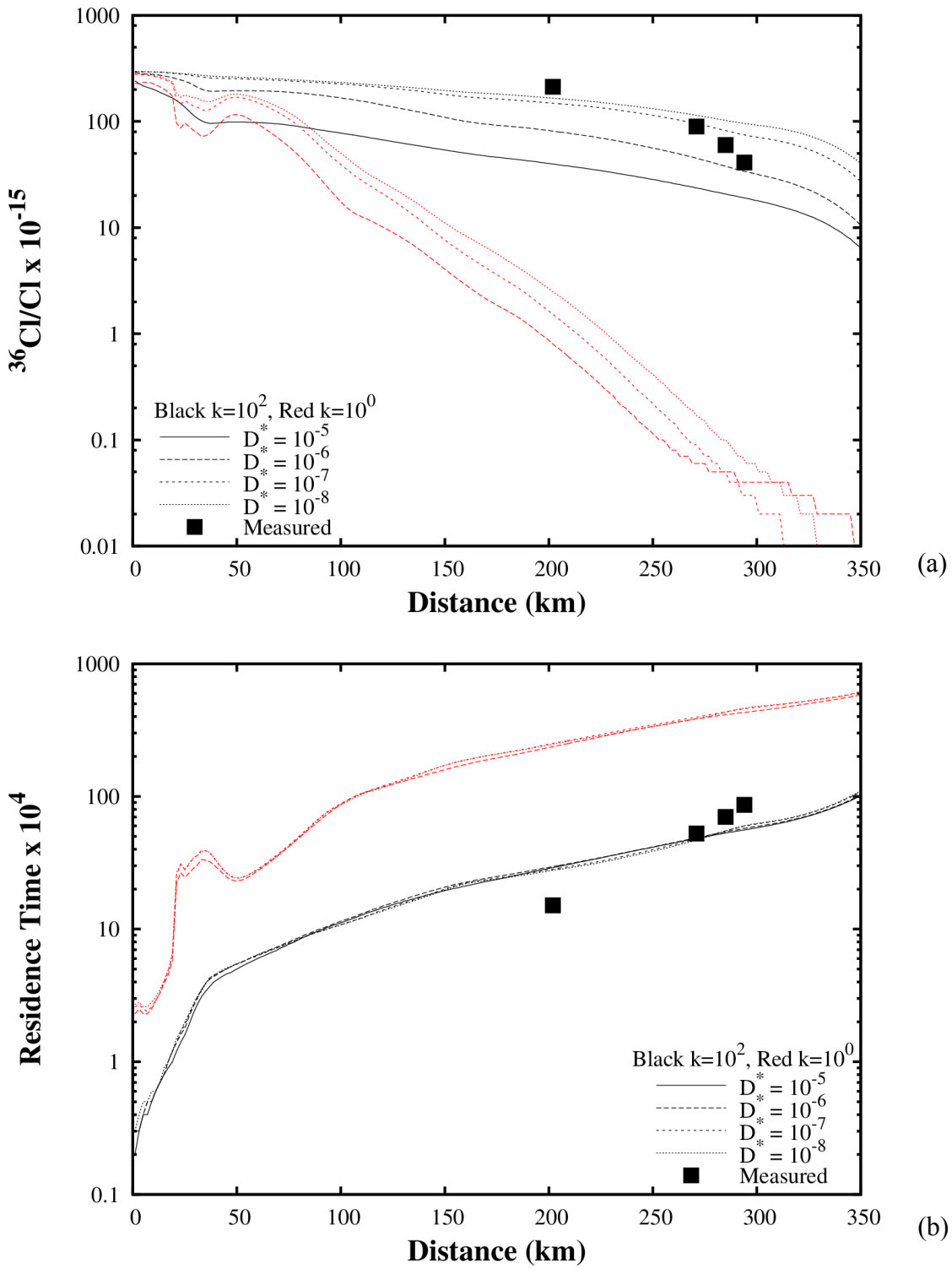

Figure 4.10: Sensitivity analysis with variable diffusion coefficient (D*). Calculated ^{36}Cl/Cl ratio (a) and corresponding groundwater residence time (b) along the lower Wilcox flow path with permeability set at k = 10^{2} darcys for sandy layers and k = 10^{-3} darcys for clayey layers.

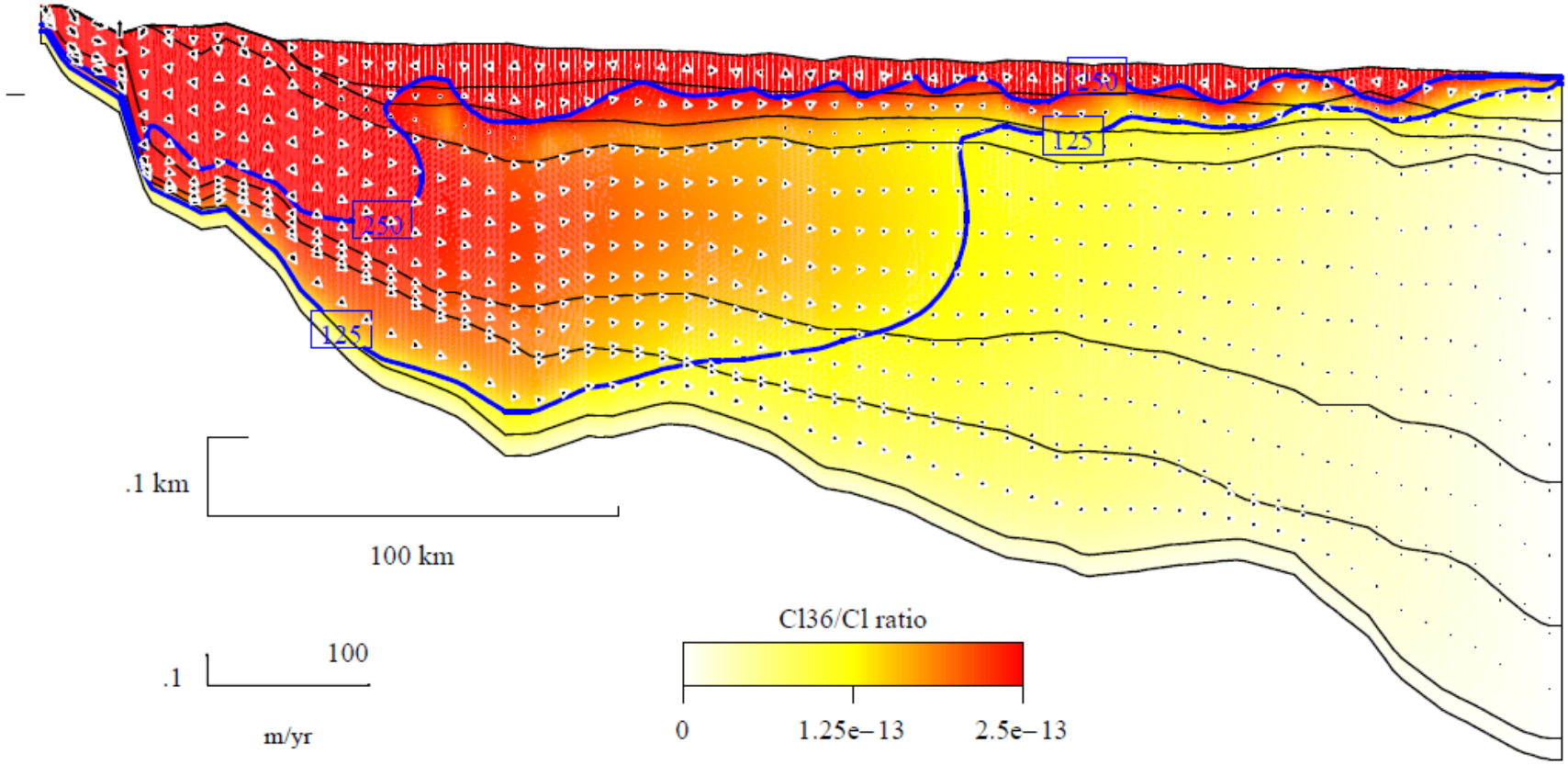

Figure 4.11: Calculated 36Cl/Cl ratio along the flow path. Atmospheric input for $^{36}Cl/Cl$ set to 250×10^{-15} (from Davis et al., 2003). Chloride is set to 2 mg/L (average value of sampled wells) at recharge (surface), and the basal chloride flux was set to zero (no cross-formational mixing), k = 10^2 darcys, $D^* = 10^{-6}$ cm^2/s. Contour lines represent $^{36}Cl/Cl$ ratio $\times10^{-15}$.

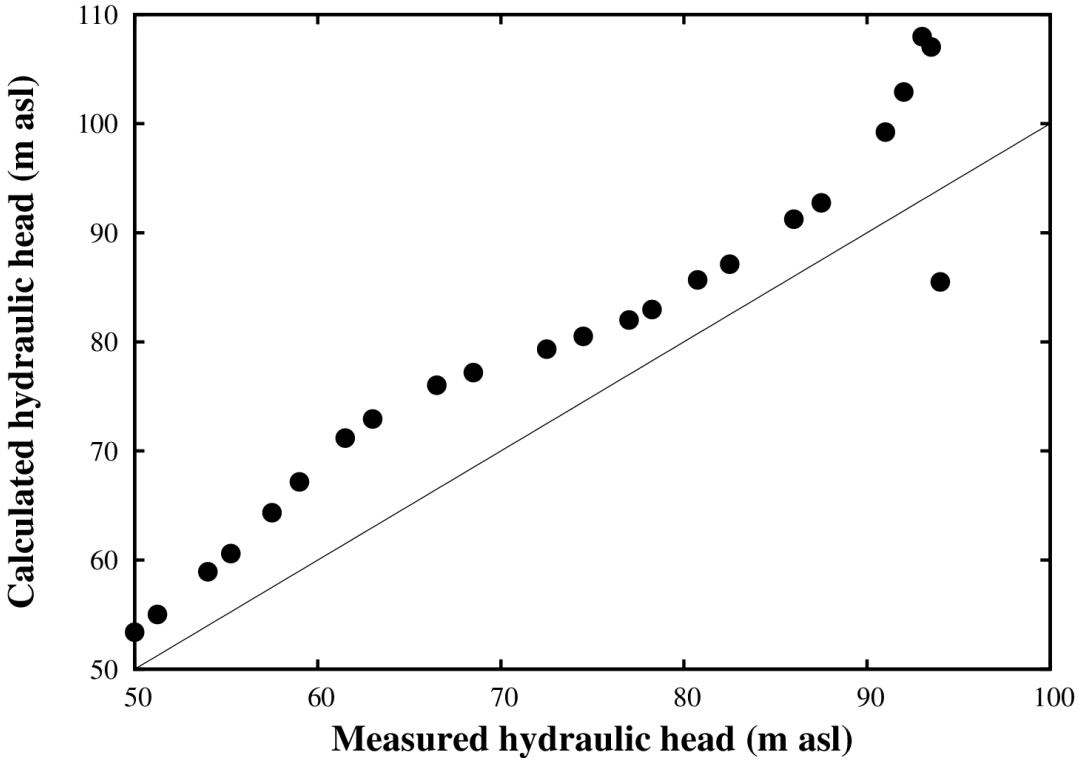

Figure 4.12: Calculated versus measured hydraulic head for the lower Wilcox aquifer. Data for hydraulic head were derived from Schrader (2007) (see Figure 2.7). The calculated values are from vertical mid-section of the lower Wilcox aquifer.

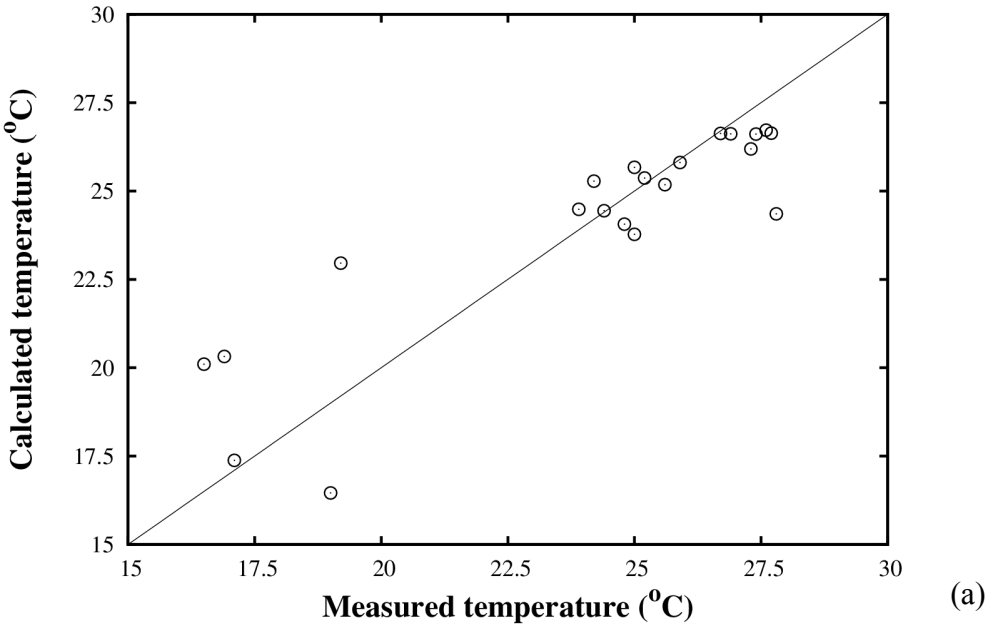

(a)

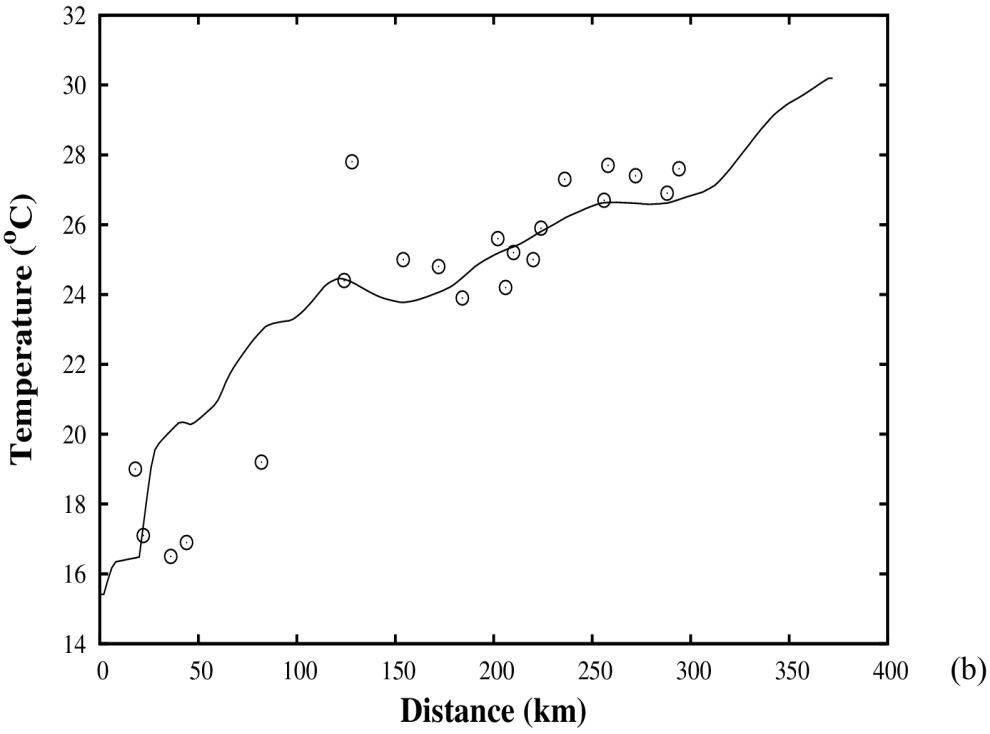

(b)

Figure 4.13: Calculated versus measured groundwater temperature (a), and (b) modeled (solid line) and measured (open circles) temperature variation along the groundwater flow path (b).

Chapter 5 Discussion and conclusions

5.1 Groundwater chemistry and geochemical modeling

Because of the regional scale of this study and associated heterogeneity of the aquifer system, a number of processes can affect groundwater geochemistry. These may include: (1) dissolution and precipitation of carbonates (e.g., calcite and siderite) and precipitation of sulfides (e.g., FeS_2); (2) weathering of silicates to clay minerals; (3) cation exchange on clay minerals; (4) bacterially mediated reduction of O_2, NO_3^-, Fe(III) (oxyhydr)oxides, and SO_4^{2-} coupled to oxidation of organic matter; and (5) diffusion and advection of solutes associated with cross-formational leakage. Upward leakage from the lower Wilcox to the middle Wilcox or Claiborne aquifer may occur via paleo-channels that cut through confining beds (as proposed by Chapelle and Knobel (1983) for the Aquia aquifer) or via minor fracture systems.

Using plots that show stoichiometric relationships of ions, it is apparent that trends in major ion chemistry are influenced initially by the dissolution of minerals that are reactive at low temperature (mainly carbonates, as indicated by Ca^{2+} and Mg^{2+} concentrations). The chromatographic trend of cations shown in Figure 4.2 suggests that the system transitions from calcite dissolution to cation exchange with distance.

A plot of $SI_{calcite}$ versus distance (Figure 5.1) indicates that calcite undersaturation is sustained along the flow path, probably as a result of exchange of dissolved Ca^{2+} for adsorbed Na^+. SI calculations indicate that groundwater is undersaturated with respect to $SiO_{2(a)}$ and chalcedony, which are precursor phases for quartz (Hem, 1992). The stability diagrams in Figure 5.2 show that samples plot in the kaolinite field (i.e., kaolinite is the thermodynamically favored aluminosilicate phase) and along the quartz stability line ($K_T = 10^{-4}$). Weathering of detrital aluminosilicates to authigenic silicates is limited by slow kinetics (dissolution times on the order of $10^5 – 10^6$ years) at low groundwater temperatures (Drever, 1997). Because SI calculations simply suggest the thermodynamic favorability of a reaction, they must be interpreted in light of other lines of evidence, such as mineralogy. For example, no SI value was obtained for pyrite (see Table A.4), even though it was observed as an authigenic phase in thin sections (Figure 4.6a, b). The availability of Fe, the decrease in SO_4^{2-} along the flow path, and the lack of HS^- suggest

that sulfide is "scrubbed" from groundwater by pyrite precipitation. Although data are sparse, the increase in $\delta^{34}S$ of groundwater along the regional flow path in the lower Wilcox, from 22.2‰ (well 7) to 37.8‰ (well 13) to 77.3‰ (well 18) (Table A.3), is consistent with progressive reduction of SO_4^{2-} to HS^-, which results in enrichment of residual SO_4^{2-} in ^{34}S (Chapelle, 1993, p. 262–263). Sulfate is probably contributed not by dissolution of anhydrite or gypsum, but by diffusion from adjoining confining units, as observed in the Atlantic Coastal Plain by Pucci and Owens (1989) and Chapelle and McMahon (1991).

In Figure 5.3, the Na^+ and Cl^- concentrations of Wilcox groundwater samples plot above the halite dissolution line. This implies that contribution by mixing with brackish (saline) water is minimal. The possibility of cross-formational mixing between the Wilcox and underlying or overlying strata was considered during formulation of the geochemical models. A mixing ratio of 0.99 (Wilcox) to 0.01 (Claiborne or McNairy) was commonly enough to account for Cl^- and SO_4^{2-} added into the system, assuming that there was no source of these solutes in the aquifer.

Reactions that contribute carbon to groundwater are decomposition of organic matter (OM) and dissolution of solid carbonates. Microbial oxidation of OM via electron acceptors such as H_2O, Fe^{3+}, or SO_4^{2-} produces CO_2. This is substantiated by the small amount of measured dissolved O_2 in the samples (<1 mg/L). In addition, 18 of the samples, mostly from the lower Wilcox aquifer, have Eh levels between -149 and -50 mV. This range typically represents Fe(III) reduction, SO_4^{2-} reduction, and/or reduction of organic matter (OM) to CO_2 (fermentation) (Stumm and Morgan, 1996; McMahon and Chapelle, 2008). To simplify the geochemical models, all CH_4 production was assumed to result from CO_2 reduction. Organic matter in the form of CH_2O was included as a constraint according to the following half-reaction:

$$CH_2O + H_2O \rightarrow CO_2 + 4H^+ + 4e^-$$

The production of acid (right-hand side of the above reaction) causes the dissolution of calcite,

$$CaCO_3 + H^+ \rightarrow Ca^{2+} + HCO_3^-$$

provided that there is a congruent loss of Ca^{2+} from the solution, which is usually exchanged for other base cations:

$$Ca^{2+} + 2X^{-} \rightarrow CaX_2$$

$$(Na, K, 0.5Mg)X \rightarrow X + (Na^{+}, K^{+}, 0.5Mg^{2+})$$

Plummer et al. (1994) concluded that calcite dissolution can go to completion as Ca^{2+} is lost from solution, provided that an increase in pH occurs. This process is explained by Appelo (1994) as proton exchange, in which desorbed protons are consumed as bicarbonate from calcite dissolution and via hydrolysis of CO_2 from organic matter oxidation:

$$Ca^{2+} + 2HX \rightarrow CaX_2 + 2H^{+}$$

$$CaCO_3 \rightarrow Ca^{2+} + CO_3^{2-}$$

$$CO_3^{2-} + H^{+} \rightarrow HCO_3^{-}$$

A more complicated series of reactions can be anticipated to link C, Fe, and S cycling via reductive dissolution of Fe(III) (oxyhydr)oxide, reduction of SO_4^{2-}, and dissolution of siderite to form pyrite:

$$CH_2O + 4Fe(OH)_{3(a)} + 8H^{+} \rightarrow CO_2 + 4Fe^{2+} + 11H_2O$$

$$2CH_2O + SO_4^{2-} + 2H+ \rightarrow H_2S + 2CO_2 + 2H_2O$$

$$2SO_4^{2-} + Fe^{3+} + 16H^{+} + 15e^{-} \rightarrow FeS_2 + 8H_2O$$

$$FeCO_3 + H^{+} \rightarrow Fe^{2+} + HCO_3^{-}$$

The above-mentioned processes (Stumm and Morgan, 1996) are consistent with the observed pyrite rims around siderite (Figure 4.6a, b).

Models were further constrained using ^{13}C balance between data points. An increase or decrease of ^{13}C in groundwater can result from addition or removal of carbonates and organic matter, which have distinct ranges of carbon isotopic compositions. Common sources of dissolved C in groundwater flow systems include marine carbonate shell material, with $\delta^{13}C \sim 0‰$ VPDB, solid organic matter (SOM; e.g., lignite), with $\delta^{13}C \sim -25‰$ VPDB, and soil-gas CO_2, which can have intermediate ^{13}C values, depending on the composition of vegetation being oxidized (Faure, 1986, Cook and Böhlke, 2000). With

progressive reaction and increasing residence time of groundwater in the subsurface, several processes can affect ^{13}C values in groundwater. These include methanogenesis, which can produce isotopically heavy DIC (Chapelle and Knobel, 1985); cycling of carbon between carbonate mineral phases (continuous dissolution of and precipitation of calcite cement), which can enrich ^{13}C; and diffusion of DIC from confining units. Typical values for SOM (-25‰) and calcite (0‰) were used as model constraints. The test for hydraulic connectivity between pairs of wells using $\delta^{13}C$ of DIC as a constraint did not give plausible reaction models. The observed $\delta^{13}C$ range (-12.4‰ to -6.9‰) for all samples suggests mixing of DIC pools derived from dissolution of calcite and oxidation of SOM, as inferred by McMahon and Chapelle (1991) and Kennedy and Genereux (2007) for confined Coastal Plain aquifers in South Carolina and North Carolina, respectively.

5.2 Oxygen-18, deuterium, and residence time

Stable isotopic values in groundwater similar to those of modern precipitation are not distinctive markers of recent recharge (Siegel, 1991). Paleorecharge studies in major aquifers of the central and eastern United States using ^{14}C dating have shown that several of the aquifer systems were recharged during the Pleistocene (Table 2.3). Examination of the spatial distribution of ^{2}H and ^{18}O from the same studies that encompass ^{14}C ages between 10 and 30 ka (Figure 5.4) reveals that the isotopic signatures of the Pleistocene-recharged aquifers can be either depleted or enriched relative to modern recharge or to predicted values based on paleotemperatures. Predicted values reflect the modern global $\delta^{18}O$ – temperature (T) relationship of Dansgaard (1964), $\delta^{18}O = 0.695T - 13.6$. Paleotemperatures are inferred from noble gas concentrations (Stute et al., 1992, 1995; Clark et al., 1998; Aeschbach-Hertig et al., 2002; Ma et al., 2004; Klump et al., 2008).

Instances of $\delta^{18}O$ and $\delta^{2}H$ depletion in regional confined aquifers include the Madison aquifer in the northern Plains states (Plummer et al., 1990) and Dockum aquifer in the High Plains of Texas and New Mexico (Dutton and Simpkins, 1986; Dutton, 1995). Conversely, enriched $\delta^{18}O$ and $\delta^{2}H$ values have been observed in Iowa (Siegel, 1991), the Cambro-Ordovician aquifer of southeastern Wisconsin (Klump et al., 2008), and the Marshall aquifer of the Michigan basin (Ma et al., 2004). Along the Atlantic Coastal

Plain, enrichment of $\delta^{18}O$ and $\delta^{2}H$ was not observed in the Aquia aquifer of Maryland (Aeschbach-Hertig et al., 2002), but was observed in the Black Creek aquifer of North Carolina (Kennedy and Genereux, 2007) and the Floridan aquifer in southeastern Georgia and Florida (Plummer, 1993; Plummer and Sprinkle, 2001). Regional variability in groundwater $\delta^{18}O$ and $\delta^{2}H$ values during the last glacial maximum has been attributed to various factors, including differences in moisture source areas, proximity to the ice sheet, seasonality of recharge, and atmospheric circulation patterns (Plummer, 1993; Dutton, 1995; Kennedy and Genereux, 2007).

One well-known control on stable isotopic compositions of precipitation and recharge is the continental effect. Following a pattern of Rayleigh distillation, precipitation becomes progressively depleted in $\delta^{18}O$ and $\delta^{2}H$ because of rain-out of the heavier isotopes with distance from the ocean (Dutton et al., 2005; Mukherjee et al., 2007). In the midcontinental USA, for which the Gulf of Mexico is a primary source of moisture, $\delta^{18}O$ and $\delta^{2}H$ of precipitation decrease with increasing latitude following the empirical relationship $\delta^{18}O = -0.0057\ LAT^{2} + 0.1078\ LAT - 1.6544$ for land surface < 200 m asl (Dutton et al., 2005). The continental effect could be a plausible explanation for the observed increases in $\delta^{18}O$ and $\delta^{2}H$ with distance downgradient (i.e., southward) in the Wilcox aquifer if recharge by downward cross-formational leakage is significant. However, because BASIN2 simulations indicate that such leakage is negligible, other explanations are needed, such as progressive depletion of $\delta^{18}O$ and $\delta^{2}H$ in precipitation in the recharge zone over time, or isotopic fractionation along the flowpath. The distinct differences in $\delta^{18}O$ and $\delta^{2}H$ between the upgradient and downgradient Wilcox aquifer suggest that the latter preserves a paleoclimatic signal.

In a homogeneous system with low permeability (and thus slow groundwater velocity), transport by diffusion is the limiting factor for fractionation of heavy isotopes (Solomon and Sudicky, 1991; Solomon et al., 1993; Desaulniers et al., 1986). LaBolle et al. (2008) argued that because diffusion is a slow process, detectable isotopic depletion in such systems by diffusion within small time intervals is not apparent. For a heterogeneous system, using ^{3}H - ^{3}He dating, LaBolle et al. (2008) found groundwater age to be relatively young along major flow paths and relatively old within aquitards as compared to mean age. The same study showed enrichment of heavy isotopes in the

aquifer as compared to depletion in the aquitards. Based on an experimental study, LaBolle et al. (2006) reported an isotopic enrichment along distal parts of principal flow paths (high-permeability zones).

The flow model developed has shown that the flow path is compartmentalized between the unconfined and confined sections of the Wilcox aquifer (Figure 4.11), which is consistent with the separate trends of the stable isotopes along the flow path. Hence it is possible that present-day recharge tends to remain near the top of the MEAS and does not mix with the water in the confined section of the Wilcox aquifer. Calculated residence time in Figure 4.10b might not be representative because of the assumption that $^{36}Cl/Cl$ has been constant from the time of recharge (> 100 ka) (Purdy et al., 1996). Nonetheless, the relative distribution of $^{36}Cl/Cl$ values along the groundwater flow path (as shown in Figure 4.11) suggests that downgradient flushing is sufficiently slow that diffusion plays an important role in solute transport in the aquifer.

5.3 Conclusions

Determining the mode and timing of groundwater recharge and the controls on groundwater geochemistry requires adequate and systematically collected data about the physical and chemical properties of an aquifer. With verifiable hydraulic data, this study has attempted to integrate geochemical methods and 2-D groundwater flow modeling to substantiate the processes controlling the groundwater chemistry and residence time of groundwater in the Wilcox aquifer. The geochemical and groundwater flow models presented in previous sections approximate a heterogeneous system. Due to the scale of the aquifer it is difficult to obtain model uniqueness. Calibration and sensitivity analysis were performed to a limited extent on the flow model. Nonetheless, the results provide insights about the compartmentalization of the Wilcox aquifer.

Under the anaerobic oxidation state of the aquifer, oxidation of OM coupled to reduction of Fe(III) (oxyhydr)oxides and SO_4^{2-} results in dissolution of carbonate minerals. The main conclusions from the geochemical data analysis are: (1) the upgradient (unconfined to semi-confined) and downgradient (confined) sections of the aquifer have distinctive hydrochemical facies; (2) groundwater chemistry in the upgradient section of the aquifer is controlled by the dissolution/precipitation of

carbonate minerals; and (3) cation exchange and continued dissolution of carbonates coupled to redox reactions control the downgradient water chemistry. Low TDS in the aquifer suggests that cross-formational flow of more saline water is negligible.

Measured ^{36}Cl data in conjunction with the transport modeling supports the interpretation of separate flow conditions in the upgradient and downgradient sections of the aquifer. Groundwater age derived from the flow model and ^{36}Cl is almost triple the age of estimates from groundwater age studies for surrounding regional aquifer systems which used ^{14}C for dating. Regardless of the magnitude of the discrepancy, it is likely that diffusion is a more important control on solute transport in the downgradient section of the aquifer than in the upgradient section of the aquifer, where advection is more important.

Based on multiple lines of evidence, this research deduces that the upgradient and downgradient sections of the Wilcox aquifer have little to no hydraulic connectivity. One plausible explanation could be offset by faults in the New Madrid seismic zone. Further investigation focused at the interface (presumably the fault zone) is warranted. A more rigorous study should include calibration of the flow and transport model with a more extensive isotopic data set, including ^{14}C, ^{36}Cl, and He isotopes. At a minimum, development of a model that explicitly incorporates ^{18}O and ^{2}H diffusion, to evaluate the inference that downgradient enrichment of those isotopes is an artifact of diffusion, would be helpful.

The findings of this study have implications for water-resources management in the Mississippi Embayment. In eastern Arkansas, extensive pumping of the alluvial aquifer for agriculture resulted in water-table declines of at least 12 m in the last four decades of the 20th century, and pumping of the middle Claiborne aquifer for industrial and municipal water supplies has resulted in potentiometric-surface declines of more than 110 m since the 1920s (Clark and Hart, 2009). Potentiometric-surface declines in the lower Wilcox aquifer in eastern Arkansas declined ~ 12 m from 1958 to 2000 before appearing to stabilize (Figure 2.5). If depletion of overlying aquifers results in increased exploitation of the Wilcox, which appears to be compartmentalized in eastern Arkansas, accelerated depressurization is likely. In addition, degradation of water quality by

induced cross-formational flow of more mineralized water from underlying and downdip strata could result.

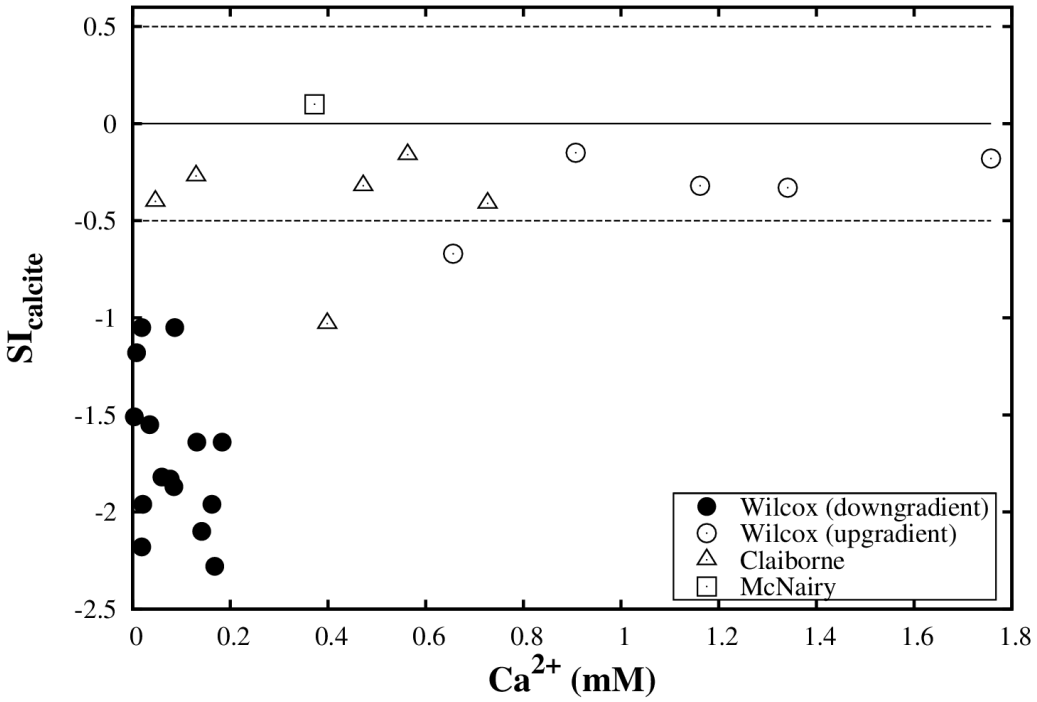

(a)

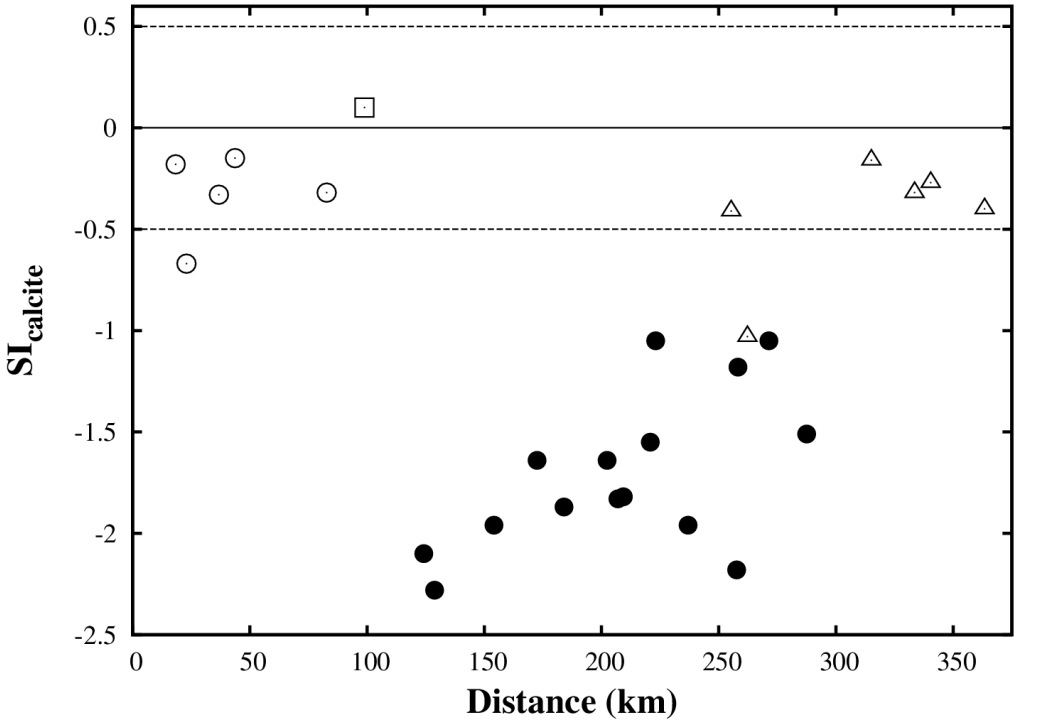

(b)

Figure 5.1: Graphs showing the saturation state of calcite (near saturation upgradient to undersaturated downgradient) as a function of (a) dissolved Ca2+ and (b) distance along flow path.

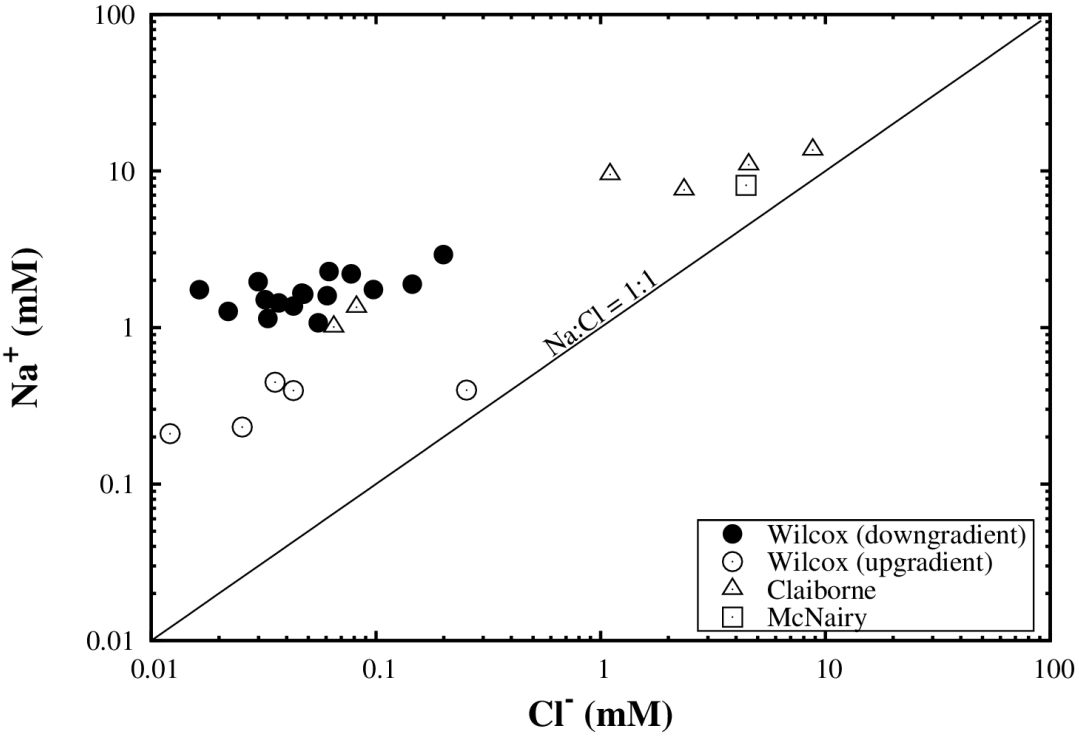

Figure 5.2: Graph showing the relation of Na+ to Cl-. The 1:1 line represents halite dissolution. Samples falling above the line indicate contributions of Na+ from other processes, such as cation exchange or silicate weathering.

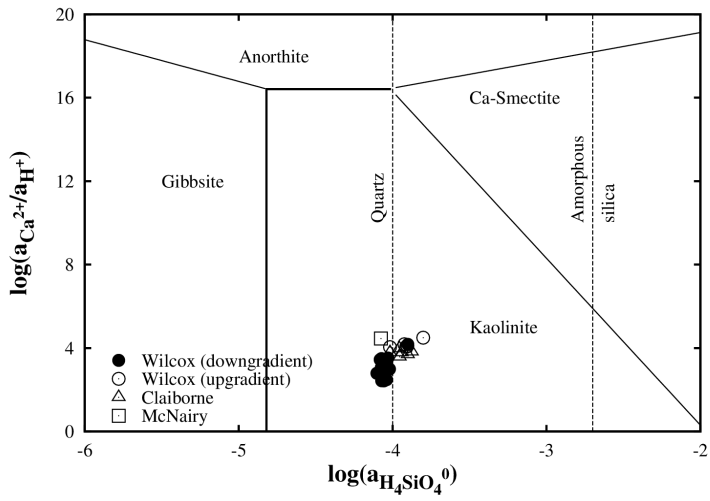

(a)

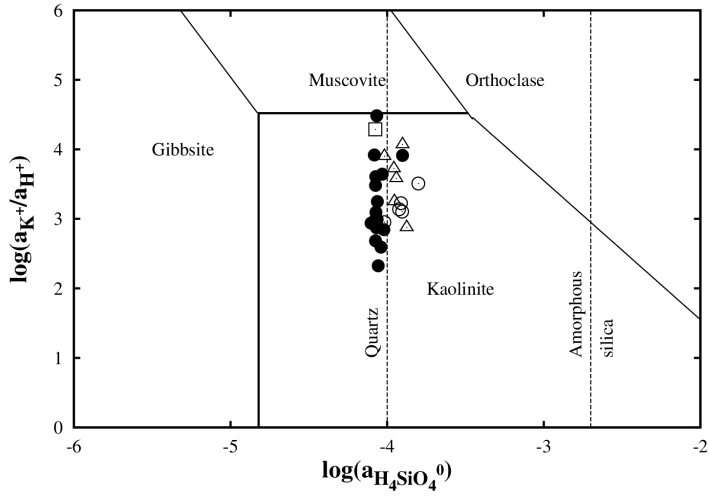

(b)

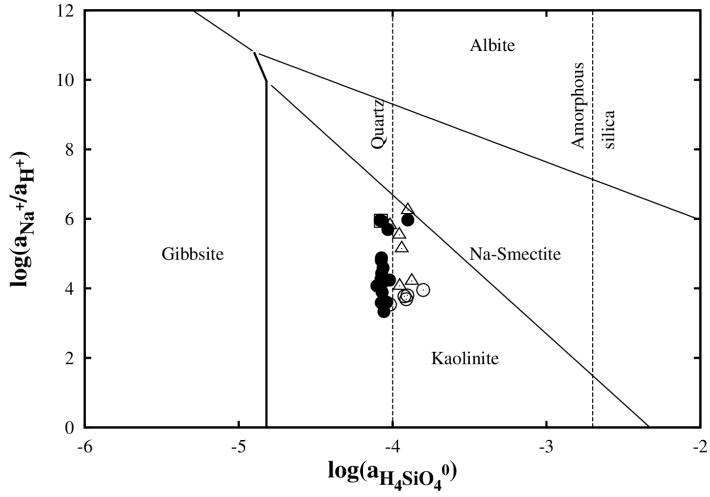

(c)

Figure 5.3: Stability diagrams for feldspar-clay mineral phases: (a) calcite, (b) potassic, and (c) sodic. Thermodynamic data from Tardy (1971) and Drever (1997).

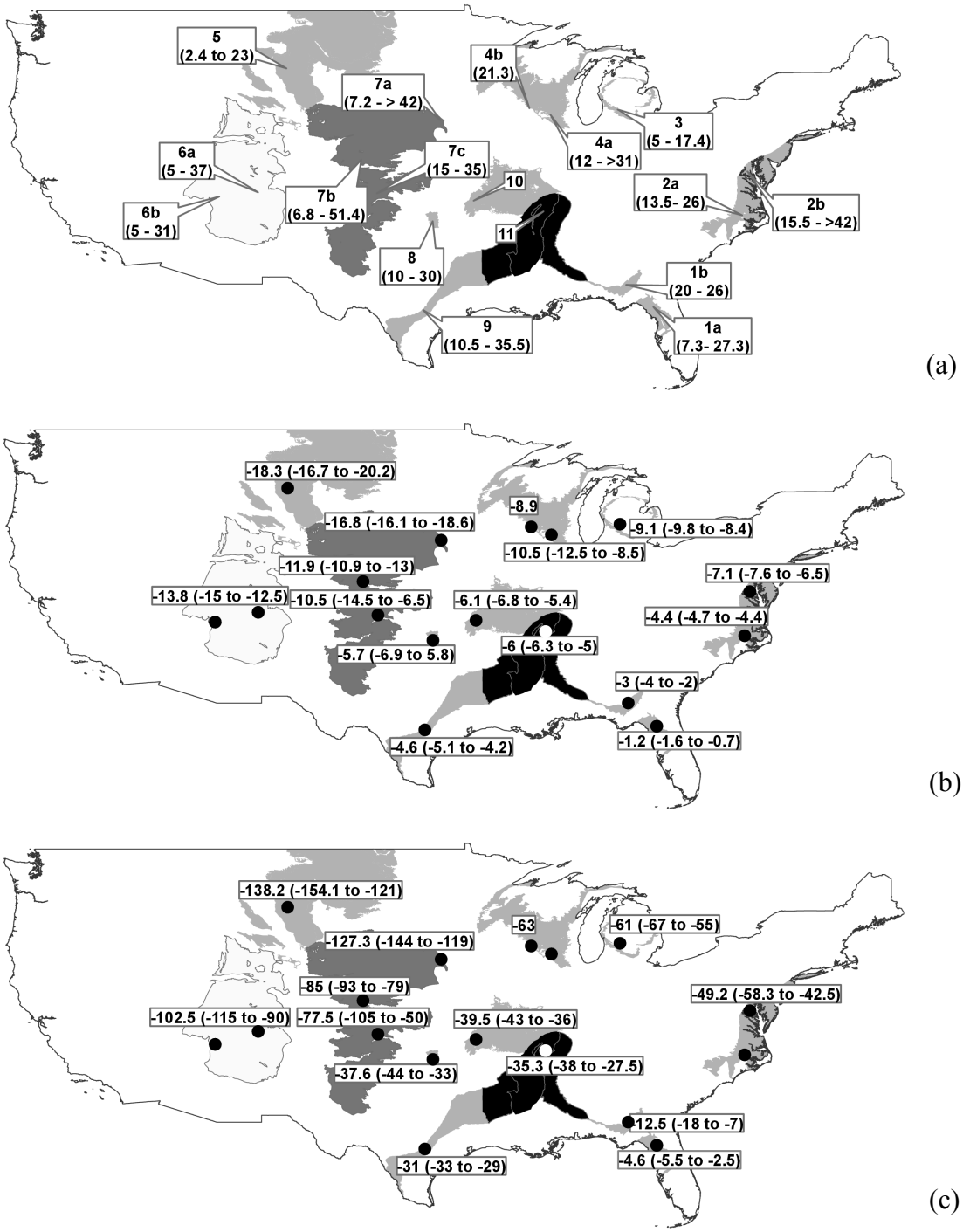

Figure 5.4: Maps showing published (a) paleorecharge dates determined using 14C-dating. Age values are given in 1000 years (in parenthesis). Alphanumeric IDs represent aquifer codes (see Table 2.3). Corresponding $\delta^{18}O$ and $\delta^{2}H$ are shown in (b) and (c), respectively. Values for ^{18}O and ^{2}H were selected for the age range between ~10 ka and 30 ka. See Table 4.1 for map legend and references.

Appendix A

Table A.1: Location, depth, and water level of sampled wells.

ID	USGS-ID	Town	County/State	Sampling Date (mm/dd/yy)	Longitude	Latitude	Alt. (masl[a])	Depth (m)	WL[b] (m)	Dist.[c] (km)
Unconfined Wilcox										
1	MO4010160108	Charleston	Mississippi/MO	07/07/06	-89.34156	36.91213	97.5	116.7	4.3	23
2	MO4010876101	Wyatt	Mississippi/MO	07/07/06	-89.22258	36.91185	96.6	141.7	5.2	18
3	MO4010743106	Sikeston	Scott/MO	07/09/06	-89.58370	36.87954	99.7	123.1	19.8	37
4	MO4010235110	East Prairie	Mississippi/MO	07/08/06	-89.38017	36.77157	93.0	182.9	3.7	44
5	MO4010626103	Parma	New Madrid/MO	07/09/06	-89.81567	36.61279	86.3	144.8	3.7	83
Confined Wilcox										
6	MO4010354108	Hayti	Pemiscot/MO	07/10/06	-89.75050	36.24502	82.3	395.6	4.9	124
7	MO4010143109	Caruthersville	Pemiscot/MO	05/29/07	-89.67190	36.15632	80.8	414.2	5.5	129
8	MO4024448105	Pemiscot	Pemiscot/MO	07/10/06	-89.91543	36.04437	75.0	411.5	5.2	154
9	355323089552101	Dogwood	Mississippi/AR	07/11/06	-89.92259	35.88980	76.2	426.7	4.8	173
10	355252090095701	Manila	Mississippi/AR	07/11/06	-90.16432	35.88488	73.2	353.0	7.3	184
11	AR6160?	Little River	Mississippi/AR	07/13/06	-90.23333	35.69583	70.1	426.7	NA[d]	209
12	354033090055201	Keiser	Mississippi/AR	07/13/06	-90.09675	35.67577	70.1	442.6	5.8	207
13	353917089561501	Osceola	Mississippi/AR	05/30/07	-89.93832	35.65468	74.7	457.2	12.0	202
14	353629090195501	Lepanto	Poinsett/AR	07/12/06	-90.33316	35.60647	65.8	443.8	5.3	221
15	353216090074001	Joiner	Mississippi/AR	07/15/06	-90.15000	35.50833	72.2	481.6	11.0	223
16	352238090151801	Gilmore	Crittenden/AR	07/15/06	-90.27889	35.41083	67.1	460.6	7.3	237

Continued on next page

Table A.1: Continued

ID	USGS-ID	Town	County/State	Sampling Date (mm/dd/yy)	Longitude	Latitude	Alt. (masl[a])	Depth (m)	WL[b] (m)	Dist.[c] (km)
17	351614090275401	Earle	Crittenden/AR	07/14/06	-90.46458	35.27069	65.5	518.2	8.7	258
18	AR6541?	Shell Lake	St Francis/AR	05/31/07	-90.48389	35.12528	60.7	483.1	NA	271
19	345705090284201	Hughes	St Francis/AR	07/14/06	-90.47493	34.95326	61.6	487.7	15.4	288
20	345448090182701	Horseshoe Lake	Crittenden/AR	06/01/07	-90.30775	34.91349	61.3	499.3	9.7	285
21	345416090313801	Brickeys	Lee/AR	06/01/07	-90.52663	34.90369	59.7	487.7	13.5	294
Memphis Sand										
22	352231090421501	Vandale-Birdeye	Cross/AR	05/30/07	-90.70514	35.37552	130.8	319.7	77.4	255
23	351544090334101	Parkin	Cross/AR	05/31/07	-90.55829	35.26059	63.7	182.9	9.5	262
Sparta Sand										
24	344631090455801	Marianna	Lee/AR	06/04/07	-90.76611	34.77472	70.1	149.7	?	315
25	343324090544601	Marvell	Phillips/AR	06/05/07	-90.91539	34.55676	64.3	179.8	20.5	340
26	343242090390201	West Helena	Phillips/AR	06/04/07	-90.65194	34.54524	76.2	184.7	33.1	334
27	341822090512401	Elaine	Phillips/AR	06/05/07	-90.85597	34.30672	50.6	283.8	9.7	363
McNairy										
28	4010490108	Malden	Dunklin/MO	05/29/07	-89.96860	36.55307	85.3	275.8	2.7	99

[a] meters above sea level; [b] water level measurements from Schrader (2007); [c] distance from recharge area (see Figure 3.2); [d] data not available

Table A.2: Field measured parameters and major ion concentrations of sampled wells.

ID	Temp	Cond	pH	Eh	O_2	HCO_3^-	CO_3^{2-}	F^-	Cl^-	Br^-	SO_4^{2-}	Ca^{2+}	Mg^{2+}	Na^+	K^+
	°C	µS/cm		mV	mg/L	mg/L	mg/L	mg/L	mg/L	mg/L	mg/L	mg/L	mg/L	mg/L	mg/L
DL[a]								0.02	0.10	0.01	0.10	0.10	0.10	0.10	0.10
Unconfined Wilcox															
1	17.1	198	7.35	-64.7	1.00	113.7	0.1	0.20	0.90	–	3.37	26.31	6.39	5.32	3.11
2	19.0	534	6.98	0.0	0.26	353.8	0.3	0.27	1.52	–	13.33	70.47	19.21	9.09	4.03
3	16.5	379	7.21	-82.4	0.60	197.3	0.2	0.24	8.96	–	29.37	53.78	11.61	9.16	3.60
4	16.9	233	7.66	-147.8	0.54	139.2	0.3	0.12	0.43	–	2.48	36.37	6.93	4.83	2.94
5	19.2	341	7.18	-30.2	0.46	217.0	0.2	0.20	1.26	–	4.95	46.58	10.74	10.29	3.55
Confined Wilcox															
6	24.4	234	6.45	32.2	0.74	121.4	0.0	0.10	1.14	–	19.42	5.68	2.1	34.58	5.77
7	27.8	175	6.30	103.3	0.96	82.0	0.0	0.07	1.17	–	13.17	6.74	1.36	26.26	4.37
8	25.0	188	6.58	6.0	0.62	102.9	0.0	0.09	1.96	–	10.44	6.51	2.21	24.66	5.24
9	24.8	208	6.81	-89.9	0.56	113.9	0.1	0.08	0.78	–	13.30	7.35	2.22	29.15	4.77
10	23.9	187	6.96	-71.3	0.74	104.0	0.1	0.11	1.52	–	10.38	3.39	0.94	31.57	3.92
11	25.2	207	7.05	-102.1	0.52	128.5	0.2	0.13	3.45	–	6.46	2.41	0.55	40.22	3.60
12	24.2	181	7.04	-75.5	0.62	102.7	1.7	0.12	1.31	–	5.48	3.09	0.75	33.02	3.66
13	25.6	197	6.97	-42.6	0.80	105.3	0.1	0.09	1.06	–	4.90	5.28	0.54	45.16	3.09
14	25.0	187	7.61	-149.0	0.62	111.2	0.5	0.11	1.66	–	5.59	1.41	0.42	38.13	3.06
15	25.9	215	7.66	-120.6	0.58	127.1	0.2	0.10	0.58	–	5.71	3.46	0.84	40.10	3.65
16	27.3	171	7.40	-116.5	0.78	108.8	0.1	0.12	1.69	–	3.06	0.84	0.18	37.59	2.90

Continued on next page

Table A.2: Continued

ID	Temp	Cond	pH	Eh	O_2	HCO_3^-	CO_3^{2-}	F^-	Cl^-	Br^-	SO_4^{2-}	Ca^{2+}	Mg^{2+}	Na^+	K^+
	°C	µS/cm		mV	mg/L	mg/L	mg/L	mg/L	mg/L	mg/L	mg/L	mg/L	mg/L	mg/L	mg/L
DL								0.02	0.10	0.01	0.10	0.10	0.10	0.10	0.10
17	26.7	172	7.25	-111.1	0.52	105.8	0.4	0.13	2.15	–	2.66	0.75	0.15	36.74	2.86
18	27.4	200	8.36	-9.9	1.80	116.4	1.2	0.11	2.19	–	0.16	0.75	<0.10	52.37	0.79
19	26.9	205	8.67	-125.3	0.60	113.6	2.5	0.12	5.14	–	2.88	0.14	<0.10	43.50	2.67
20	27.7	197	8.64	-79.5	0.82	106.9	2.2	0.10	2.75	–	0.59	0.33	<0.10	50.61	0.78
21	27.6	262	8.53	-149.0	0.70	136.6	2.7	0.52	7.07	–	<0.10	2.38	<0.10	67.25	1.00
Memphis Sand															
22	22.0	528	7.12	-50.8	0.92	308.2	0.3	0.13	2.90	–	6.51	29.14	17.37	31.05	2.43
23	20.7	235	7.09	-16.6	0.96	131.0	0.1	0.09	2.30	–	1.18	15.98	4.49	23.16	5.99
Sparta Sand															
24	21.8	1692	7.46	-63.6	0.86	404.4	0.8	0.23	311.18	–	<0.10	22.58	8.82	313.81	8.17
25	20.5	904	7.88	36.0	0.44	486.8	2.1	0.38	39.03	–	<0.10	5.21	0.17	218.24	4.54
26	21.0	981	7.31	-75.0	0.42	432.0	0.6	0.04	83.30	–	<0.10	18.93	6.28	174.47	8.12
27	22.9	1250	8.25	-93.4	0.34	431.7	4.4	0.21	161.34	–	<0.10	1.87	<0.10	252.44	2.88
McNairy															
28	23.6	945	8.08	-35.4	0.98	227.1	1.4	0.15	157.18	–	16.67	14.94	3.64	186.13	6.99

[a] Detection limit

Table A.3: Trace solutes, dissolved methane and stable isotope compositions of groundwater samples.

ID	Fe^{2+}	Fe_{tot}	Mn_{tot}	Si	Sr^{2+}	HS^-	CH_4	NH_4	TOC	$\delta^{13}C$	$\delta^{34}S$	$\delta^{18}O$	$\delta^{2}H$
	mg/L	mg/L	mg/L	mg/L	mg/L	mg/L	µg/L	mg/L		‰	‰	‰	‰
DL[a]	0.1	0.10	0.01	0.10	0.10	–	0.10	0.02	0.5	±0.3	±0.15	±0.08	±0.9
Unconfined Wilcox													
1	1.0	0.99	0.06	7.38	0.15	–	0.79	0.12	NA[b]	-9.08	–	-6.05	-36.18
2	2.0	1.41	0.18	5.77	0.62	–	0.73	0.26	<0.5	-8.49	–	-5.90	-35.94
3	2.0	1.77	0.23	7.16	0.39	–	1.06	0.14	1.7	-9.71	–	-6.11	-36.97
4	2.0	1.49	0.22	9.54	0.16	–	0.74	0.11	0.5	-8.56	–	-5.91	-35.15
5	2.0	1.16	0.40	7.50	0.17	–	0.28	0.15	0.7	-11.52	–	-5.51	-33.13
Confined Wilcox													
6	3.0	3.05	<0.01	5.49	0.24	–	0.03	0.22	<0.5	-10.45	–	-6.79	-41.31
7	3.0	2.82	<0.01	5.27	<0.10	–	1.39	0.34	<0.5	-11.68	22.2	-6.82	-39.41
8	3.0	3.29	0.03	5.07	0.30	–	0.34	0.18	<0.5	-9.08	–	-6.36	-37.82
9	3.0	2.98	0.05	5.14	0.33	–	0.35	0.26	<0.5	-8.01	–	-6.24	-36.94
10	2.0	1.15	<0.01	4.75	0.14	–	0.30	0.20	<0.5	-8.32	–	-6.34	-35.70
11	0.8	0.63	<0.01	5.06	<0.10	–	0.54	0.25	<0.5	-12.38	–	-6.04	-34.90
12	1.0	0.85	<0.01	5.20	0.12	–	–	0.16	<0.5	-11.55	–	-5.99	-35.18
13	0.2	1.60	<0.01	5.74	<0.10	–	0.42	0.38	<0.5	-10.92	37.8	-6.29	-35.33
14	0.2	<0.10	<0.01	5.10	<0.10	–	0.62	0.16	<0.5	-10.02	–	-5.94	-34.16
15	0.6	0.41	<0.01	5.12	0.15	–	0.44	0.24	<0.5	-10.79	–	-6.06	-35.49
16	0.4	0.20	<0.01	5.23	<0.10	–	2.04	0.19	<0.5	-9.03	–	-5.93	-34.12
17	0.2	<0.10	<0.01	5.11	<0.10	–	2.96	0.18	<0.5	-9.08	–	-5.90	-33.74
18	<0.1	<0.10	<0.10	5.81	<0.10	0.2	2.22	0.43	<0.5	-11.06	77.3	-5.92	-33.60
19	<0.1	<0.10	<0.10	5.56	<0.10	–	10.54	0.18	<0.5	-7.62	–	-5.71	-33.06
20	<0.1	<0.10	<0.10	5.35	<0.10	0.05	3.50	0.44	<0.5	-11.01	–	-5.86	-32.74
21	<0.1	<0.10	<0.10	7.97	<0.10	0.05	10.55	0.50	<0.5	-7.26	–	-5.87	-35.15

Continued on next page

ID	Fe^{2+}	Fe_{tot}	Mn_{tot}	Si	Sr^{2+}	HS^-	CH_4	NH_4	TOC	$\delta^{13}C$	$\delta^{34}S$	$\delta^{18}O$	$\delta^{2}H$
	mg/L	mg/L	mg/L	mg/L	mg/L	mg/L	µg/L	mg/L		‰	‰	‰	‰
DL[a]	0.1	0.10	0.01	0.10	0.10	–	0.10	0.02	0.5	±0.3	±0.15		
Memphis Sand													
22	1.0	0.92	<0.10	8.01	<0.10	–	0.57	0.43	<0.5	-10.86	4.1	-5.91	-33.15
23	1.0	1.03	<0.10	6.69	0.66	–	0.49	0.52	<0.5	-9.77	14.5	-6.04	-34.57
Sparta Sand													
24	0.7	0.49	<0.10	6.63	1.38	–	435.99	1.37	0.8	-6.89	–	-5.54	-31.45
25	0.2	<0.10	<0.10	5.82	<0.10	–	264.84	1.42	0.9	-11.4	–	-5.50	-31.15
26	1.0	0.92	<0.10	6.88	1.05	–	292.28	1.88	0.8	-8.73	–	-5.14	-28.07
27	<0.1	<0.10	<0.10	7.72	<0.10	–	341.71	1.06	1.9	-7.83	–	-5.10	-28.69
McNairy													
28	0.2	<0.10	<0.10	5.13	0.40	–	0.62	0.89	<0.5	-11.4	42.5	-6.14	-32.45

[a] Detection limit, for stable isotopes reported as standard deviation 1σ; [b] not analyzed

Table A.4: Calculated saturation indices of minerals that may control the groundwater chemistry.

ID	%err[a]	$CO_{2(g)}$	Calcite	Dolomite	Anhydrite	Gypsum	$Fe(OH)_{3(a)}$	Goethite	Siderite	Pyrite	Halite	Chalcedony	$SiO_{2(a)}$
Unconfined Wilcox													
1	5.5	-2.34	-0.67	-1.71	-3.56	-3.31	-2.08	3.52	0.10	–	-9.85	-0.27	-1.13
2	-4.0	-1.48	-0.18	-0.66	-2.70	-2.46	-2.03	3.64	0.25	–	-9.42	-0.39	-1.25
3	1.2	-1.98	-0.33	-1.09	-2.42	-2.17	-2.63	2.95	0.36	–	-8.63	-0.27	-1.14
4	7.6	-2.57	-0.15	-0.79	-3.58	-3.33	-2.51	3.08	0.63	–	-10.21	-0.15	-1.02
5	1.3	-1.89	-0.32	-1.01	-3.22	-2.99	-1.94	3.74	0.24	–	-9.43	-0.28	-1.14
Confined Wilcox													
6	-4.3	-1.36	-2.10	-4.30	-3.42	-3.20	-2.51	3.36	-0.16	–	-8.95	-0.48	-1.32
7	4.9	-1.36	-2.28	-4.88	-3.47	-3.26	-1.68	4.31	-0.43	–	-9.06	-0.54	-1.37
8	-3.1	-1.56	-1.96	-4.04	-3.61	-3.39	-2.45	3.44	-0.04	–	-8.86	-0.52	-1.36
9	-2.4	-1.75	-1.64	-3.46	-3.46	-3.24	-3.42	2.46	0.18	–	-9.18	-0.51	-1.35
10	-5.2	-1.94	-1.87	-3.96	-3.88	-3.66	-3.10	2.76	-0.13	–	-8.85	-0.54	-1.38
11	-6.9	-1.93	-1.82	-3.94	-4.24	-4.02	-3.57	2.32	-0.20	–	-8.40	-0.53	-1.36
12	-1.5	-2.02	-1.83	-3.93	-4.19	-3.97	-3.08	2.79	-0.17	–	-8.90	-0.50	-1.34
13	13.3	-1.93	-1.64	-3.92	-4.02	-3.80	-2.39	3.53	0.05	–	-8.86	-0.48	-1.31
14	-3.7	-2.55	-1.55	-3.29	-4.52	-4.30	–	–	–	–	-8.74	-0.52	-1.36
15	-2.6	-2.54	-1.05	-2.36	-4.13	-3.92	-2.24	3.68	0.20	–	-9.18	-0.53	-1.37
16	-3.2	-2.34	-1.96	-4.22	-4.99	-4.78	-3.26	2.71	-0.38	–	-8.74	-0.54	-1.37
17	-3.5	-2.20	-2.18	-4.69	-5.10	-4.88	–	–	–	–	-8.64	-0.54	-1.37
18	8.8	-3.28	-1.05	–	-6.34	-6.13	–	–	–	–	-8.48	-0.51	-1.34

Continued on next page

Table A.4: Continued

ID	%err[a]	$CO_{2(g)}$	Calcite	Dolomite	Anhydrite	Gypsum	$Fe(OH)_{3(a)}$	Goethite	Siderite	Pyrite	Halite	Chalcedony	$SiO_{2(a)}$
19	-2.4	-3.62	-1.51	–	-5.82	-5.61	–	–	–	–	-8.19	-0.54	-1.37
20	10.2	-3.61	-1.18	–	-6.13	-5.92	–	–	–	–	-8.40	-0.56	-1.39
21	11.4	-3.39	-0.34	–	–	–	–	–	–	–	-7.87	-0.38	-1.21
Memphis Sand													
22	-9.8	-1.66	-0.41	-0.74	-3.32	-3.09	-2.60	3.19	0.22	–	-8.60	-0.29	-1.14
23	3.6	-1.99	-1.03	-2.31	-4.21	-3.97	-1.95	3.78	-0.02	–	-8.81	-0.35	-1.21
Sparta Sand													
24	1.4	-1.90	-0.16	-0.41	–	–	-2.16	3.62	0.29	–	-5.61	-0.37	-1.22
25	4.6	-2.24	-0.27	-1.74	–	–	–	–	–	–	-6.64	-0.41	-1.27
26	-0.1	-1.71	-0.32	-0.82	–	–	-2.53	3.22	0.46	–	-6.41	-0.34	-1.20
27	-1.9	-2.65	-0.40	–	–	–	–	–	–	–	-5.97	-0.33	-1.17
McNairy													
28	4.5	-2.75	0.10	-0.08	-3.23	-3.01	–	–	–	–	-6.11	-0.51	-1.35

[a] Charge-balance error in percent

Table A.5: Summary of calculated mass transfer amounts. Mass transfer amounts reported in this table correspond to model outputs with dilution factor of 1.0 between initial and final wells.

Model ID	Initial well	Final well	No. of models	CH_2O	Calcite	Dolomite	Siderite	$Fe(OH)_{3(a)}$	Pyrite	NaCl	Anhydrite	CaX_2	MgX_2	NaX	KX
1	1	3	7	0.00	0.04	0.23	1.07	-0.98	-0.07	0.23	0.41	0.02	0.00	-0.06	0.01
2	4	6	3	1.44	0.00	0.26	0.44	0.00	-0.41	0.02	0.99	-1.10	0.39	1.35	0.07
3	6	7	1	50.00	0.22	0.18	-0.52	0.54	-0.03	0.00	0.00	0.30	-0.03	-0.49	-0.04
4	6	8	1	50.00	0.37	0.16	-0.84	0.89	-0.04	0.02	0.00	0.25	0.00	-0.49	-0.01
5	7	8	2	0.16	0.05	0.00	-0.33	0.35	-0.02	0.02	0.00	-0.05	0.03	0.00	0.02
6	9	12	1	0.29	0.00	0.00	-0.60	0.60	-0.04	0.01	0.00	-0.05	0.00	0.14	-0.03
7	9	13	2	0.19	0.02	0.00	-0.21	0.23	-0.04	0.01	0.00	-0.10	-0.07	0.38	-0.04
8	10	11	6	0.32	0.00	0.00	0.08	0.00	-0.09	0.05	0.15	-0.17	-0.02	0.38	-0.01
9	14	16	5	0.04	0.00	0.00	0.02	0.00	-0.02	0.00	0.00	0.01	0.01	-0.03	-0.01
10	15	16	1	40.00	0.08	0.05	-0.15	0.16	-0.01	0.03	0.00	0.10	-0.03	-0.13	-0.02
11	16	19	2	0.06	0.05	0.00	-0.21	0.20	-0.01	0.10	0.00	-0.07	-0.01	0.15	-0.01
12	16	20	2	0.09	0.07	0.00	-0.17	0.18	-0.01	0.03	0.00	-0.08	-0.01	0.23	-0.05
13	16	21	4	0.27	0.23	0.00	0.07	0.00	-0.08	0.15	0.12	-0.33	-0.01	0.72	-0.05
14	17	18	3	0.00	0.17	0.00	0.02	0.00	-0.02	0.00	0.00	-0.17	-0.01	0.41	-0.05
15	17	19	2	0.21	0.00	0.00	-0.30	0.35	-0.04	0.09	0.08	-0.09	-0.01	0.20	0.00
16	17	20	2	0.07	0.10	0.00	-0.18	0.19	-0.01	0.02	0.00	-0.11	-0.01	0.28	-0.06
17	18	19	3	0.00	0.00	0.00	-0.10	0.08	0.01	0.07	0.00	-0.02	0.00	0.00	0.04
18	18	21	5	0.25	0.00	0.04	0.07	0.00	-0.07	0.14	0.14	-0.15	-0.04	0.36	0.01
19	19	21	5	0.48	0.07	0.00	0.14	0.00	-0.14	0.05	0.24	-0.26	0.00	0.57	-0.04
20	20	21	5	0.42	0.06	0.00	0.12	0.00	-0.12	0.12	0.23	-0.25	0.00	0.49	0.01

Mole transfer amounts are reported in mmol/L; positive (+) sign indicates dissolution, and negative (-) sign indicates precipitation of mineral phases

Table A.6: Deuterium and ^{18}O amounts in rainwater.

No	Sample ID	Rainfall Events		Precip.[a]	$\delta^{18}O$[b]	$\delta^{18}O$[c]	$\delta^{2}H$
		From	To	cm	‰	‰	‰
1	TVA01/22/97	01-01-1997	01-21-1997	4.22	-8.01	-7.82	-41.86
2	TVA02/06/97	01-22-1997	02-05-1997	5.33	-8.45	-7.95	-50.44
	DOE02/06/97	01-22-1997	02-05-1997	5.33	-8.29	-7.64	-50.25
	Average					*-7.80*	*-50.35*
3	TVA03/07/97	02-06-1997	03-06-1997	23.27	-5.38	-4.60	-24.08
4	TVA03/26/97	03-07-1997	03-25-1997	5.79	-4.19	-3.50	-15.52
	DOE03/26/97	03-05-1997	03-25-1997	5.79	-4.64	-3.91	-16.90
	Average					*-3.71*	*-16.21*
5	TVA04/23/97	03-26-1997	04-22-1997	10.77	-6.10	-5.25	-27.10
	DOE04/23/97	03-26-1997	04-22-1997	10.77	-5.26	-5.02	-24.61
	Average					*-5.14*	*-25.86*
6	DOE05/20/97	04-23-1997	05-19-1997	16.41	-4.44	-4.00	-20.73
	TVA05/22/97	04-23-1997	05-21-1997	16.41	-6.51	-6.14	-36.41
	Average					*-5.07*	*-28.57*
7	DOE06/02/97	05-20-1997	06-01-1997	8.08	-8.79	-8.45	-55.74
8	DOE06/24/97	06-02-1997	06-23-1997	8.15	-6.44	-6.13	-37.81
9	TVA08/20/97	06-24-1997	08-19-1997	19.58	-4.06	-3.15	-14.55
	DOE08/20/97	06-24-1997	08-19-1997	19.58	-2.94	-2.41	-9.95
	Average					*-2.78*	*-12.25*
10	TVA10/16/97	08-20-1997	10-15-1997	9.22	NA	-4.27	-21.12
	DOE10/16/97	08-20-1997	10-15-1997	9.22	NA	-4.54	-21.33
	Average					*-4.41*	*-21.23*
11	TVA12/01/97	10-16-1997	11-30-1997	8.84	NA	-10.44	-67.2
	DOE12/01/97	10-16-1997	11-30-1997	8.84	NA	-10.42	-67.62
	Average					*-10.43*	*-67.41*
12	TVA01/11/98	12-01-1997	01-10-1998	11.99	-10.36	-9.52	-63.74
	DOE01/12/98	12-01-1997	01-11-1998	12.04	-10.43	-10.29	-65.79
	Average					*-9.91*	*-64.77*
	VWM[c]					**-5.80**	**-33.39**

[a] cumulative precipitation during sampling intervals; [b] measured at the University of Georgia (January-February 1998); [b] measured at the University of Arizona (July 2007); [c] volume weighted mean; TVA = Tennessee Valley Authority Shawnee Plant (long. 88.79E, lat. 37.16N); DOE = U S Department of Energy Paducah Gaseous Diffusion Plant (long. 88.82E, lat. 37.11N)

Appendix B

Table B.1: Water level data used to create potentiometric surface map. Data collected by Schrader (2007).

Index	Station	Lat.	Long.	Elev.	Well depth	Water depth	Date
				m	m	m	
Clay County							
1	20N07E01CBB1	36.3964	-90.2842	140.2	61.0	28.1	03/07/2006
2	21N08E14CBB1	36.4544	-90.1906	115.8	47.9	25.5	03/07/2006
Craighead County							
3	13N07E14BBA2	35.7572	-90.3197	67.4	313.3	8.2	03/08/2006
4	14N05E25DCB1	35.8119	-90.5081	71.0	271.3	12.9	03/08/2006
5	14N05E34DDD1	35.7936	-90.5358	69.8	266.4	12.6	03/08/2006
6	14N06E27ACB2	35.8161	-90.4369	69.2	304.5	9.4	03/08/2006
7	14N07E17DCB1	35.8356	-90.3672	70.7	326.1	10.8	03/08/2006
8	15N07E33BAD1	35.8875	-90.3519	70.7	315.2	8.5	03/08/2006
Crittenden County							
9	04N07E36ADB1	34.9136	-90.3078	61.3	499.3	18.0	03/09/2006
10	05N07E29ACC1	35.0247	-90.3736	61.0	518.2	18.8	03/09/2006
11	06N07E01ABB1	35.0889	-90.3019	63.1	469.7	20.1	03/09/2006
12	06N09E07CAC1	35.1519	-90.1783	64.0	448.1	27.6	03/09/2006
13	07N07E14CCC1	35.2217	-90.3250	68.0	482.8	21.0	03/09/2006
14	07N08E24CAB1	35.2106	-90.1967	67.4	469.4	20.8	03/09/2006
15	08N06E33CBD1	35.2706	-90.4644	65.5	533.4	16.4	03/09/2006
16	09N08E29ADD1	35.3736	-90.2544	68.6	476.7	17.1	03/09/2006
Greene County							
17	16N05E13BAB1	36.0231	-90.5072	88.4	166.1	30.3	03/07/2006
18	17N04E36BCA1	36.0633	-90.6161	153.9	94.8	46.5	03/07/2006
19	17N06E31DCB1	36.0578	-90.4839	86.9	140.8	31.7	03/07/2006
20	18N06E10DCD1	36.2025	-90.4222	97.5	36.6	7.2	03/07/2006

Continued on next page

Table B.1: Continued

Index	Station	Lat.	Long.	Elev. m	Well m	Water m	Date
Lee County							
21	01N04E09DCC1	34.7025	-90.7056	62.2	574.5	19.1	03/09/2006
22	03N05E01BAB1	34.9036	-90.5267	59.7	518.8	15.6	03/09/2006
Mississippi County							
23	10N08E17ADD1	35.4897	-90.2514	68.6	463.6	16.0	03/08/2006
24	11N08E10AAC2	35.5939	-90.2169	67.1	420.6	12.2	03/08/2006
25	11N09E33AAB1	35.5372	-90.1275	72.2	475.5	15.9	03/08/2006
26	11N10E20ADA1	35.5636	-90.0369	71.6	431.9	14.3	03/08/2006
27	12N09E11DBB1	35.6758	-90.0967	70.1	442.6	10.7	03/08/2006
28	12N11E17CDD1	35.6547	-89.9383	74.7	457.2	16.1	03/08/2006
29	13N11E08DDA1	35.7578	-89.9297	74.7	440.4	18.0	03/08/2006
30	13N11E31CCCC1	35.7058	-89.9686	73.5	457.2	16.3	03/08/2006
31	14N11E20CCA1	35.8164	-89.9406	73.2	462.7	11.5	03/08/2006
32	15N08E08DBC3	35.9353	-90.2575	72.5	323.1	7.8	03/08/2006
33	15N09E31ACD1	35.8850	-90.1644	73.2	353.0	12.4	03/08/2006
34	15N10E01ADC1	35.9533	-89.9683	75.6	411.5	12.2	03/08/2006
35	15N12E23DBC1	35.9072	-89.7836	72.5	454.5	17.2	03/08/2006
Poinsett County							
36	10N07E16CBB2	35.4903	-90.3581	66.4	457.2	15.6	03/07/2006
37	11N05E06CCD1	35.6061	-90.6050	65.2	302.4	13.0	03/07/2006
38	11N05E36AAA1	35.5428	-90.5025	65.2	358.1	11.4	03/07/2006
39	11N06E35CDA3	35.5311	-90.4222	65.5	396.5	9.3	03/07/2006
40	11N07E03BDD1	35.6081	-90.3319	65.8	443.8	12.5	03/07/2006
41	12N05E13BBB1	35.6772	-90.5164	67.7	326.4	14.4	03/07/2006
St. Francis County							
42	04N06E16CCB1	34.9533	-90.4750	61.6	492.3	16.6	03/09/2006
43	04N06E21BAD2	34.9469	-90.4708	61.3	530.4	18.8	03/09/2006

Table B.2: Depth to top of surface of individual layers used for BASIN2 modeling. Negative sign indicates above sea level. All units are in meters.

No	Midway (conf. unit)	Lower Wilcox	Middle Wilcox	Lower-middle Claiborne	M Claiborne (conf. unit)	Upper Claiborne	Alluv.
1	-122	-137	-137	-137	-137	-137	-137
2	-70	-86	-136	-136	-136	-136	-136
3	84	54	9	-101	-101	-101	-101
4	83	76	36	-112	-112	-112	-112
5	117	107	91	-75	-110	-110	-110
6	139	119	102	-72	-91	-114	-114
7	189	145	117	-44	-75	-91	-91
8	217	158	134	-28	-62	-62	-93
9	285	192	169	5	-27	-37	-90
10	312	209	185	17	-12	-35	-88
11	335	245	220	32	-11	-32	-86
12	350	255	223	40	-12	-32	-89
13	395	279	237	60	-1	-33	-89
14	392	300	238	61	11	-34	-83
15	370	289	226	44	10	-40	-81
16	372	290	226	40	9	-43	-79
17	356	298	223	45	16	-38	-79
18	359	309	224	43	14	-35	-78
19	379	327	241	32	7	-30	-73
20	393	333	251	31	3	-28	-76
21	432	345	265	43	7	-28	-66
22	439	352	266	42	7	-29	-72
23	459	366	274	35	6	-24	-66
24	477	374	281	38	8	-20	-69
25	507	386	280	38	7	-24	-63
26	519	391	274	44	12	-27	-67
27	528	417	271	64	26	-22	-64
28	542	414	281	64	25	-24	-61
29	536	419	292	57	21	-26	-63
30	529	426	295	62	26	-21	-61
31	522	454	315	63	26	-14	-62

Continued on next page

B.2: Continued

No	Midway (conf. unit)	Lower Wilcox	Middle Wilcox	Lower-middle Claiborne	M Claiborne (conf. unit)	Upper Claiborne	Alluv.
32	519	471	320	61	24	-13	-57
33	537	486	341	44	12	-9	-56
34	565	490	357	41	7	-13	-52
35	615	508	360	48	9	-26	-58
36	661	530	378	69	29	-17	-56
37	704	539	385	60	31	-2	-54
38	719	554	395	52	29	6	-52
39	750	603	439	65	35	7	-50
40	761	623	452	76	46	9	-48

References

Aeschbach-Hertig, W., Stute, M., Clark, J. F., Reuter, R. F., Schlosser, P., 2002. A paleotemperature record derived from dissolved noble gases in groundwater of the Aquia Aquifer (Maryland, USA). Geochim. Cosmochim. Acta 66, 797–817.

Andrews, J. N., Fontes, J. C., Michelot, J. L., Elmore, D., 1986. In-situ neutron flux, Cl production and groundwater evolution in crystalline rocks at Stripa, Sweden. Earth Planet. Sci. Lett. 77, 49–58.

APHA, 1992. Standard Methods for the Examination of Water and Wastewater. American Public Health Association, 18th edition, method 4500-NH-C, pp. 4–78.

APHA, 1995a. Standard Methods for the Examination of Water and Wastewater. American Public Health Association, 19th edition, method 4500-NO-E, pp. 4–87.

APHA, 1995b. Standard Methods for the Examination of Water and Wastewater. American Public Health Association, 19th edition, method 4500-NO-B, pp. 4–85.

APHA, 1995c. Standard Methods for the Examination of Water and Wastewater. American Public Health Association, 19th edition, method 4500-S-D, pp. 4–124.

Appelo, C., 1994. Cation and proton exchange, pH variations, and carbonate reactions in a freshening aquifer. Water Resour. Res. 30, 2793–2805.

Appelo, C. A. J., Postma, D., 1999. Geochemistry, Groundwater and Pollution. Balkema, Rotterdam, 536 p.

Arthur, J. K., Taylor, R. E., 1986. Mississippi Embayment aquifer system in Mississippi: Geohydrologic data compilation for flow model simulation. Water Resour. Bull. 22, 1021–1029.

Arthur, K. J., Taylor, R. E., 1998. Ground-water flow analysis of the Mississippi Embayment aquifer system, south-central United States. U.S. Geological Survey, Professional Paper 1416-I.

Bentley, H. W., Phillips, F. M., Davis, S. N., Habermehl, M. A., Airey, P. L., Calf, G. E., Elmore, D., Gove, H. E., Torgersen, T., 1986. Chlorine 36 dating of very old groundwater: 1. The Great Artesian Basin, Australia. Water Resour. Res. 22, 1991–2001.

Bethke, C. M., 1985. A numerical model of compaction-driven groundwater flow and heat transfer and its application to the paleohydrology of intracratonic sedimentary basins. J. Geophys. Res. 90, 6817–6828.

Bethke, C. M., Lee, M., Park, J., 2002. A guide to using the BASIN2 software package: Basin modeling with BASIN2 - Release 5.0. Hydrogeology Program - University of Illinois, Champaign.

Boghici, R., 2008. The Carrizo-Wilcox aquifer of Texas: Groundwater chemistry, origin, and ages. Gulf Coast Association of Geological Societies Transactions 58, 105–123.

Böttcher, J., Strebel, O., Voerkelius, S., Schmidt, H. L., 1990. Using isotope fractionation of

nitrate-nitrogen and nitrate-oxygen for evaluation of microbial denitrification in a sandy aquifer. J. Hydrol. 114, 413–424.

Brahana, J. V., Mesko, T. O., Busby, J. F., Kraemer, T. F., 1985. Ground-water quality data from the northern Mississippi Embayment; Arkansas, Missouri, Kentucky, Tennessee, and Mississippi. U.S. Geological Survey, Open-File Report 85-683.

Carmody, R. W., Plummer, L. N., Busenberg, E., Coplen, T. B., 1998. Methods for collection of dissolved sulfate and sulfide and analysis of their sulfur isotopic composition. U.S. Geological Survey, Open-File Report 97-234.

Castro, M. C., Goblet, P., 2003a. Calibration of regional groundwater flow models: Working toward a better understanding of site-specific systems. Water Resour. Res. 39, 1172.

Castro, M. C., Goblet, P., 2003b. Noble gas thermometry and hydrologic ages: evidence for late Holocene warming in Southwest Texas. Geophys. Res. Lett. 30, 2251.

Castro, M. C., Goblet, P., 2005. Calculation of groundwater ages—a comparative analysis. Ground Water 43, 368–380.

Cederstrom, D. J., 1946. Genesis of ground waters in the coastal plain of Virginia. Econ. Geol. 41, 218–245.

Chapelle, F. H., 1993. Ground-Water Microbiology and Geochemistry. John Wiley & Sons, New York, 424 p.

Chapelle, F. H., 2003. Geochemistry of groundwater. In: Drever, J. I. (Ed.), Surface and Ground Water, Weathering, and Soils. Treatise on Geochemistry, Vol. 5. Elsevier, Oxford, pp. 425–449.

Chapelle, F. H., Knobel, L. L., 1983. Aqueous geochemistry and the exchangeable cation composition of glauconite in the Aquia aquifer, Maryland. Ground Water 21, 343–352.

Chapelle, F. H., Knobel, L. L., 1985. Stable carbon isotopes of DIC in the Aquia aquifer, Maryland: Evidence for an isotopically heavy source of CO_2. Ground Water 23, 592–599.

Chapelle, F. H., McMahon, P. B., 1991. Geochemistry of dissolved inorganic carbon in a Coastal Plain aquifer: 1. Sulfate from confining beds as an oxidant in microbial CO_2 production. J. Hydrol. 127, 85–108.

Clark, B. R., Hart, R. M., 2009. The Mississippi Embayment Regional Aquifer Study (MERAS): Documentation of a groundwater-flow model constructed to assess water availability in the Mississippi Embayment. U.S. Geological Survey, Scientific Investigations Report 2009-5172.

Clark, J. F., Davisson, M. L., Hudson, G. B., Macfarlane, P. A., 1998. Noble gases, stable isotopes, and radiocarbon as tracers of flow in the Dakota aquifer, Colorado and Kansas. J. Hydrol. 211, 151–167.

Clark, J. F., Stute, M., Schlosser, P., Drenkard, S., 1997. A tracer study of the Floridan aquifer in southeastern Georgia: Implications for groundwater flow and paleoclimate. Water Resour. Res. 33, 281–289.

Cook, P. G., Böhlke, J. K., 2000. Determining timescale for groundwater flow and solute transport. In: Cook, P. G., Herczeg, A. L. (Eds.), Environmental Tracers in Subsurface Hydrology. Kluwer Academic Publishers, Boston, pp. 1–30.

Cook, P. G., Herczeg, A. L., 2000. Environmental Tracers in Subsurface Hydrology. Kluwer, Boston, 529 p.

Craig, H., 1961. Isotopic variations in meteoric waters. Science 133, 1702–1703.

Cushing, E. M., Boswell, E. H., Speer, P. R., Hosman, R. L., 1970. Water resources of the Mississippi embayment; availability of water in the Mississippi Embayment. U.S. Geological Survey, Professional Paper 448A.

Czarnecki, J. B., 2006. Simulation of various management scenarios of the Mississippi River Valley alluvial aquifer in Arkansas. U.S. Geological Survey, Scientific Investigations Report 2006-5052.

Dansgaard, W., 1964. Stable isotopes in precipitation. Tellus 16, 436–468.

Davis, S. N., Cecil, D. W., Zreda, M., Sharma, P., 1998. Chlorine-36 and the initial value problem. Hydrogeol. J. 6, 104–114.

Davis, S. N., Moysey, S., Cecil, D. W. L., Zreda, M., 2003. Chlorine-36 in groundwater of the United States: empirical data. Hydrogeol. J. 11, 217–227.

Desaulniers, D. E., Kaufmann, R. S., Cherry, J. A., Bentley, H. W., 1986. ^{37}Cl-^{35}Cl variations in a diffusion controlled groundwater system. Geochim. Cosmochim. Acta 50, 1757–1764.

Drever, J. I., 1997. The Geochemistry of Natural Waters, 3rd edition. Prentice Hall, Upper Saddle River, NJ, 436 p.

Dutton, A., Wilkinson, B. H., Welker, J. M., Bowen, G. J., Lohmann, K. C., 2005. Spatial distribution and seasonal variation in $^{18}O/^{16}O$ of modern precipitation and river water across the conterminous USA. Hydrol. Proc. 19, 4121–4146.

Dutton, A. R., 1995. Groundwater isotopic evidence for paleorecharge in US High Plains aquifers. Quaternary Res. 43, 221–231.

Dutton, A. R., Simpkins, W. W., 1986. Hydrogeochemistry and water resources of the Triassic lower Dockum Group in the Texas Panhandle and eastern New Mexico. Bureau of Economic Geology, University of Texas at Austin, Report of Investigations 161.

EPA, 1979. Methods for Chemical Analysis of Water and Wastes, method 376.2. U.S. Environmental Protection Agency, Washington, DC.

Faure, G., 1986. Principles of Isotope Geology, 2nd edition. John Wiley & Sons, Inc., New York, 589 p.

Fetter, C. W., 2001. Applied Hydrogeology, 4th edition. Prentice Hall, Upper Saddle River, NJ, 598 p.

Fillon, R. H., Lawless, P. N., Waterman, A. S., 2005. Paleocene-Eocene deposystems and evolution of the Gulf of Mexico basin petroleum system. Gulf Coast Association of

Geological Societies Transactions 55, 195–222.

Fogg, G. E., Kreitler, C. W., 1982. Ground-water hydraulics and hydrochemical facies in Eocene aquifers of the east Texas basin. Bureau of Economic Geology, University of Texas at Austin, Report of Investigations 127.

Fontes, J., Brissaud, I., Michelot, J., 1984. Hydrological implications of deep production of chlorine-36. Nucl. Instrum. Meth. B 5, 303–307.

Foster, M. D., 1950. The origin of high sodium bicarbonate waters in the Atlantic and Gulf Coastal Plains. Geochim. Cosmochim. Acta 1, 33–48.

Galloway, W. E., Bebout, D. G., Fisher, W. L., Dunlap, J. B., Cabrera-Castro, R., Lugo-Rivera, J. E., Scott, T. M., 1991. Cenozoic. In: Salvador, A. (Ed.), The Geology of North America: the Gulf of Mexico basin. Vol. J. Geological Society of America, Boulder, Colorado, pp. 245–324.

Gat, J. R., 1996. Oxygen and hydrogen isotopes in the hydrologic cycle. Annu. Rev. Earth Planet. Sci. 24, 225–262.

Geyh, M., 2001. Environmental Isotopes in the Hydrological Cycle: Principles and Applications. Volume IV: Groundwater. UNESCO/IAEA, 196 p.

Grubb, H. F., 1998. Summary of hydrology of the regional aquifer systems, Gulf Coastal Plain, south-central United States. U.S. Geological Survey, Professional Paper 1416-A.

Hart, R. M., Clark, B. R., 2008. Geophysical log database for the Mississippi Embayment Regional Aquifer Study (MERAS). U.S. Geological Survey, Scientific Investigations Report 2008-5192.

Hart, R. M., Clark, B. R., Bolyard, S. E., 2008. Digital surfaces and thicknesses of selected hydrogeologic units within the Mississippi Embayment Regional Aquifer Study (MERAS). U.S. Geological Survey, Scientific Investigations Report 2008-5098.

Heath, R. C., 1983. Basic ground-water hydrology. U.S. Geological Survey, Water Supply Paper 2220.

Hem, J. D., 1992. Study and interpretation of the chemical characteristics of natural water. U.S. Geological Survey, Water-Supply Paper 2254.

Hendry, M. J., Schwartz, F. W., 1990. The chemical evolution of ground water in the Milk River aquifer, Canada. Ground Water 28, 253–261.

Hosman, R. L., 1996. Regional stratigraphy and subsurface geology of Cenozoic deposits, Gulf Coastal Plain, south-central United States. U.S. Geological Survey, Professional Paper 1416-G.

Hosman, R. L., Long, A. T., Lambert, T. W., Jeffery, H. G., 1968. Water resources of the Mississippi embayment; Tertiary aquifers in the Mississippi embayment, with discussions of quality of the water. U.S. Geological Survey, Professional Paper 448-D.

Hosman, R. L., Weiss, J. S., 1991. Geohydrologic units of the Mississippi Embayment and Texas Coastal Uplands aquifer systems, south-central United States. U.S. Geological Survey,

Professional Paper 1416-B.

Hubbert, M. K., 1940. The theory of ground-water motion. J. Geol. 48, 785–944.

Jackson, S. T., Webb, R. S., Anderson, K. H., Overpeck, J. T., Webb III, T., Williams, J. W., Hansen, B. C. S., 2000. Vegetation and environment in eastern North America during the last glacial maximum. Quaternary Sci. Rev. 19, 489–508.

Kane, M. F., Hildenbrand, T. G., Hendricks, J. D., 1981. Model for the tectonic evolution of the Mississippi Embayment and its contemporary seismicity. Geology 9, 563–568.

Kennedy, C. D., Genereux, D. P., 2007. ^{14}C groundwater age and the importance of chemical fluxes across aquifer boundaries in confined Cretaceous aquifers of North Carolina, USA. Radiocarbon 49, 1181–1203.

Klump, S., Grundl, T., Purtschert, R., Kipfer, R., 2008. Groundwater and climate dynamics derived from noble gas, ^{14}C, and stable isotope data. Geology 36, 395–398.

LaBolle, E. M., Fogg, G. E., Eweis, J. B., 2006. Diffusive fractionation of ^{3}H and ^{3}He in groundwater and its impact on groundwater age estimates. Water Resour. Res. 42, W07202.

LaBolle, E. M., Fogg, G. E., Eweis, J. B., Gravner, J., Leaist, D. G., 2008. Isotopic fractionation by diffusion in groundwater. Water Resour. Res. 44, W07405.

Lee, M. -K., Griffin, J., Saunders, J., Wang, Y., Jean, J. S., 2007. Reactive transport of trace elements and isotopes in the Eutaw coastal plain aquifer, Alabama. J. Geophys. Res. 112, G02026.

Liu, L., Zoback, M. D., 1997. Lithospheric strength and intraplate seismicity in the New Madrid seismic zone. Tectonics 16, 585–595.

Ma, L., 2009. Noble gases dissolved in groundwaters of the Michigan Basin: Implications for paleoclimatology, hydrogeology, tectonics and mantle geochemistry. Ph.D. thesis, University of Michigan.

Ma, L., Castro, M. C., Hall, C. M., 2004. A late Pleistocene-Holocene noble gas paleotemperature record in southern Michigan. Geophys. Res. Lett. 31, L23204.

Maupin, M. A., Barber, N. L., 2005. Estimated withdrawals from principal aquifers in the United States, 2000. U.S. Geological Survey, Circular 1279.

McMahon, P. B., Chapelle, F. H., 1991. Geochemistry of dissolved inorganic carbon in a Coastal Plain aquifer: 2. Modeling carbon sources, sinks, and $\delta^{13}C$ evolution. J. Hydrol. 127, 109–135.

McMahon, P. B., Chapelle, F. H., 2008. Redox processes and the water quality of selected principal aquifer systems of the United States. Ground Water 44, 259–271.

Mook, W. G., 2001. Environmental Isotopes in the Hydrological Cycle: Principles and Applications. Volume I: Introduction -Theory, Methods, Review. UNESCO/IAEA, 280 p.

Mukherjee, A., Fryar, A. E., 2008. Deeper groundwater chemistry and geochemical modeling of the arsenic affected western Bengal basin, West Bengal, India. Appl. Geochem. 23, 863–894.

Mukherjee, A., Fryar, A. E., Rowe, H. D., 2007. Deeper groundwater chemistry and geochemical modeling of the arsenic affected western Bengal basin, West Bengal, India. J. Hydrol. 334, 151–161.

Musgrove, M. L., Banner, J. L., 1993. Regional ground-water mixing and the origin of saline fluids: Midcontinent, United States. Science 259, 1877–1882.

Oman, J. K., 1986. Stratigraphic framework and correlation of the Tertiary lignite-bearing formations from southeast Missouri to the Fort Pillow test well of west Tennessee. U.S. Geological Survey, Bulletin 1644.

Park, J., Bethke, C. M., Torgersen, T., Johnson, T. M., 2002. Transport modeling applied to the interpretation of groundwater ^{36}Cl age. Water Resour. Res. 38, 1043.

Parkhurst, D. L., Appelo, C. A. J., 1999. User's guide to PHREEQC (version 2)— a computer program for speciation, batch-reaction, one-dimensional transport, and inverse geochemical calculations. U.S. Geological Survey, Water-Resources Investigations Report 99-4259.

Parkhurst, D. L., Christenson, S., Breit, G. N., 1996. Ground-water-quality assessment of the Central Oklahoma aquifer, Oklahoma: Geochemical and geohydrologic investigations. U.S. Geological Survey, Water Supply Paper 2357-C.

Penny, E., Lee, M. K., Morton, C., 2003. Groundwater and microbial processes of Alabama coastal plain aquifers. Water Resour. Res. 39, 1320, doi:10.1029/2003WR001963.

Pettijohn, R. A., 1996. Geochemistry of ground water in the Gulf Coast aquifer systems, south-central United States. U.S. Geological Survey, Water-Resources Investigations Report 96-4107.

Phillips, F. M., Castro, M. C., 2003. Groundwater dating and residence-time measurements. In: Drever, J. I. (Ed.), Surface and Ground Water, Weathering, and Soils. Treatise on Geochemistry, Vol. 5. Elsevier, Oxford, pp. 451–497.

Phillips, F. M., Peeters, L. A., Tansey, M. K., Davis, S. N., 1986. Paleoclimatic inferences from an isotopic investigation of groundwater in the central San Juan Basin, New Mexico. Quaternary Res. 26, 179–193.

Phillips, F. M., Tansey, M. K., Peeters, L. A., Cheng, S., Long, A., 1989. An isotopic investigation of groundwater in the central San Juan basin, New Mexico: carbon 14 dating as a basis for numerical flow modeling. Water Resour. Res. 25, 2259–2273.

Piper, A. M., 1944. A graphic procedure in the geochemical interpretation of water analyses. Trans. Am. Geophys. Union 25, 914–923.

Plummer, L. N., 1993. Stable isotope enrichment in paleowaters of the southeast Atlantic Coastal Plain, United States. Science 262, 2016–2020.

Plummer, L. N., Back, W., 1980. The mass balance approach; application to interpreting the chemical evolution of hydrologic systems. Am. J. Sci. 280, 130–142.

Plummer, L. N., Busby, J. F., Lee, R. W., Hanshaw, B. B., 1990. Geochemical modeling of the Madison aquifer in parts of Montana, Wyoming, and South Dakota. Water Resour. Res. 26,

1981–2014.

Plummer, L. N., Prestemon, E. C., Parkhurst, D. L., 1994. An interactive code (NETPATH) for modeling NET geochemical reactions along a flow PATH, version 2.0. U.S. Geological Survey, Water-Resources Investigations Report 94-4169.

Plummer, L. N., Sprinkle, C. L., 2001. Radiocarbon dating of dissolved inorganic carbon in groundwater from confined parts of the Upper Floridan aquifer, Florida, USA. Hydrogeol. J. 9, 127–150.

Prudic, D. E., 1991. Estimates of hydraulic conductivity from aquifer-test analyses and specific-capacity data, Gulf Coast regional aquifer systems, south-central United States. U.S. Geological Survey, Water-Resources Investigations Report 90-4121.

Pucci, A. A. J., Owens, J. P., 1989. Geochemical variations in a core of hydrogeologic units near Freehold, New Jersey. Ground Water 27, 802–812.

Pugh, A. L., 2008. Summary of aquifer test data for Arkansas - 1940-2006. U.S. Geological Survey, Scientific Investigations Report 2008-5149.

Pugh, A. L., 2010. Potentiometric surfaces and water-level trends in the Cockfield (Upper Claiborne) and Wilcox (Lower Wilcox) aquifers of southern and northeastern Arkansas, 2009. U.S. Geological Survey, Scientific Investigations Report 2010-5014.

Purdy, C. B., Helz, G. R., Mignerey, A. C., Kubik, P. W., Elmore, D., Sharma, P., Hemmick, T., 1996. Aquia aquifer dissolved Cl^- and $^{36}Cl/Cl$: Implications for flow velocities. Water Resour. Res. 32, 1163–1171.

Scholl, M., 2006. Precipitation isotope collector designs, http://water.usgs.gov/nrp/proj.bib/hawaii/precip_methods.htm, accessed 2 November 2011.

Schrader, T. P., 2007. Potentiometric surfaces and water-level trends in the Cockfield and Wilcox aquifers of southern and northeastern Arkansas, 2006. U.S. Geological Survey, Scientific Investigations Report 2007-5218.

Schwartz, F. W., Zhang, H., 2003. Fundamentals of Ground Water. John Wiley & Sons, Inc., New York, 583 p.

Siegel, D. I., 1991. Evidence for dilution of deep, confined ground water by vertical recharge of isotopically heavy Pleistocene water. Geology 19, 433–436.

Solomon, D. K., Schiff, S. L., Poreda, R. J., Clarke, W. B., 1993. A validation of the $^3H/^3He$ method for determining groundwater recharge. Water Resour. Res. 29, 2951–2962.

Solomon, D. K., Sudicky, E. A., 1991. Tritium and helium 3 isotope ratios for direct estimation of spatial variations in groundwater recharge. Water Resour. Res. 27, 2309–2319.

Speer, P. R., Golden, H. G., Patterson, J. F., Welborne, W. J., 1964. Water resources of the Mississippi Embayment; low-flow characteristics of streams in the Mississippi Embayment in Mississippi and Alabama, with a section on quality of the water. U.S. Geological Survey, Professional Paper 448-I.

Stearns, R. G., 1957. Cretaceous, Paleocene, and Lower Eocene geologic history of the northern

Mississippi Embayment. Geol. Soc. Am. Bull. 68, 1077–1100.

Stotler, R., Harvey, F. E., Gosselin, D. C., 2010. A Black Hills-Madison aquifer origin for Dakota aquifer groundwater in northeastern Nebraska. Ground Water 48, 448–464.

Stumm, W., Morgan, J. J., 1996. Aquatic Chemistry: Chemical Equilibria and Rates in Natural Waters, 3rd edition. John Wiley & Sons, Inc., New York, 1022 p.

Stute, M., Clark, J. F., Schlosser, P., Broecker, W. S., Bonani, G., 1995. A 30,000 yr continental paleotemperature record derived from noble gases dissolved in groundwater from the San Juan basin, New Mexico. Quaternary Res. 43, 209–220.

Stute, M., Schlosser, P., Clark, J. F., Broecker, W. S., 1992. Paleotemperatures in the southwestern United States derived from noble gases in ground water. Science 256, 1000–1003.

Tardy, Y., 1971. Characterization of the principal weathering types by the geochemistry of waters from some European and African crystalline massifs. Chem. Geol. 7, 253–271.

Tetlow, J. A., Wilson, A. L., 1964. The absorptiometric determination of iron in boiler feed-water. Part III. Method for determining the total iron content. Analyst 89, 442–452.

Thomas, W. A., 1991. The Appalachian-Ouachita rifted margin of southeastern North America. Geol. Soc. Am. Bull. 103, 415–431.

Thorstenson, D. C., Fisher, D. W., Croft, M. G., 1979. Geochemistry of the Fox Hills–Basal Hell Creek aquifer in southwestern North Dakota and northwestern South Dakota. Water Resour. Res. 15, 1479–1498.

Warwick, P. D., Breland, F. C., Hackley, P. C., 2008. Biogenic origin of coalbed gas in the northern Gulf of Mexico Coastal Plain, U.S.A. Int. J. Coal Geol. 76, 119–137.

Weiss, J. S., 1992. Geohydrologic units of the Coastal Lowlands aquifer system, south-central United States. U.S. Geological Survey, Professional Paper 1416-C.

Williamson, A. K., Grubb, H. F., 2001. Ground-water flow in the Gulf Coast aquifer systems, south-central United States. U.S. Geological Survey, Professional Paper 1416-F.

Wood, W. W., 1981. Guidelines for collection and field analysis of ground-water samples for selected unstable constituents. U.S. Geological Survey, Techniques of Water-Resources Investigations book 1, chapter D2.

Yeatts, D. S., 2004. Potentiometric surfaces in the Cockfield and Wilcox aquifers of southern and northeastern Arkansas, 2003. U.S. Geological Survey, Scientific Investigations Report 2004-5169.

Zhu, C., 2000. Estimate of recharge from radiocarbon dating of groundwater and numerical flow and transport modeling. Water Resour. Res. 36, 2607–2620.

Zhu, C., Waddell, R. K., Star, I., Ostrander, M., 1998. Responses of ground water in the Black Mesa basin, northeastern Arizona, to paleoclimatic changes during the late Pleistocene and Holocene. Geology 26, 127–130.

ZoBell, C. E., 1946. Studies on redox potential of marine sediments. Bull. Am. Assoc. Petrol. Geol. 30, 477–513.

Vita

Estifanos Haile

Date of Birth – September 17, 1977

Place of Birth – Asmara, Eritrea

PRIOR EDUCATION

– Royal Institute of Technology, Sweden
Licentiate Degree in Groundwater chemistry, December 2005
Thesis: Groundwater chemistry and recharge rate in crystalline rocks: case study from the Eritrean highland
Advisor: Prof. Em. Gunnar Jacks

– Addis Ababa University, Ethiopia, B.Sc., Geology [June 1998]
B.Sc in Geology, June 1998

PRIOR EXPERIENCE

– Department of Earth and Environmental Sciences, University of Kentucky, USA
Teaching and research assistant – January 2006 to May 2011

– Department of Land and Water Resources Engineering, Royal Institute of Technology, Sweden
Research and Teaching assistant – January 2003 to May 2005

– Department of Earth Sciences, University of Asmara, Eritrea
Graduate assistant – September 1998 to December 2002

ABSTRACTS OF PRESENTATIONS

Haile, E., and Fryar, A.E. [2008], Geochemical modeling of regional hydrochemical evolution in the Wilcox aquifer of Missouri and Arkansas: Gulf Coast Association of Geological Societies Transactions, v. 58, p. 339 – 342.

Haile, E., and Fryar, A.E. [2007], Recharge and regional-scale chemical evolution of groundwater in the Wilcox aquifer, northern Mississippi Embayment, USA: Geological Society of America Abstracts with Programs, v. 39, no. 6, p. 267.

Harikumar, P. S., Haile, E., Bhattacharya, P., Madhavan, K., Jacks, G. [2006], Groundwater quality problems of coastal aquifers of Alappuzha, India with Reference to excess fluoride and defluoridation using domestic filters. Groundwater for sustainable development: Problems, Perspectives and Challenges, New Delhi, India. Abstract No 81.

Haile, E., and Jacks, G. [2005], Rainwater and groundwater chemistry in the Eritrean highlands – Inference for groundwater recharge, Eos Trans. AGU, 86(52), Fall Meet. Suppl., San Francisco CA. Abstract H23F-1488